Thermodynamic optimisation of a boiler feed water desalination plant

PJ van der Walt

21588260

Dissertation submitted in fulfilment of the requirements for the degree *Magister* in Chemical Engineering at the Potchefstroom Campus of the North-West University

Supervisor: Prof L Liebenberg

November 2014

Abstract

In the process of electricity generation, water is used as the working fluid to transport energy from the fuel to the turbine. This water has to be ultrapure in order to reduce maintenance cost on the boilers.

For the production of ultrapure water, a desalination process is used. This process consists of an ultrafiltration pretreatment section, two reverse osmosis stages and a continuous electrodeionisation stage. Reverse osmosis desalination plants are, however, inherently inefficient with a high specific energy consumption. In an attempt to improve the efficiency of low recovery seawater applications, energy recovery devices are installed on the brine outlet of the reverse osmosis stages. The energy recovery device recovers the energy that is released through the high pressure brine stream and reintroduces it to the system.

The investigated desalination process has a fresh water feed with a salinity of 71 ppm and is operated at recoveries above 85%. The plant produces demineralised water at a salinity lower than 0.001ppm for the purpose of high pressure boiler feed.

A thermodynamic analysis determined the Second Law efficiencies for the first and second reverse osmosis sections as 3.85% and 3.68% respectively. The specific energy consumption for the reverse osmosis plants is 353 Wh/m^3 and 1.31 Wh/m^3. This was used as the baseline for the investigation. An exergy analysis determined that energy is lost through the brine throttling process and that a pressure exchanging system can be installed on all reverse osmosis brine streams. Energy recovery devices are untested in high recovery fresh water applications due to the low brine pressure and low brine flow.

It was determined that pressure exchanging systems can reduce the specific energy consumption of the first reverse osmosis stage with 12.2% whereas the second RO stage energy consumption can be improved with 7.7%. The Second Law efficiency can be improved by 25.6% for the first reverse osmosis stage while the efficiency is improved with 18.1% for the second stage. The optimal operating recovery for the PES is between 80% and 90%.

Key Words: Reverse osmosis, energy recovery, energy consumption, Second Law efficiency

Acknowledgements

I would like to thank my supervisor, Prof Leon Liebenberg for his guidance and patience. His mentorship, willingness and passion have been an inspiration. Thank you for the hours of reading, expert advice and the professional manner in which you assisted.

Thank you to the two external examiners for their thorough and incisive comments. Your contribution is greatly appreciated.

A special word of thanks should go to my colleagues for their support and understanding.

My family, Jannie, Louine and Karlien van der Walt has been supportive in the superlative sense. Thank you for the belief, kindness and countless prayers.

Finally I would like to praise the LORD for His countless blessings and everlasting grace. Without Your power, nothing would be possible.

Table of Contents

List of Figures

List of Tables

List of symbols

Symbol	Description	Unit (if applicable)
$\bar{v}$	Average membrane flux	ℓ/m^2h
μ	Chemical potential	J/mol
B	Salt permeability coefficient	m^2/s
C	Concentration	g/ ℓ
c	Molar concentration	mol/ℓ
C^*	Activated carbon	
CF	Concentration factor	
C_p	Specific heat capacity	kJ/kg
Da	Dalton	Da
E	Energy	J
Eff	Present efficiency	%
FCE	Feed water conductivity equivalent	μS/cm
f_{os}	Osmotic pressure coefficient	Pa
FV	Future value	
g	Specific Gibbs energy	kJ/kg
h	Specific enthalpy	kJ/kg
I	Current	A
i	Interest rate	%
J	Flux	m^3/m^2s
L	Permeability coefficient	kg $m/m^2s.kPa$
l	Membrane thickness	mm
LSI	Langelier saturation Index	
m	Mass	kg
mf	Mass fraction	
M_W	Molecular weight	kg/mol
n	years	
NTU	Normal turbidity units	-
P	Pressure	kPa

Symbol	Description	Unit (if applicable)
ppm-h	Parts per million during hours of exposure	ppm-h
PV	Present value	
Q	Volumetric flow	m^3/h
R	Recovery	%
R_g	Universal Gas Constant (8.314)	J/molK
R_m	Membrane resistance	m^{-1}
R_s	Salt rejection	%
S	Salinity	ppm
s	Specific entropy	kJ/kgK
SDI	Silt density index	
SEC	Specific energy consumption	Wh/m^3
SI	Salinity increase	%
S_o	Solubility	mol/ℓ
T	Temperature	K
V	Potential difference	V
V	Volume	m^3
VM	Volumetric mixing	%
W	Work	Wh
x	Mole fraction	
η	Efficiency	%
π	Osmotic pressure	kPa
ρ	Density	kg/m^3
ψ	Specific exergy	kW

Glossary

Term	Description
Aquifer	A body of permeable rock which can contain groundwater
Array	An ordered arrangement
Brackish water	Water with a salinity higher than 500 ppm but lower than 30 000 ppm
Brine	The high salinity, concentrated, by-product of a cross-flow membrane process
Coagulant	A substance that neutralises the electrostatic forces between suspended particles
Colloid	A substance microscopically dispersed in the water. These substances do not settle out and are usually unreactive
Corrosion	The destruction of a material due to a chemical reaction with its environment
Cross-flow	A filtration process producing a permeate and concentrate stream
Dalton	A unit mass. 1 Dalton is the mass of a hydrogen atom
Dead-end	A filtration process producing only a permeate stream
Demineralised water	Water with a conductivity lower than 0.1 µS/cm
Desalination	The process where salinity is removed from water
Driving pressure	The pressure required in a reverse osmosis vessel in order to produce water at a specific recovery
Exergy	The energy that can be converted into work. Therefore the quantity of work that can be performed by a fluid relative to a reference state
Flocculant	A substance binding smaller suspended particles to form flocks
Fouling	The formation of an encrusted deposit on a membrane surface
Fresh water	Water with a salinity lower than 500 ppm
Hardness	The mineral content of water. Usually related to magnesium and calcium

Term	Description
Hydrophilic	Substances with a high affinity for water
Hydrophobic	Substances with a low affinity for water
Oleophilic	Substances with a strong affinity for oils
Osmotic pressure	The pressure required to prevent natural osmosis from occurring
Permeate	The substance passing through a filter or membrane
Polishing	Final step in demineralised water production that removes the residual ions from the water
Polyamide	A synthetic polymer consisting of amino groups and carboxylic acid groups
Polysulfone	A thermoplastic polymer consisting of aryl-SO_2-aryl groups
Potable water	Water suitable for domestic and drinking purposes
Propagation	The movement of a wave through a medium
Recovery	Relationship of the volume of water purified versus the feed water volume
Salt water	Water with a salinity higher than 30 000 ppm
Scaling	Small, plate-like structures adhering to the membrane surface due to chemical reactions
Seawater	Water with a salinity of 30 000 ppm and higher found in the oceans
Silt	Fine sand, clay or suspended material carried by water
Skids	Identical sections of the water treatment plant that can be operated independently from one another
Solute	The minor component in a solution. The solute is dissolved in the solvent
Ultrapure water	Water of a demineralised quality
Van der Waals forces	The sum of the attractive or repulsive forces between molecules other than covalent or electrostatic forces
Zeolite	A large group of minerals consisting of hydrated aluminosilicates of sodium, potassium, calcium or barium
Zeta potential	The degree of repulsion between two similarly charged particles

Abbreviations

Abbreviation	Description
AOC	Assimilable Organic Carbon
BOD	Biochemical Oxygen Demand
CA	Cellulose Acetate
CEB	Chemically Enhanced Backwash
CEDI	Continuous Electrode Deionisation
CF	Concentration Factor
CIP	Cleaning in Place
COD	Chemical Oxygen Demand
DOC	Dissolved Oxygen Content
ED	Electrodialysis
EDR	Electrodialysis Reversal
ERD	Energy Recovery Device
ERT	Energy Recovery Turbine
HP	High Pressure
IX	Ion Exchange
LSI	Langelier Saturation Index
MF	Microfiltration
NF	Nanofiltration
NTU	Nephelometric Turbidity Units
ORP	Oxidisation-reduction potential
PA	Polyamide
PES	Pressure Exchange System
ppb	Parts Per Billion
ppm	Parts per Million
ppt	Parts Per Thousand
RO	Reverse Osmosis
SBA	Strong Base Anion
SDI	Silt Density Index

Abbreviation	Description
SEC	Specific Energy Consumption
SWRO	Saltwater Reverse Osmosis
TA	Total Anions
TC	Total Cations
TDS	Total Dissolved Solids
TEA	Total Exchangeable Anions
TEC	Total Exchangeable Cations
TH	Total Hardness
TMP	Trans-Membrane Pressure
TOC	Total Organic Content
UF	Ultrafiltration
UV	Ultra Violet
VSD	Variable Speed Drive
WBA	Weak Base Anion
ZLD	Zero Liquid Discharge

Chapter 1

Introduction

This chapter provides background to the problem statement and establishes a clear objective for the study. Chapter 1 also elucidates the purpose and the scope of the study, as well as the research methodology that was followed.

1.1 Introduction

Water is the chemical compound that supports life (Flynn, 2009).

Of the 1.4 billion km^3 water on planet earth only 2.5% is fresh water. 70% of all the fresh water is absorbed in the polar ice caps or permanent glaciers and 29.7% consists of ground water. The remaining 0.3% makes up the freshwater lakes, dams and rivers. (United Nations, 2012)

Human activity relies heavily on freshwater sources like dams, lakes and rivers. These sources combined are less than 0.008% of the total water on planet earth.

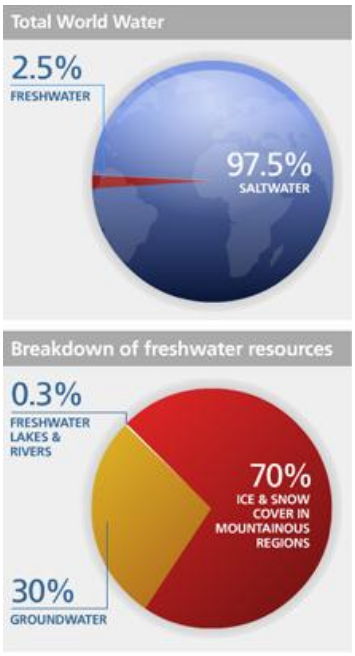

Figure 1: Breakdown of the world's water resources (United Nations, 2012)

Due to the immense population growth and the resulting stress on water resources, water purification technology, especially reverse osmosis (RO) technology, is currently one of the fastest growing fields in engineering (Penate & Garcia-Rodriguez, 2010).

1.2 Problem relevance and research significance

Reverse osmosis is widely used in municipal wastewater treatment, saltwater desalination and demineralised water production (Flynn, 2009). This study will focus on the reverse osmosis process typically used to produce demineralised water from fresh water for the purpose of electricity generation.

The production of demineralised water is achieved primarily by either ion exchange (IX) or reverse osmosis (RO). Ion exchange has a high operating cost and consumes large amounts of both acids and caustics.

RO on the other hand uses considerably less chemicals and has a lower operating cost, which makes it a more environmentally friendly design (Kucera, 2010).

A major drawback in the RO process is the energy consumption and low Second Law efficiency of 4% (Cuda, *et al.*, 2006). By reducing the energy consumed by the RO plant, both the carbon footprint and the production cost of the demineralized water will be considerably reduced (Malaeb & Ayoub, 2011). This study will aim to determine where energy recovery is possible on a current industrial RO plant and determine the feasibility of an alternative design.

A vast majority of low recovery, seawater reverse osmosis plants (SWRO) already have incorporated energy recovery devices (ERDs) to reduce the specific energy costs to potable water production (Geisler, *et al.*, 2001). This thermodynamic analysis investigates the feasibility to integrate an ERD into the current RO design of a specific fresh water plant operating at high recoveries.

The subsequent reduction in energy costs will further improve the already comparatively low carbon footprint of the RO plant design and will contribute to lower operating costs.

1.3 Scope of the study

Through rigorous application of previous research, coupled with mathematical formalism and empirical work, specific areas where energy recovery is possible will be identified on the fresh water desalination plant.

Available means to recover energy will be researched and evaluated. The two most promising ERDs will be compared on a practical and economic base to ensure the compatibility with the current plant design and ensure that the implementation of these devices does not hamper the process performance whilst maximising financial benefit.

The feasibility of the design will be evaluated through descriptive evaluating methods in the form of an informed argument that is based on literature from previous research (Henver, et al., 2004). Experimental evaluation methods based on simulations will be conducted in order to validate all mathematical models and results obtained (Henver, et al., 2004).

The proposed design will be instantiated and the feasibility determined through technical and economical evaluations.

The scope of the study will ensure that the seven guidelines for design based research as set out by Henver et al. will be satisfied (Henver, et al., 2004). This will ensure:

- a viable artefact instantiation or feasibility study is done by establishing the design as an artefact,
- that the problem relevance is stated,
- the design is assessed according to well executed evaluation methods,
- the novelty or significance of the research is clear and concise,
- rigorous evaluation methods and effective combination of knowledge, empirical work and practical applications where met,
- the design as search process has utilised all available means to reach the desired results that satisfy the problem statement
- and that all results are clearly communicated in a professional manner.

These seven guidelines will be met by following the research methodology as stated below.

1.4 Research Methodology

An investigation on current technologies used in desalination plants and the methods used to recover energy will be conducted and summarised in a literature review. This will include thermodynamic evaluation methods and process fundamentals.

Research will be done by conducting an exergy analysis on an industrial 240m^3/h desalination plant configuration. This analysis will determine if an energy recovery device can be installed and if so, where the appropriate location is for the installation.

In order to establish a baseline from which the proposed design will be evaluated, Second Law efficiency as well as the specific energy consumption will be calculated for the current plant.

After the appropriate location for the installation of the energy recovery devices is established, a second exergy analysis will be performed. The Second Law efficiency as well as the SEC will be calculated for the proposed design. This will be compared with the baseline established from the first analysis.

Two types of energy recovery devices, an ERT and PES will be compared with each other and with the base case in order to make a recommendation.

The effect that recovery has on the specific energy consumption and on the amount of energy recovered will be investigated to determine optimal operational conditions.

The energy saved, if any, will then be used to determine if a financial gain can be established from the installation.

1.5 References

Flynn, D. J., 2009. The Nalco Water Handbook. 3 ed. New York: McGraw Hill.

Geisler, P., Krumm, W. & Peters, T. A., 2001. Reduction of energy demand for seawater RO with the pressure exchange system PES. *Desalination,* 1(135):205-210.

Henver, A., March, S., Park, J. & Ram, S., 2004. Design Science in information systems research. *MIS Quarterly,* 1(28):75-105.

Kucera, J., 2010. *Reverse Osmosis: Design, Processes and Application for Engineers.* Hoboken: Wiley and Sons.

Penate, B. & Garcia-Rodriguez, L., 2010. Energy optimisation of existing SWRO (seawater reverse osmosis) plants with ERT (energy recovery turbines): Technical and thermoeconomic assessment. *Energy,* 1(36):613-626.

United Nations, 2012. *Water resources.* [Online]
Available at: http://www.unwater.org/statistics_res.html
[Accessed 16 September 2013].

Chapter 2

Literature Study: Water treatment

This chapter surveys the state-of-the-art technology in water treatment. It outlines the need for demineralised water and the related production methods. Attention is especially focussed on the reverse osmosis process and the pretreatment to reverse osmosis. The most contemporary energy recovery systems and their application thereof are discussed. A thermodynamic overview of a desalination plant is given.

2.1 Introduction

Water, due to its molecular structure, is an excellent solvent and, therefore, will not be found in nature as a pure liquid. Substances bonded with ionic bonds and covalent bonds, for example salts and minerals, will readily be dissolved into the liquid (American Water Works Association, 1999). These minerals can be either present in an ionic state or in a colloidal state in the fluid (Meltzer, 1992). Biological components such as viruses, bacteria and proteins will also be present in most fresh water, rendering it unsafe for human consumption (Kucera, 2010)

Continuous strain on the environment and on water reserves has led to stringent environmental laws on wastewater quality and on the amount of wastewater discharged by industries (Kucera, 2010). Water purification technology, therefore, forms a crucial part of the modern society, not only for domestic use, but also for industrial activity (American Water Works Association, 1999).

In the electricity generation industry, water is used as the working fluid. This requires rigorous and inflexible ultrapure water to ensure minimal damage to equipment (Vidojkovic, *et al.*, 2013).

This chapter provides information on the advantages of using ultrapure water and the production methods thereof. Desalination methods are introduced, focussing on membrane processes for demineralised water production.

In order to better understand the production methods, the impurities found in water and the effect of these impurities on high pressure boilers are discussed.

2.2 Water impurities

The electrical polarity of water molecules provides the perfect medium to dissolve most ionic and covalent compounds (Flynn, 2009). Sugars, salts, acids, alkalis and gases such as oxygen and nitrogen readily dissolve in water (Clifford & Letterman, 1999). Other gases such as carbon dioxide and ammonia react with water to form weak acids or alkalis (Flynn, 2009).

The density and viscosity of water together with the turbulent motion of flowing water cause solids to be suspended in the water for prolonged periods (Flynn, 2009). These particles can include inorganic solids, organic material or biological organisms (Flynn, 2009).

The quality of the water is intimately related to geological surroundings and climate of the water source (Flynn, 2009). The rainfall, geological surroundings of the watershed, underground aquifer properties, biological activity of the soil and the human population have a major effect on the contaminants trapped in the raw water (Flynn, 2009).

Surface water (lakes, dams and rivers) composition is affected by the properties of the ground it comes into contact with (Flynn, 2009). If the rock bed contains limestone, the water will have a high alkalinity and will be high in calcium and magnesium (hardness) (Flynn, 2009). Surface water from rivers will have higher turbidity than water from lakes and dams. Phosphates and nitrates may also be present due to agricultural activity. Surface water from lakes and dams will have a lower hardness (Clifford & Letterman, 1999). The water in lakes may also be more prone to algae growth and, therefore, will have higher biological contents. These sources mainly provide fresh water with a salinity lower than 500 ppm (Flynn, 2009).

Groundwater typically has a constant temperature throughout the year (Flynn, 2009). The hardness of the water can range between extremes according to the aquifer properties (Flynn, 2009). The suspended material and biological content of groundwater is generally low; however, anaerobic bacteria may be present (Clifford & Letterman, 1999). Typically groundwater is a source of brackish water with a salinity between 500 ppm and 25 000 ppm (Flynn, 2009).

Seawater has a high concentration of dissolved solids with salinity in the region of 30 000 ppm (Malaeb & Ayoub, 2011), (El-Emam & Dincer, 2013). The biological content in seawater is also high (Malaeb & Ayoub, 2011), (El-Emam & Dincer, 2013). The large volume of seawater ensures a more predictable temperature range (Flynn, 2009). Suspended particles will also be present in seawater (Flynn, 2009).

Impurities in water can be classed into 6 groups (Flynn, 2009). These are:

a) Soluble matter
b) Insoluble matter
c) Organic contaminants
d) Biological contaminants
e) Dissolved gases

Soluble matter includes impurities such as calcium, magnesium, chloride, bicarbonate, silica and sulphates (Vidojkovic, *et al.*, 2013), (Romero-Ternero, et al., 2005). This makes up the

salinity of the water (Vidojkovic, *et al.*, 2013). Conductivity and pH are excellent measures of the amount of soluble matter impurities contained within water (American Water Works Association, 1999). Table 1: Common soluble matter impurities and the effect on an industrial system discusses the impact on an industrial system if these impurities are excessively present (American Water Works Association, 1999).

Table 1: Common soluble matter impurities and the effect on an industrial system (Flynn, 2009)

Impurity	**Impact on system**
Calcium	Forms insoluble calcium scale at higher concentrations.
Magnesium	More soluble than calcium but can form scale at higher concentrations. Magnesium silicate can form at high pH if water contains silica.
Chloride	Corrosive to most metals. Higher concentrations indicate a higher corrosion potential.
Bicarbonate	Provides a buffer capacity. Calcium carbonate scale can occur at a high pH and calcium concentration.
Silica	Silica can form scale or precipitate at lower pH levels. Solubility increases as the pH increase. Colloidal silica can form and cause damage to high pressure turbo machinery.
Sulphate	Can cause corrosion at high concentrations. Calcium sulphate scale can form at concentrations exceeding 800mg/ℓ as $CaCO_3$

Insoluble materials like silt, sand and soil add to the turbidity of water (Flynn, 2009). The suspended particles are not true colloids; however, colloidal properties keep these particles in suspension (Flynn, 2009). The negative electrostatic charge (zeta charge) of particles in water (-14mV to -30mV) will act on other particles (Flynn, 2009). This interaction will keep the particles in suspension (Clifford & Letterman, 1999).

Van der Waals forces also interact with the particles (Flynn, 2009). The attraction of the Van der Waals force, together with the negative charge of the particles, will create a temporary dipole moment (Flynn, 2009). This dipole will then induce another dipole moment on a nearby particle (Flynn, 2009). The particles then attract each other while the Van der Waals forces keep the particles in suspension (Clifford & Letterman, 1999). If these forces are neutralised, the particles will agglomerate and settle out of suspension. This can be done with the addition of coagulants (Clifford & Letterman, 1999).

The organic matter in water originates from soil, rotting vegetation or even larger particles like twigs and leaves (Clifford & Letterman, 1999). This is measured in numerous ways including BOD, COD, TOC and DOC (Clifford & Letterman, 1999). Organic material is a major factor in water treatment due to membrane fouling and exhaustion of anion exchange resins (Flynn, 2009).

Dissolved gases accumulate in water due to turbulent flow conditions or dissolve from the atmosphere (Clifford & Letterman, 1999). These gases, especially oxygen, can cause major problems in equipment as corrosion of boiler tubes becomes a reality (Clifford & Letterman, 1999). Oxygen scavengers like hydrazine and/or mechanical equipment like deaerators are used to remove dissolved gases and prevent corrosion (Flynn, 2009). Figure 2 shows the role oxygen plays in the corrosion reaction (Flynn, 2009).

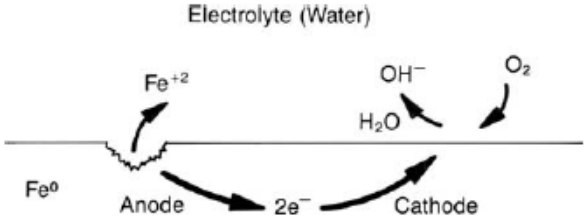

Figure 2: Corrosion reaction (Flynn, 2009)

For industrial purposes, these above mentioned impurities are managed and removed in order for water to be used safely and efficiently in processes such as the pharmaceutical, power generation, petroleum, food and pulp and paper industries (Meltzer, 1992).

Table 2: Water quality indicators

Indicator	Property indicated	Unit
pH	Concentration hydrogen ions	pH scale (1 - 14)
Conductivity	Ability to conduct an electrical current	µS/cm
Turbidity	Clarity of the water	NTU
Salinity	Dissolved salts present in water	%
DO	Dissolved Oxygen	mg/ℓ
TDS	Total dissolved solids	mg/ℓ
TC	Total cations	mg/ℓ as $CaCO_3$
TA	Total anions	mg/ℓ as $CaCO_3$
TH	Total hardness (sum of calcium and magnesium ions)	mg/ℓ as $CaCO_3$
SDI	Silt Density Index (Suspended solid content indication)	SDI (no units)

2.3 Ultrapure water in the electricity generation process

Water heated above its boiling point (100^0C at 101.3 kPa) evaporates into steam (Vidojkovic, *et al.*, 2013). Due to the availability, relatively high energy content and high heat transfer coefficient of steam, water is the substance preferred as the working fluid in the electricity generation process (Vidojkovic, *et al.*, 2013).

The electricity generation process is an energy exchanging system (Cuda, *et al.*, 2006). The chemical energy from the fuel is transferred to the water as heat energy (Cuda, *et al.*, 2006). The water/steam cycle then transports the heat energy to the turbine where it is converted into mechanical energy (Cuda, *et al.*, 2006). The mechanical energy from the turbine shaft then rotates the generator to transform the mechanical energy into electrical energy (Cuda, *et al.*, 2006).

This process utilises large amounts of water to produce steam. In the year 2000, the USA used a total of 1500 billion litres of water per day (US Geological Survey, 2004). 48% of that was utilised by thermal electric power generators (US Geological Survey, 2004).

Water is pumped to the boiler where it enters the boiler tubes under pressure (Cuda, *et al.*, 2006). The combustion process of the fuel inside the boiler releases the chemical energy in

the fuel emitting heat energy in the process (Cuda, *et al.*, 2006). Through convection and conduction, this heat energy is absorbed by the water (Cuda, *et al.*, 2006). This heat evaporates the water into steam. The steam, now rich in energy, is released to the turbine where the heat energy is converted into mechanical energy (Vidojkovic, *et al.*, 2013).

The water that is fed to the boiler needs to be of a specific quality (Kucera, 2010). This aids the prevention of boiler tube failures and prevents damage to the turbine blades (Kucera, 2010). The presence of any foreign ions or dissolved solids will cause fouling or corrosion of the boiler tubes (Kucera, 2010).

Fouling or scaling inside the boiler tubes poses serious threats due to the low thermal conductivity of the foreign, deposited, matter (Flynn, 2009). Scaling occurs when foreign matter precipitates and adheres to the inside of the boiler tubes (Flynn, 2009).

As the water in the boiler tubes absorb the heat energy released from the combustion process, it also cools the boiler tube metal to a temperature at which failure probability is low (Cuda, *et al.*, 2006).

Scaling in the tubes, however, impedes the efficiency with which the water regulates the temperature of the boiler tubes (Cuda, *et al.*, 2006). Heat transfer, depending on the type and composite of the scale, can be reduced by up to 12% (Flynn, 2009). This will cause overheating of the metal and will lead to tube leaks or failures (Flynn, 2009).

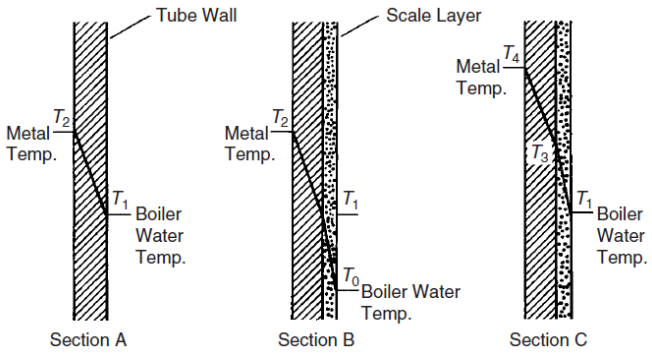

Figure 3: Effect on temperature caused by scaling of boiler tubes (Flynn, 2009)

Figure 3 shows the effect that scaling has on the temperature of the boiler tube metal. Section A has no scaling and operates at the normal water temperature (T_1) and metal temperature (T_2). Section B shows a drop in the boiler water temperature (T_3) due to the adverse effect of scaling on the heat transfer. This will lower the overall boiler efficiency as more fuel needs to be combusted to generate the sufficient water temperature. Scaling will also raise the metal

temperature (T_4), as evident in Section C. If temperature T_4 rises above the safe maximum temperature of the metal (458^0C), the boiler tube will fail causing a production loss (Flynn, 2009).

Chemical reactions such as corrosion are prevented by the use of ultrapure water (Flynn, 2009). Corrosion or ductile gauging of the boiler tubes occur when chemicals in the water react with the parent metal of the boiler tubes (Cuda, *et al.*, 2006).

Sodium hydroxide is the most common corrosive agent and reacts according to Equations 1 and 2 (Flynn, 2009).

$$4NaOH + Fe_3O_4 \rightarrow 2NaFeO_2 + Na_2FeO_2 + H_2O \quad \textbf{Equation 1}$$

In this reaction, the sodium hydroxide reacts with the protective magnetite (Fe_3O_4) layer (Vidojkovic, *et al.*, 2013). This exposes the parent metal (Fe) which then reacts according to Equation 2 and 3 (Vidojkovic, *et al.*, 2013).

$$Fe + NaOH + H_2O \rightarrow NaFeO_2 + 3H^+ \quad \textbf{Equation 2}$$

$$3Fe + 4H_2O \rightarrow Fe_3O_4 + 8H \quad \textbf{Equation 3}$$

The second reaction reforms the protective magnetite layer; however, the hydrogen released in both reactions are free to react with the carbon in the carbon-steel alloy (Flynn, 2009). This reaction forms methane which is in a vapour form and forms pits or ductile gauging (Flynn, 2009).

Scaling and corrosion can only take place if foreign matter such as sodium hydroxide is present in the water. Therefore, in order to protect the boiler tubes, ultrapure water is preferred (Vidojkovic, *et al.*, 2013).

Ultrapure water is a product of a process called demineralisation. This entails the removal of the vast majority of impurities dissolved or suspended in the water (Wood & Gifford, 2004).

Demineralised water specifications will vary according to the application thereof. A typical composition of demineralised water is given in Table 3 (Kremser, *et al.*, 2006).

Table 3: Typical demineralised water composition (Kremser, *et al.*, 2006)

Property	Quantity
Conductivity (µS/cm)	< 0.1
SiO_2 (µg/ℓ)	< 15
TOC (mg/ℓ)	< 0.2
Na^+ (µg/ℓ)	< 20
K^+ (µg/ℓ)	< 20

As water in its purest form does not conduct any electricity, conductivity is an excellent measure used to determine the amount of ions and/or dissolved solids in the water (Kucera, 2010). The typical conductivity for use in high pressure boiler systems is 0.055 µS/cm (Vidojkovic, *et al.*, 2013).

Ultrapure, demineralised water is industrially produced primarily by two methods, namely ion exchange and reverse osmosis desalination (Vidojkovic, *et al.*, 2013). The ion exchange process will be discussed in Appendix A.

Demineralisation through membrane processes typically consists of three process steps to produce the ultrapure water (Macedonio & Drioli, 2010). These processes are pretreatment, reverse osmosis and polishing.

2.4 Pretreatment to reverse osmosis

Membrane fouling is regarded as the most common and undesirable problem in RO desalination (Ma, *et al.*, 2007). Scaling, organic fouling, colloidal fouling, biofouling and mineralisation are generally the types of fouling that takes place on RO membranes (Flynn, 2009). With the exception of mineralisation, the other four problems are easily avoided with proper pretreatment (Ma, *et al.*, 2007).

Pretreatment protects RO membranes, provides a better reliability of the desalination plant and improves the overall performance of the plant (Bae, *et al.*, 2011).

Conventional pretreatment includes screens for coarse pre-filtration, chemical dosing (including flocculation and coagulation), clarification and sand-filtration (Ma, *et al.*, 2007).

Membrane technologies can also be used as pretreatment options. The membrane systems include microfiltration (MF), ultrafiltration (UF) and nanofiltration (NF) (Flynn, 2009).

Membrane systems are preferred over conventional methods due to the possibility of lower operating costs (Bae, *et al.*, 2011), (Macedonio & Drioli, 2010).

Pretreatment sections are designed specifically for the feed water quality. This should ensure the water that enters the reverse osmosis section is within the required quality (Flynn, 2009). Table 4 shows the general feed water inlet quality requirements for RO and the processes that can be used to produce this water (Kucera, 2010).

Table 4: Guideline feed water quality to reverse osmosis as well as pretreatment methods (Kucera, 2010)

Species	**Units/ Measure**	**Guideline Value**	**Treatment Methods**
Calcium Carbonate	LSI	Close to 0	pH adjustments and antiscalant dosing
Chlorine	ppm	< 1	Carbon filtration and/or sodium bisulphite dosing
Colloids	SDI	< 5	Coagulation, flocculation, clarification, filtration (Sand filtration, MF, UF, NF)
Colour	APHA*	< 3	UF, NF and activated carbon adsorption
Hydrogen Sulphite	ppm	< 0.1	Complex combinations of oxidation, coagulation, filtration, sulphide addition and rechlorination.
Metals	ppm	< 0.05	Sodium softening and iron filters
Microbes	AOC**	< 5 µg/ℓ	Chlorine, ozone, UV radiation, non-oxidising biocides
Organics	TOC	< 3 ppm	Clarification, UV radiation, carbon filters
Silica	ppm	140 - 200	Reactive silica – antiscalants and pH adjustments Colloidal silica – Coagulation, UF, NF
Suspended Solids	NTU	< 1	Coagulation, flocculation, clarification, filtration (Sand filtration, MF, UF, NF)

* APHA American Public Health Association's dimensionless measure of colour intensity in water.

** AOC is a measure of the growth potential of a sample of microorganisms.

The quality of the raw water feed should be investigated thoroughly prior to the design of the pretreatment section. As evident from Table 4 the quality of the water will determine which processes will be in the final design for the desalination plant (Huang, *et al.*, 2011).

Pretreatment to RO can be divided into four categories: chemical, mechanical, mechanical plus chemical and sequenced pretreatment types that are readily used in industry (Kucera, 2010).

2.4.1 Chemical pretreatment

Chemical pretreatment is focussed on the removal of hardness, oxidising agents, bacterial content and scale formation (Macedonio & Drioli, 2010). Table 5 shows the available chemical pretreatment methods and the addressed species.

Table 5: Chemical pretreatment processes and the species addressed thereby (Kucera, 2010)

Chemical pretreatment	Species addressed
Chlorine	Microbes, TOC, colour
Ozone	Microbes, TOC, colour
Antiscalants	Hardness, silica
Sodium metabisulphite	Oxidisers (free chlorine)
Non-oxidising biocides	Microbes

2.4.2 Mechanical pretreatment

Mechanical pretreatment includes clarification, filtration, UV radiation and membrane technologies. Table 6 provides mechanical pretreatment processes and the problems addressed by the pretreatment (Flynn, 2009).

Table 6: Mechanical pretreatment processes and the species addressed thereby (Kucera, 2010)

Mechanical pretreatment	Species addressed
Clarification	Suspended solids, colloids, organics, colour, SDI, turbidity
Multimedia filtration	Turbidity, suspended solids, SDI
High-efficiency filtration	Suspended solids
Carbon filters	TOC, Chlorine
Iron filters	Iron, Manganese, Hydrogen sulphide
Sodium softeners	Hardness, soluble iron
UV radiation	Organics, Microbes

Membranes (MF, UF, NF)	Colloids, microbes, algae, colour, suspended solids, turbidity, SDI

Clarification and multimedia filtration are discussed in Appendix A.

2.4.2.1 Membrane processes as pretreatment

Membrane processes remove impurities according to the size of the membrane pores (Flynn, 2009). The spectrum shown in Figure 4 is indicative of the purities removed by various membranes (Kucera, 2010).

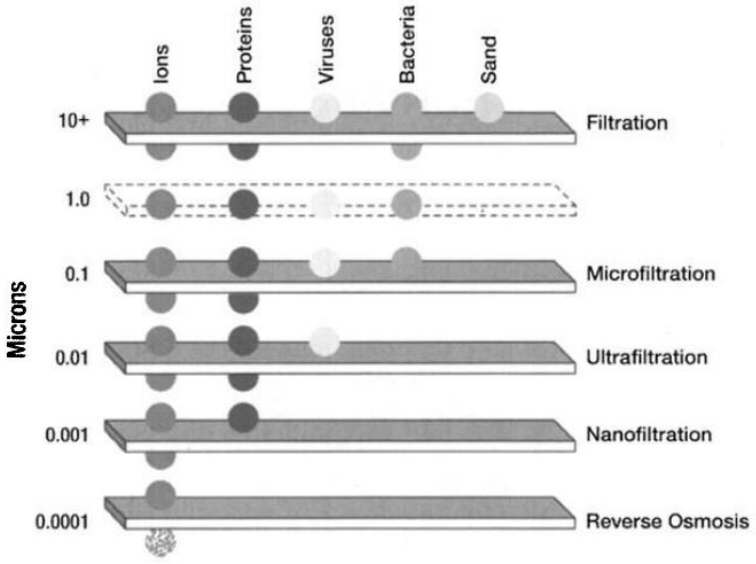

Figure 4: Filtration spectrum and impurities removed by specific membranes (Flynn, 2009)

Membrane separation can either be dead-end filtration or cross-flow filtration. Dead-end filtration has one inlet and one outlet stream (Flynn, 2009). Dead-end filtration consumes less energy than cross-flow filtration; however, it is more prone to fouling (Flynn, 2009). This is shown in Figure 5 (Flynn, 2009).

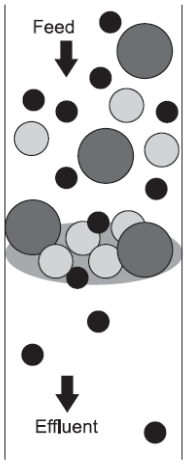

Figure 5: Dead-end filtration (Flynn, 2009)

Cross-flow separation consists of a feed stream with permeate and concentrate streams. The permeate flows through the membrane while the larger particles remain in the concentrate stream (Flynn, 2009). This configuration is less prone to fouling but consumes more energy than dead-end filtration (Flynn, 2009). This process is illustrated in Figure 6 (Flynn, 2009).

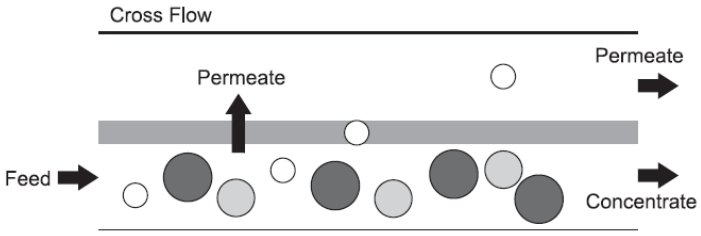

Figure 6: Cross-flow filtration (Flynn, 2009)

Reverse osmosis pretreatment may consist of microfiltration, ultrafiltration or nanofiltration or a combination of these processes (Kucera, 2010).

Microfiltration

Microfiltration membranes typically have a pore size ranging from 0.05 µm to 2 µm (Flynn, 2009). This pressure driven separation process is based on size exclusion. Particles larger than the pore size will be removed from the water (Flynn, 2009).

The usual configuration for microfiltration is a dead-end system; however, cross-flow filtration is possible (Singh, 2006).

Microfiltration membranes need to be cleaned if the differential pressure over the membrane is excessively high (Flynn, 2009). This can be done by chemically enhanced backwashing (CEB) or cleaning in place (CIP) (Cuda, *et al.*, 2006).

Backwashing, depending on feed water quality, can take place every 15 min to 60 min and usually lasts for half a minute (Flynn, 2009). CIP is done as frequently as needed to remove all the foreign matter not removed by the CEB (Flynn, 2009).

Microfilters remove suspended solids, turbidity and algae from water. Depending on the quality of the feed water, UF may be required (Hwang & Kammermeyer, 1984).

Ultrafiltration

This process is widely used in industry, not only for RO pretreatment, but also for concentration of proteins, bottled water production, waste oil treatment and paint recovery (Flynn, 2009).

Ultrafiltration removes colloidal silica, viruses, bacteria and high molecular weight organic material (Flynn, 2009). As shown in Table 7, UF-pretreated water has a significantly lower SDI than conventional pretreatment methods. A higher SDI will have a directly negative effect on the RO efficiency (Rosberg, 1997).

Table 7: SDI of different pretreatment methods

Pretreatment Method	**SDI**
Conventional methods*	5 - 6
MF-pretreated	2
UF-pretreated	< 1

* Conventional methods include clarification and media filtration

With UF as a pretreatment process, as opposed to conventional methods, the system recovery of the RO process will increase. This will lead to smaller pipe sizes, less pretreatment chemicals, smaller RO dimensions, less RO stages, RO membranes lifetime increases and less frequent cleaning (Rosberg, 1997).

According to Rosberg (1997), this will have a significant effect on both the capital and operating cost of the desalination plant.

Either cross-flow or dead-end flow can be used; however, dead-end is preferred (Rosberg, 1997). The membranes consist of large numbers of capillaries that are permanently hydrophilic (Figure 7). This reduces fouling potential (Singh, 2006). The membrane capillaries are made from a blend of polyethersulfone and polyvinylpyrrolidone (Hwang & Kammermeyer, 1984).

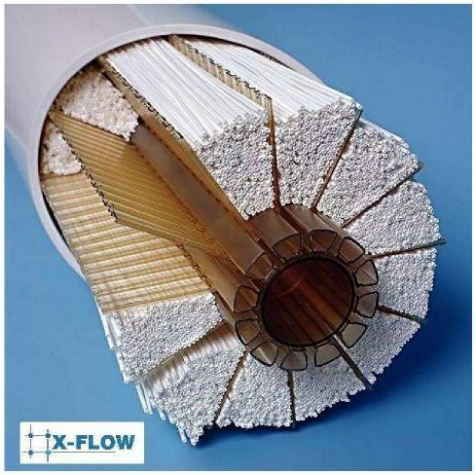

Figure 7: UF membrane capillaries

The UF process operates at around 1.6 bar with 15% of the filtered water produced, used for backwash purposes (Wood & Gifford, 2004).

Nanofiltration

Reverse osmosis and NF are very similar processes. Both are pressure driven and rely on a combination of size exclusion and diffusion permeation (Flynn, 2009).

Nanofiltration is not as effective in desalination as RO modules. RO modules typically reject 96% of salts whereas NF only rejects 75% (Flynn, 2009). Therefore, NF is not effective as a final desalination step and is thus used as a pretreatment process (Flynn, 2009). Table 8 compares the rejection of RO and NF.

Table 8: RO and NF membrane rejection

Species	**RO membranes**	**NF membranes**
Divalent ions (Ca^{2+}, Mg^{2+})	98 - 99%	90 - 98%
Monovalent ions (Na^{+}, Cl^{-})	96 - 99%	50 - 95%
Gases (O_2, Cl_2, CO_2)	0%	0%

Table 8 shows that NF is not as effective in removing monovalent ions from solutions and that neither RO nor NF removes any gases.

NF usually makes use of cross-flow filtration, producing a reject/brine stream as well as a product stream (Kucera, 2010).

This process is primarily used as a replacement for sodium softening to produce drinking water (Flynn, 2009).

The pretreatment section should produce water that is of an acceptable quality for the downstream RO process.

2.5 Reverse Osmosis

Reverse osmosis is a separation technology that utilises membranes to remove dissolved solids from solution (Flynn, 2009). The membranes act as a perm-selective barrier that allows some species (water) to pass through (Nermatollahi, et al., 2013). Species such as ions, that do not permeate the membrane, are then concentrated and removed from the water (Flynn, 2009).

The process of reverse osmosis is widely used in the production of ultrapure water, potable water or to recover dissolved solids from water (dewatering) (Kucera, 2010).

2.5.1 Reverse osmosis fundamentals

Osmosis and semipermeable membranes were first recorded by Abbe Nollet in 1748 (Munir, 1998). Osmosis is the spontaneous process where water moves from a low concentration solution to a high concentration solution. This is done through a semipermeable membrane in an effort to dilute the high concentration solution (Kucera, 2010).

The water will continue to move through the membrane until equilibrium is achieved. Equilibrium will be achieved when the concentrations on either side of the membrane are the same (Flynn, 2009). Figure 8 shows the process of osmosis.

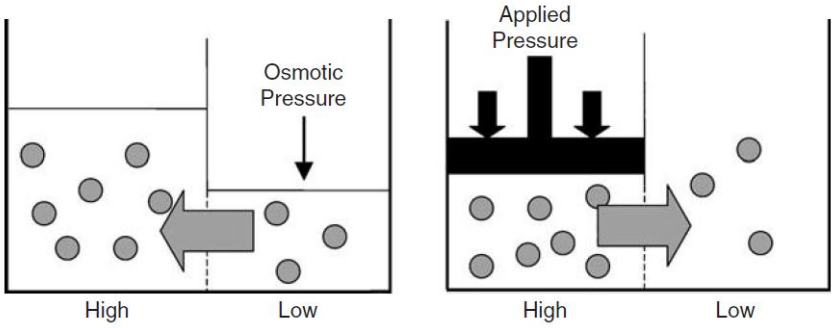

Figure 8: Osmosis, reverse osmosis and osmotic pressure (Flynn, 2009)

2.5.1.1 Osmotic pressure

Osmotic pressure is the difference in height between the two compartments either side of the membrane, as shown in Figure 8. The process of reverse osmosis requires osmotic pressure to be overcome in order to move the water from a high concentration to a low concentration (Kucera, 2010).

Osmotic pressure is related to the concentration and temperature of the solution. This relationship is given by Equation 4 (Greenlee, *et al.*, 2009), (Blanco-Marigorta, et al., 2014), (Aljundi, 2009).

$$\pi = CR_gT \qquad \textbf{Equation 4}$$

Where π = Osmotic pressure

C = ion concentration (molar)

R_g = Ideal gas constant

T = Temperature

Osmotic pressure for fresh and brackish water ranges between 100 kPa and 300 kPa (Sagle & Freeman, 2004). For seawater, osmotic pressure varies between 2300 kPa and 2600 kPa (Perry & Green, 1997).

The osmotic pressure in the concentrate is related to recovery according to Equation 5 (Perry & Green, 1997).

$$\pi_{concentrate} = \frac{1}{1-R} \qquad \textbf{Equation 5}$$

Where R is the recovery and is defined by Equation 13 (Greenlee, *et al.*, 2009).

2.5.1.2 Recovery

Recovery is an excellent measure of membrane performance and is given by Equation 6.

$$R = \frac{Q_P}{Q_F} \qquad \textbf{Equation 6}$$

Where Q_P is the volumetric flow rate of the product stream and Q_F is the volumetric flow rate of the feed stream.

Recovery in reverse osmosis systems can vary between 35% and 85% (Greenlee, *et al.*, 2009).

2.5.1.3 Solution-diffusion model

Modern RO technology dates back to 1948, when Dr Gerald Hassler at the UCLA investigated osmotic properties of cellophane (Kucera, 2010).

Hassler assumed that osmosis takes place via evaporation at one membrane surface, followed by transfer through an air film to the surface of the other membrane. At the other membrane surface, condensation was proposed to take place (Glater, 1998).

Today, the solution-diffusion model is widely used to describe ideal membrane transport (Kucera, 2010). This model was first proposed by Lonsdale *et al.* (1965) and suggested that the molecule of interest dissolves in the membrane and diffuses through the membrane.

The solution-diffusion model assumes that the membranes are without imperfections (Wijmans & Baker, 1995). In this model, the transport of solvent and solute are independent of each other. The flux of solvent through the membrane is given by Equation 7 (Lonsdale, *et al.*, 1965).

$$J_w = L(\Delta P - \Delta\pi) \qquad \textbf{Equation 7}$$

Where J_W = Flux solvent

L = Water permeability coefficient

ΔP = Transmembrane pressure difference

Δπ = Osmotic pressure difference between influent and permeate

Here it is shown that the solvent flux is linearly proportional to the pressure difference across the membrane surface (Kucera, 2010).

The solute flux, as given by the solution-diffusion model, is proportional to the solute concentration difference across the membrane. See Equation 1 (Lonsdale, *et al.*, 1965).

$$J_s = B(C_{A2} - C_{A3}) \qquad \textbf{Equation 8}$$

Where J_s = solute flux

B = Salt permeability coefficient

C_{A2} = molar solute concentration at the boundary layer of the feed stream

C_{A3} = molar solute concentration in the permeate

Equations 7 and 8 are most common in the description of transport of water and solute through a membrane. This is due to the simplicity and close correlation to empirical data of these equations (Kucera, 2010).

The permeability coefficient in Equation 8 can be calculated using Equation 10 (Wijmans & Baker, 1995). It is unique to a given membrane and is not constant (Wijmans & Baker, 1995). Newer polyamide membranes' permeability coefficient may also vary with pH (Kucera, 2010).

$$L = \frac{DS_oV}{R_gTl} \quad \textbf{Equation 9}$$

Where D = the diffusivity of the water

S_o = Water solubility

V = Partial molar volume of the water

R_g = Ideal gas constant

T = Operating temperature

l = Membrane thickness

The salt permeability coefficient can be calculated using Equation 10 (Greenlee, *et al.*, 2009).

$$B = \frac{D_sK_s}{l} \quad \textbf{Equation 10}$$

Where D_s = Salt diffusivity

K_s = Salt partition coefficient between the solution and membrane phase

l = Membrane thickness

2.5.1.4 Rejection

Salt rejection of a membrane is a measure of overall system performance. Salt rejection through a cross-flow RO process is given by Equation 11 (Bartels, *et al.*, 2005), (Sorin, et al., 2006)

.

$$R_s = \left(1 - \frac{C_{permeate}}{C_{feed}}\right) \times 100\% \qquad \textbf{Equation 11}$$

Where R_s = Salt rejection

C = Ion concentration of a salt in either the permeate or feed streams

Most industrial membranes are not normal cross-flow (Kucera, 2010). The membranes are spiral wound (Flynn, 2009). In spiral wound membranes, the feed is increasingly concentrated from the beginning to the end of the tube (Bartels, *et al.*, 2005). For spiral wound membranes, the salt rejection is given by Equation 12 (Greenlee, *et al.*, 2009).

$$R_s = \left(1 - \frac{C_{permeate}}{\frac{C_{feed}+C_{concentrate}}{2}}\right) \times 100\% \qquad \textbf{Equation 12}$$

According to Greenlee *et al.* (2009), typical RO rejection of NaCl is 98 - 99.8%. This, however, will reduce by 10% per year over the membrane lifetime (Greenlee, *et al.*, 2009).

2.5.1.5 Concentration Factor

The concentration factor (CF) of the concentrate stream can be calculated by the ratio of TDS in the concentrate to the TDS in the feed ($CF = C_C / C_F$) (Kucera, 2010). The CF can also be expressed as a function of recovery and salt rejection (Le Gouellec & Elimelech, 2002) as seen in Equation 13

$$CF = \left(\frac{1}{1-R}\right) \times [1 - R\,(1 - R_s)] \qquad \textbf{Equation 13}$$

Concentration factor is a useful indication of the overall concentrate salinity (Kucera, 2010). The salinity of the concentrate will exponentially increase as the recovery is increased for a constant salt rejection (Greenlee, *et al.*, 2009). Small increases in recovery can greatly affect the concentration of dissolved solids in the brine stream (Greenlee, *et al.*, 2009). This will affect downstream processes such as precipitation. Figure 9 shows the effect of increasing recovery on the CF (Greenlee, *et al.*, 2009).

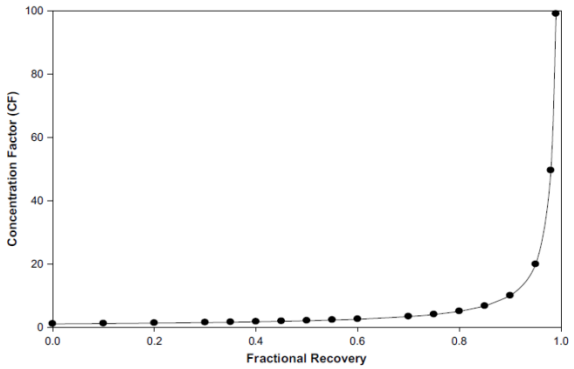

Figure 9: Effect of fractional recovery on the TDS in the concentrate stream (Greenlee, *et al.*, 2009)

2.5.1.6 Concentration polarisation

The water flow pattern past an RO membrane is similar to the flow of water through a pipe (Kucera, 2010). Figure 10 shows typical flow in a pipe with the boundary layers that are formed (Kucera, 2010). Lower flow velocities will lead to thicker boundary layers (Kucera, 2010).

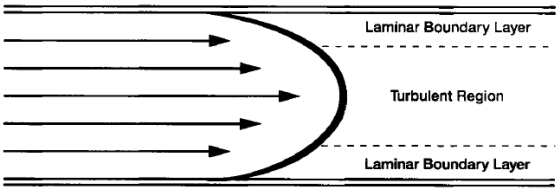

Figure 10: Flow pattern of water in a pipe (Kucera, 2010)

For a membrane system, the flow pattern is similar, except that there is a net flow through the membrane (Kucera, 2010). This flow is perpendicular to the membrane surface. A convective flow to the membranes exists; however, only a diffusional flow is evident away from the membrane (Kucera, 2010). Due to the fact that diffusion is slower than convection, the material rejected by the membrane has a high concentration in the boundary layer (Kucera, 2010). The high concentration boundary layer is known as concentration polarisation. Figure 11 shows the concentration distribution in the boundary layer (Kucera, 2010).

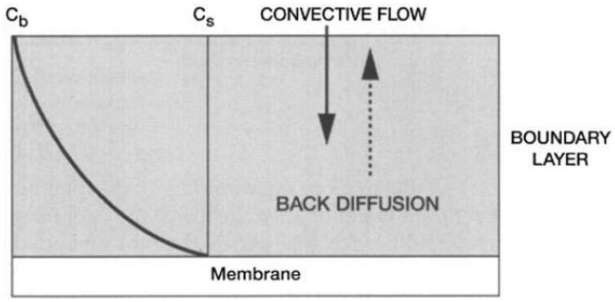

Figure 11: Concentration polarisation, where C_b is the bulk concentration and C_s is the concentration at the membrane surface (Kucera, 2010)

Concentration polarisation has three influences on the membrane (Kucera, 2010):

1. It increases the hydraulic resistance of water flowing through the membrane;
2. The higher concentration in the boundary layer increases the osmotic pressure. This effectively reduces the driving force of the water through the membrane;
3. The salt rejection will decrease due to the higher salt concentration at the membrane surface. The high concentration of a solute at the membrane surface will lead to a high amount of solute passing into the permeate stream.

These 3 factors negatively affect the performance of an RO membrane system. Concentration polarisation can lead to scaling (Kucera, 2010). This will happen when the concentration is high enough that saturation can be reached and precipitation takes place (Kucera, 2010).

Concentration polarisation is quantified by a Beta value. A high Beta value will show a high scaling probability (Kucera, 2010). The Beta value is the ratio of the concentration in the bulk solution to that at the membrane surface (Kucera, 2010).

Beta is not a membrane property, but is selected in the design phase of the system. Beta values also show the dewatering tempo of a system (Kucera, 2010). A high Beta value will imply that water is removed rapidly from the system (Kucera, 2010). This leaves a high amount of dissolved solids on the membrane surface due to the high water flux (Kucera, 2010).

2.5.2 Reverse osmosis membranes

The first RO membranes used for commercial purposes were asymmetric cellulose acetate (CA) membranes (Kucera, 2010). These membranes are still in use for applications with high fouling.

Modern RO membranes for commercial use consist of polyamide (PA) composites. PA membranes are made up of a thin skin (typically 0.2 µm thick) (Kucera, 2010). The skin is interfacially polymerised on top of a polysulfone layer. This polysulfone layer acts as a support for the skin (Singh, 2006).

PA membranes are classified under the thin-film composite membrane family (Flynn, 2009). The layering of the PA membrane composites can be seen in Figure 12 (Flynn, 2009).

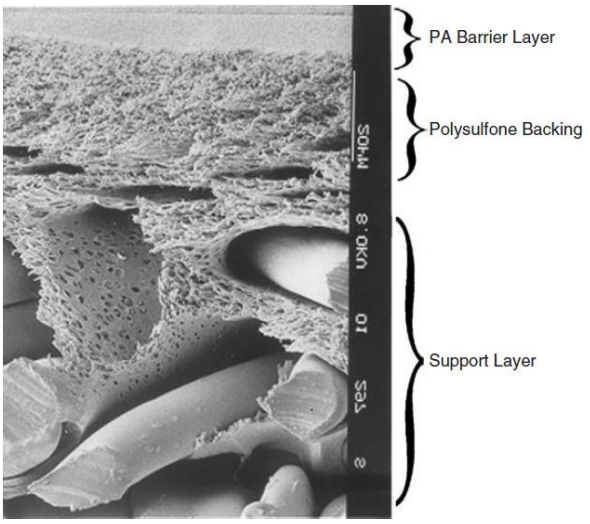

Figure 12: Cross-section of a PA membrane (Flynn, 2009)

The polyamide membranes exhibit superior solute rejection to the CA membranes (Kucera, 2010). Therefore, PA membranes are used for most demineralisation RO systems (Kucera, 2010). Table 9 compares PA and CA membranes (Flynn, 2009).

Table 9: PA and CA membrane comparison

Item	**PA membrane**	**CA membrane**
Surface charge	Negative	Neutral
Surface morphology	Rough	Smooth
Continuous pH range	3 - 10	4 - 6
Cleaning pH	1 - 13	3 - 7
Operating pressure (MPa)	1 - 2.8	1.4 - 4.1
Temperature (^{o}C)	45	35
Chlorine tolerance (mg/ℓ)	< 0.02	< 1.0

In order to contain a large area of membranes in a relatively small volume, RO membranes are modularised (Flynn, 2009). RO membranes can be arranged into four basic modules that include flat sheet, tubular, spiral wound and hollow fibre configurations (Flynn, 2009). As shown in Table 10, spiral wound modules are a compromise between the various characteristics (Flynn, 2009).

Table 10: RO module comparison

Module Type	**Packing density**	**Cleaning Ability**	**Cost per m^2**
Flat Sheet	Low	Easy	Moderate to high
Tubular	Moderate	Moderate	Moderate
Spiral wound	Moderate to high	Moderate	Moderate
Hollow Fibre	High	Complex	Moderate to low

Spiral wound membranes are the most common for industrial use. These membranes consist of sheets of membranes, placed between feed and permeate spacers. Two membranes are placed back-to-back and are separated by the permeate spacer. Three of the sides of the sheet are then glued.

This forces the permeate to flow through one side of the sheet. The open end of the sheet is then placed closest to the permeate tube (Flynn, 2009). Several of these sheets are formed and are then wound around the permeate tube (Flynn, 2009). Each of the sheets is separated by feed spacers. The module configuration is shown by Figure 13 (Flynn, 2009).

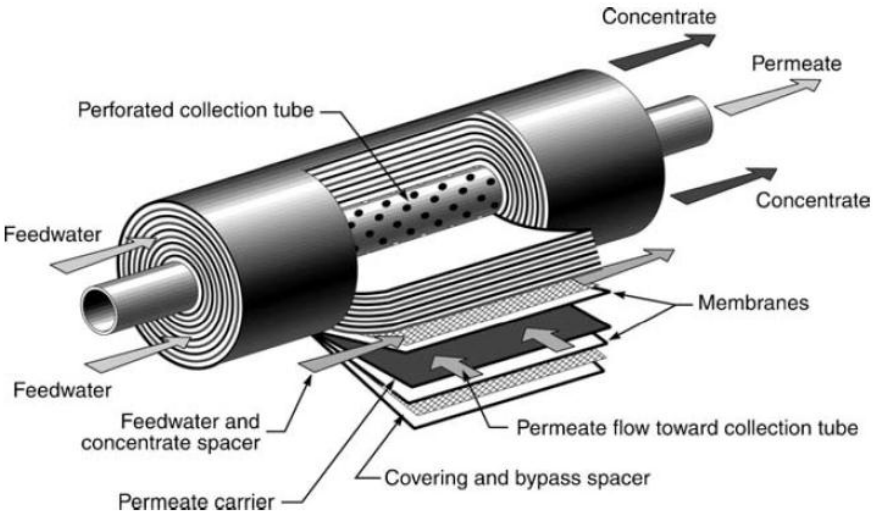

Figure 13: Spiral wound RO module configuration (Flynn, 2009)

Feed water enters at one end and runs along the feed channel created by the feed spacers (Flynn, 2009). The permeate is collected in the gap formed by the permeate spacers and moves to the open end of the sheet (Flynn, 2009). The permeate then flows into the perforated permeate tube. The feed water, that is now concentrated, exits on the opposite end to where the feed water entered (Kucera, 2010).

Spiral wound membranes are available in 63.5 mm, 102 mm, 203 mm and 406 mm diameter sizes (Flynn, 2009). These contain more than 93 m^2 of membrane surface (Flynn, 2009).

These RO modules are arranged in various flow configurations to provide the quality of water required by the end user (Flynn, 2009).

2.5.3 Process flow arrays

Spiral wound modules are typically arranged in a taper skid. This entails an array where the number of modules is halved in each subsequent stage (Flynn, 2009). Therefore a 12:6:3 configuration will consist of 3 stages (Kucera, 2010). The first stage will contain 12 pressure vessels, the second will contain 6 and the last will contain 3 (Flynn, 2009).

The number of pressure vessels is determined by the flow rate of the influent to the system. To maintain an acceptable cross-flow velocity, the feed to each pressure vessel should be between 150 ℓ/min and 230 ℓ/min (Kucera, 2010).

The influent is split equally between the pressure vessels in each skid (Flynn, 2009). Water that permeates the membranes form the product stream and the brine streams are combined to form the influent of the second stage (Flynn, 2009). The second stage product is combined with the product from the first stage while the brine stream from the second stage is dispensed for treatment. The process flow of a typical 2:1 RO configuration is shown by Figure 14 (Flynn, 2009).

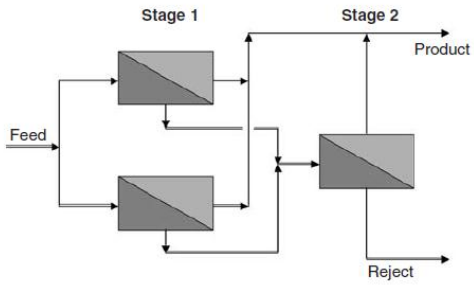

Figure 14: Schematic of a 2:1 RO process flow configuration (Kucera, 2010)

The permeate from the first RO stage can also be used as the feed for the second RO stage. This is normally done in the production of demineralised water (Flynn, 2009).

In the production of demineralised water, the product stream is pumped to a polishing unit to remove the residual ionic substances (Flynn, 2009).

The brine or reject stream can be neutralised and discarded, or can be treated to recover the dissolved salts (Flynn, 2009).

2.5.4 Brine treatment

The brine stream is usually returned to the main body of water from where it has been taken. This could be saltwater lakes or the sea (Flynn, 2009).

Brackish water RO plants, however, can change the salinity of the water source if the brine is returned to the main water body. The higher salinity will affect the DO content of the receiving water which will adversely affect aquatic life (Al-Zahrani, *et al.*, 2012).

The brine stream from brackish water RO plants is disposed of in many ways; these can include evaporation ponds, deep well injection, irrigation and surface water discharge (Clifford & Letterman, 1999). All of these processes entail the loss of water and entail additional cost to the plant (Clifford & Letterman, 1999).

Evaporation ponds have been widely used as these are inexpensive to build and have little to no operating cost (Cuda, *et al.*, 2006). Care should be taken that the salts do not leach into the ground as this will cause contraventions to environmental regulations (Cuda, *et al.*, 2006).

The ultimate achievement would be a zero liquid discharge (ZLD) solution (Betz Inc, 1991). This will entail the almost complete separation of the water from the salts (Betz Inc, 1991). This can be accomplished with technologies like freeze desalination or evaporation (Betz Inc, 1991).

2.5.5 Polishing

The permeate water from the RO modules is not demineralised water. The typical quality from an RO skid is shown by Table 11 (Arar, *et al.*, 2013) (Wenten, *et al.*, 2013).

Table 11: RO permeate properties

Property	Quantity
Conductivity (µS/cm)	15
SiO_2 (mg/ℓ)	0.15
TDS (mg/ℓ)	30.5
Na^+ (mg/ℓ)	1.6
K^+ (mg/ℓ)	0.2

Comparing Table 11 with Table 3 it is visible that the effluent from the RO section is not demineralised water.

For the production of ultrapure water, RO is used in conjunction with ion exchange processes such as conventional IX or CEDI (Kucera, 2010). These IX processes are used to remove residual ions from the product stream to produce demineralised water (Kucera, 2010).

2.5.5.1 Ion Exchange

Mixed bed filters, as described in Appendix A are commonly used as a polishing unit. The mixed bed unit is usually installed after a second RO stage.

Polishing with mixed bed filters uses large amounts of regenerative acids and alkalis, as described in Appendix A, and is therefore not recommended.

2.5.5.2 Continuous Electrode Deionisation (CEDI)

The CEDI process is the preferred method to polish RO effluent in order to produce demineralised water (Flynn, 2009), (Kahraman, et al., 2004).

This technology combines ion exchange membranes, resins and electrical fields to separate trace ions from water (Flynn, 2009). The process is schematically depicted in Figure 15.

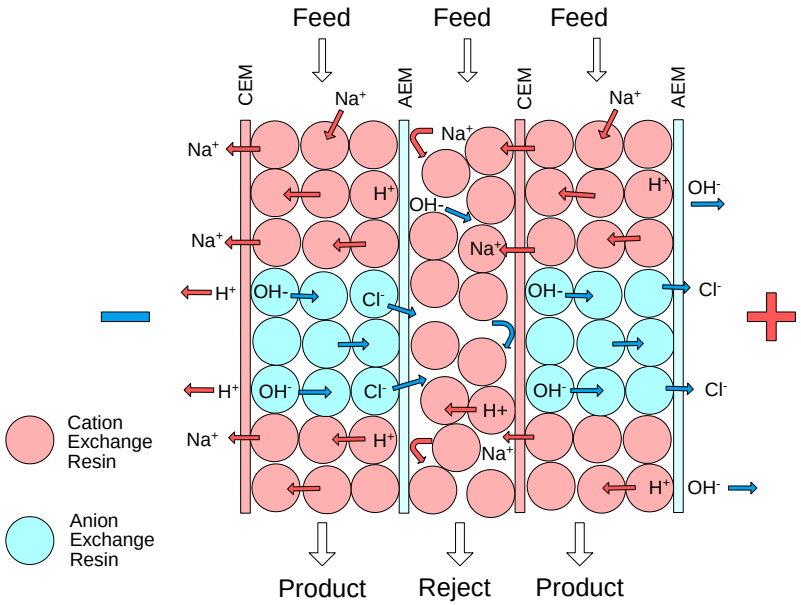

Figure 15: CEDI module schematic (Wood, *et al.*, 2009)

The CEDI system is essentially a hybrid of the ion exchange and electrodialysis processes (Wood, *et al.*, 2009) and has been in commercial use since the 1980s (Flynn, 2009).

A typical CEDI module consists of alternating cation and anion exchange membranes. A direct current electrical field is applied over the ends of the modules (Wood, *et al.*, 2009). The spaces between the membranes are filled with a mixed bed of ion exchange resins (Flynn, 2009).

The permeate from the RO system that flows through the CEDI stage is subjected to the electrical field (Wood, *et al.*, 2009). The dissolved ions present in the water are attracted to the respective counterelectrodes (Wood, *et al.*, 2009). The result of this is that the compartment bounded by the anion exchange membrane that faces the anode, is depleted of ions. This stream is diluted and will form a product stream (Wood, *et al.*, 2009).

The process is repeated on the cathode side of the module (Wood, *et al.*, 2009).

The middle compartment is called the concentrating compartment (Wood, *et al.*, 2009). This compartment traps the ions migrating from the electrodes (Wood, *et al.*, 2009). The water flowing through will collect these ions and it is removed as a reject stream (Wood, *et al.*, 2009).

The resins used between the membranes improve the transport of the ions (Flynn, 2009).

There are two distinct and constant processes inside the CEDI unit. These are enhanced transfer and electroregeneration (Wood, *et al.*, 2009).

The low ion concentrations in the feed flow consequently lower the conductivity of the water (Kahraman, et al., 2004). The ion exchange resin has an extensively higher conductivity and will improve the transfer of ions (Wood, *et al.*, 2009). In the enhanced transfer process, the resins remain in salt form and act as a transport medium for ions (Wood, *et al.*, 2009).

The second process, electroregeneration, constantly regenerates the resins. This is a product of the electrically induced dissociation of water (Wood, *et al.*, 2009). The dissociation takes place at bipolar interfaces such as resin-resin and membrane-resin interfaces within the ion-depleting compartment (Wood, *et al.*, 2009).

The continuous regeneration allows a CEDI system to remove low molecular weight organic compounds and weakly ionised compound from the water (Wood, *et al.*, 2009). These compounds would otherwise be displaced by the higher affinity compounds such as sodium or chlorine (Wood, *et al.*, 2009).

CEDI systems are superior to conventional ion exchange due to the elimination of regenerative chemicals and a water quality that remains constant over longer periods (Flynn, 2009). Conventional IX systems' effluent quality will reduce due to the exhaustion of the resins (Wood, *et al.*, 2009), (Kahraman, et al., 2004).

Typical feed water requirements to a CEDI system are visible in Table 13 (Wood, *et al.*, 2009) (Flynn, 2009).

Table 12: CEDI feed water requirements

Parameter	Maximum Value	Source
Conductivity (µS/cm)	25 - 50	(Flynn, 2009) (Wood, *et al.*, 2009)
Carbon dioxide (ppm)	10 - 20	(Wood, *et al.*, 2009)
Temperature (^{0}C)	35 - 45	(Flynn, 2009) (Wood, *et al.*, 2009)
Pressure (bar)	4 - 7	(Flynn, 2009)
Free Chlorine (ppm)	0.02 - 0.05	(Flynn, 2009)
Fe, Mn, H_2S (ppm)	0.01	(Wood, *et al.*, 2009)
Silica (ppm)	0.5 - 1	(Flynn, 2009)
Hardness (ppm as $CaCO_3$)	0.5 - 1	(Wood, *et al.*, 2009)
TOC (ppm)	0.5	(Flynn, 2009)

CEDI systems are generally operated with a voltage varying between 100 V and 600 V with a current between 3 A and 20 A (Flynn, 2009).

This process produces demineralised water with the composition that adheres to Table 3.

2.6 Conclusion

The water quality in industrial processes is of cardinal importance in preserving equipment and product quality (Betz Inc, 1991).

Traditional methods, such as ion exchange, require large amounts of caustic and acids for operation and regeneration (Meltzer, 1992). This leads to expensive operation cost and is detrimental to the environment (American Water Works Association, 1999).

Membrane technologies and reverse osmosis have revolutionised the field of separation processes and are widely used in the production of potable water and demineralised water (Flynn, 2009).

RO utilises semipermeable membranes that, under high pressure, transport water molecules through the membrane from a high salt concentration to a low salt concentration (Kucera, 2010).

The success or failure of a reverse osmosis desalination plant is determined to a large extent by the optimal combinations of three factors. These factors include the pretreatment, plant layout and cleaning procedures (Rautenbach, *et al.*, 1997).

Effective pretreatment will prolong the periods between CIP cycles and will ensure a longer membrane life. Although pretreatment sections do add to the capital expense of a desalination unit, the operating cost will be dramatically less (Kucera, 2010).

RO plants are typically arranged in a 2:1 configuration. For the production of potable water, the brine from the first RO skid is sent to a second RO skid to ensure higher recoveries (Flynn, 2009).

For demineralised RO production, the permeate from the first RO skid is passed to the second RO skid to ensure an ultra-high purity (Kucera, 2010). The permeate from the second skid is then treated with either a mixed bed or CEDI system to remove the residual unwanted ions (Flynn, 2009).

2.8 References

Al-Shammiri, M., Safar, M. & Al-Dawas, M., 2000. Evaluation of two different antiscalant in real operation at the Doha research plant. *Desalination,* 1(128):1-16.

Al-Zahrani, A., Orifi, J., Al-Suhaibani, B. & Al-Ansary, A. 2012, Thermodynamic analysis of a reverse osmosis desalination unit with energy recovery system. *Procedia Engineering,* 1(33):404-141.

Aljundi, I., 2009. Second-law analysis of a reverse osmoisis plant in Jordan. *Desalination,* 1(239):207-215.

American Water Works Association, 1999. *Water Quality and Treatment.* 5 ed. New York: McGraw-Hill.

Arar, O., Yuksel, U., Kabay, N. & Yuksel, M., 2013. Demineralisation of geothermal water reverse osmosis permeate by electrodeionisation with layerd bed configuration. *Desalination,* 1(317): 48-45.

Bae, H., Kim, H., Jeong, S. & Lee, S., 2011. Changes in the relative abundace of biofilm-forming bacteria by conventional sand-filtration and microfiltration as pretreatments for seawater reverse osmosis desalination. *Desalination,* 1(273):258-266.

Bartels, C., Franks, R., Rykbar, R., Schierach, M. & Wilf, M., 2005. The effect of feed ionic strength on salt passage through reverse osmosis membranes. *Desalination,* 1(184):185-195.

Betz Inc., 1991. *Industrial water conditioning.* 9th ed. Trevose: Betz Laboratories Inc..

Blanco-Marigorta, A., Masi, M. & Manfrida, G., 2014. Exergo-environmental analysis of a reverse osmoisis desalination palnt in Gran Canaria. *Energy,* 1(76):223-232.

Cerci, Y., 2002. Exergy analysis of a reverse osmosis desalination plant in California. *Desalination,* 3(142):257-266.

Munir, C., 1998. *Ultrafiltration and Microfiltration Handbook.* 2 ed. Boca Raton: CRC Press.

Clifford, D. A. & Letterman, R. D., 1999. *Water quality and treatment: A handbook of community water supplies.* New York: McGraw-Hill.

Cuda, P., Pospisil, P. & Tenglerova, J., 2006. Reverse osmosis in water treatment for boilers. *Desalination,* 1(198):41-46.

Dey, A. & Thomas, G., 2003. *Electronics grade water preparation.* 1 ed. Littleton: Tall Oaks Publishing Co.

Doulton USA, 2008. *Activated carbon for drinking water.* [Online]
Available at: http://doultonusa.com/HTML%20pages/activated_carbon_water_filtration.htm
[Accessed 1 October 2013].

DOW Chemical Company, 2004. *Water chemistry and pretreatment: Biological fouling prevention of FilmTec elements and DBNPA.* s.l.:DOW Chemical Co.

DOW Chemical Company, 2007. *FilmTec reverse osmosis technical manual.* s.l.:DOW liquid separations.

DOW Chemical Company, 2013. *DOWEX Marathon Anion Exchange resin,* Product Information: DOW Chemical company.

DOW Chemical Company, 2013. *DOWEX Marathon Cation Exchange resin,* Product information: Strong acid cation exchange resin.

El-Emam, R. & Dincer, I., 2013. Thermodynamic and thermoeconomic analyses of seawater reverse osmosis desalination plant with energy recovery. *Energy.* 1(64):154-163.

Flynn, D. J., 2009. *The Nalco Water Handbook.* 3 ed. New York: McGraw Hill.

Fues, P. & Kucera, J., 2007. *High-efficiency filtration for membrane pretreatment.* s.l., 68th International Water Conference.

Geisler, P., Krumm, W. & Peters, T. A., 2001. Reduction of energy demand for seawater RO with the pressure exchange system PES. *Desalination,* Issue 135:205-210.

Glater, J., 1998. The early history of reverse osmosis membrane development. *Desalination,* 1(117).

Greenlee, L., Lawler, D., Freeman, D., Marriot, B. & Moulin, P., 2009. Reverse osmosis desalination: Water sources, technology and today's challenges. *Water research,* 1(43):2317-2348.

Huang, H., Cho, H., Schwab, K. & Jacangelo, J., 2011. Effects of feedwater pretreatment on the removal of organic microconstituents by a low fouling reverse osmosis membrane. *Desalination,* 1(281):446-454.

Hwang, S. & Kammermeyer, K., 1984. *Membrane Separations.* 1 ed. Malabar: Robert E. Krieger Publishing Co.

Kahraman, N., Cengel, Y., Wood, B. & Cerci, Y., 2004. Exergy analysis of a combined RO, NF and EDR desalination plant. *Desalination.* 1(171):217-232.

Kremser, U., Drescher, G., Otto, S. & Recknagel, V., 2006. First operating experience with the treatment of 3100m3/day of Elbe river water by means of reverse osmosis to produce process water and demineralised water for use in the industry. *Desalination,* 1(189):53-58.

Kucera, J., 2010. *Reverse Osmosis: Design, Processes and Application for Engineers.* Hoboken: Wiley and Sons.

Le Gouellec, Y. & Elimelech, M., 2002. Calcium Sulfate (gypsum) scaling in nanofiltration of agricultural drainage water. *Journal of Membrane Science,* 1(205):279-291.

Liu, C., Rainwater, K. & Song, L., 2011. Energy analyses and efficiency assessment of reverse osmosis desalination process. *Desalination,* 1(276):352-358.

Lonsdale, H., Merten, U. & Riley, R., 1965. Transport properties of cellulose acetate osmotic membranes. *Journal of applied polymer science,* Volume 9.

Macedonio, F. & Drioli, E., 2010. An exergetic analysis of a membrane desalination system. *Desalination,* 1(261):293-299.

Malaeb, L. & Ayoub, G. M., 2011. Reverse osmosis technology for water treatment: State of the art review. *Desalination,* 1(267):1-8.

Ma, W., Zhao, Y. & Wang, L., 2007. The pretreatment with enhanced coagulation and UF membrane for seawater desalination with reverse osmosis. *Desalination,* 1(203):256-259.

Mehdizadeh, H., 2006. Membrane desalination plants from an energy-exergy viewpoint. *Desalination.* 1(191):200-209.

Meltzer, T. H., 1992. *High-Purity Water Preparation.* 1 ed. Littleton: Tall Oaks Publishing Company.

Morelli,C., 1996. *Basic principles of water treatment.* 1 ed. Littleton,CO: Tall Oaks Publishing Co.

Nermatollahi, F., Rahimi, A. & Gheinani, T., 2013. Experimental and theoretical energy and exergy analysis for a solar desalination system. *Desalination.* 1(317):23-31.

Penate, B. & Garcia-Rodriguez, L., 2010. Energy optimisation of existing SWRO (seawater reverse osmosis) plants with ERT (energy recovery turbines): Technical and thermoeconomic assessment. *Energy,* 1(36):613-626.

Perry, R. & Green, D., 1997. *Perry's Chemical Engineers' Handbook.* New York: McGraw Hill.

Pororov, A. & Kornilova, N., 2011. Intensive demineralisation through ion exchange. *Filtration and Separation,* 48(2):36-40.

Rautenbach, R., Linn, T. & Al-Gobaisi, D. M. K., 1997. Present and future pretreatment concepts - Strategies for reliable and low maintenance reverse osmosis seawater desalination. *Desalination,* 1(110):97-106.

Romero-Ternero, V., Garcia-Rodriguez, L. & Gomez-Camacho, C., 2005. Thermoeconomic analysis of wind powered seawater reverse osmosis desalination in the Canary Islands. *Desalination.* 1(186):291-298.

Rosberg, R., 1997. Ultrafiltration, a viable cost-saving pretreatment for reverse osmosis and nanofiltration- A new approach to reduce cost. *Desalination,* 1(110):107-114.

Sagle, A. & Freeman, B., 2004. *Fundamentals of membranes for water treatment.* The future of desalination in Texas, Texas water development board, Austin.

Sharqawy, M. H., Zubair, S. M. & Lienhard, J. H., 2011. Second Law analysis of reverse osmosis desalination plants: An alternative design using pressure retarded osmosis. *Energy,* 1(36):6617-6626.

Singh, R., 2006. *Hybrid membrane systems for water purification.* 1 ed. Amsterdam: Elsevier.

Sorin, M., Jedrzejak, S. & Bouchard, C., 2006. On maximum power of reverse osmosis separation processes. *Desalination. 1(190):*212-220.

Texas Water Development Board, 2011. *Energy optimisation of brackish groundwater reverse osmosis desalination,* Austin: Texas Water Development Board.

United Nations, 2012. *Water resources.* [Online]
Available at: http://www.unwater.org/statistics_res.html
[Accessed 16 September 2013].

US Geological Survey, 2004. *Estimated use of water in the United States in 2000,* s.l.: USGS Circular 1268.

Vidojkovic, S. *et al.*, 2013. Extensive feedwater quality control and monitoring concept for preventing chemistry-related failures of boiler tubes in a subcritical thermal power plant. *Applied Thermal Engineering,* 1(59):683-694.

Wenten, I., Khoiruddin, G., Arfianto, F. & Zudiharto, 2013. Bench scale electrodeionisation for high pressure boiler feed water. *Desalination,* 1(314):109-114.

Wijmans, J. & Baker, R., 1995. The solution-diffusion model: A review. *Journal of Membrane Science,* 1(107):1-21.

Wood, J. & Gifford, J., 2004. *Process and systems design for reliable operations of RO/CEDI systems.* Pittsburgh, Proceedings of the 65th annual inernational water conference.

Wood, J., Gifford, J., Arba, J. & Shaw, M., 2009. Production of ultrapure water by continuous electrodeionisation. *Desalination,* 1(250):973-976.

Chapter 3

Literature Study: Energy Analyses

This chapter provides a summary of the energy involved in the desalination process and provides background on the relevant calculations. A thermodynamic overview of a desalination plant is given. The newest energy recovery systems and their applications are discussed.

3.1 Introduction

Although reverse osmosis desalination uses fewer chemicals than traditional water treatment plants, it is not as efficient and therefore has relatively high specific energy consumption (3 - 4 kWh/m^3 for seawater applications) (Al-Zahrani, *et al.*, 2012), (Kahraman, et al., 2004).

A thermodynamic analysis where the Second Law efficiency is determined has become a common tool in an energy analysis (Cerci, 2002). The Second Law analysis involves the comparison of exergy input and exergy destruction along the desalination process (Cerci, 2002), (Aljundi, 2009). This provides valuable information in the energy analysis.

The use of exergy analyses is of growing importance in order to identify locations where energy is lost (Macedonio & Drioli, 2010). Once these sources of energy loss are determined, the effects can be managed and the process can be improved (Cerci, 2002), (Sorin, et al., 2006).

The processes that were introduced in Chapter 2 are discussed from a thermodynamic perspective in this chapter. The energy required to produce demineralised water and the efficiency of membrane processes are analysed. The necessary calculations that are relevant to the investigation are presented from literature with emphasis on energy consumption, exergy calculations efficiency. Energy recovery devices are introduced and the impact of these devices on the energy consumption of the plant is discussed.

3.2 Energy Consumption

The energy required to desalinate water can be as high as 8 kWh/m^3 (Malaeb & Ayoub, 2011). This can contribute up to 50% of the final product cost (Geisler, *et al.*, 2001) and 75% of the operating cost (Al-Zahrani, *et al.*, 2012). The energy consumption is, however, a direct function of feed salinity (Rautenbach, *et al.*, 1997).

3.2.1 Energy requirements

The net energy required to pump water through a cross-flow RO module is given by Equation 14 (Liu, *et al.*, 2011).

$$E = V_0 \Delta P \qquad \textbf{Equation 14}$$

Where E = Energy required

V_0 = Volume of water

ΔP = Driving Pressure

If the assumption is made that no energy is lost due to friction in the membrane channel, the energy leaving in the brine stream is given by Equation 15 (Liu, *et al.*, 2011).

$$E_B = (1 - R)V_0\Delta P \quad \textbf{Equation 15}$$

Where E_B = Energy in the brine stream

R = Recovery

Equation 16 shows the relationship between the energy in the permeate stream (E_P), recovery, pressure and flow (Liu, *et al.*, 2011).

$$E_P = RV_0\Delta P \quad \textbf{Equation 16}$$

The specific energy (E_s) required for the production of purified water through an RO membrane can be calculated using three equations (Liu, *et al.*, 2011). These equations are used in different scenarios.

$$E_{s1} = (f_{os}C_0\frac{1}{R}\ln\frac{1}{1-R})/3.6 \times 10^6 \quad \textbf{Equation 17}$$

Where E_s is in kWh/m^3 and f_{os} is the osmotic pressure coefficient.

Equation 17 is used in the case where the RO process is reversible. It is therefore not applicable to continuous processes (Liu, *et al.*, 2011).

$$E_{s2} = (f_{os}C_0\frac{1}{R}\ln\frac{1}{1-R}) \times 3.6 \times 10^{-6} + 2.78 \times 10^{-7}\Delta P_{net} \quad \textbf{Equation 18}$$

Equation 18 is used in reversible processes with concentration polarisation.

$$E_{s3} = 2.05 \times 10^{-5}C_0\frac{2-R}{2(1-R)} + 2.78 \times 10^{-7}\Delta P_{net} \quad \textbf{Equation 19}$$

Equation 19 is used to calculate the specific energy consumption for cross-flow reverse osmosis. This will be used in low recovery RO or low salinity applications where the osmotic pressure is low, even at the membrane channel exit. (Liu, *et al.*, 2011)

Thermodynamic restrictions apply for the RO process when the osmotic pressure is equal to the pressure at the exit of the membrane vessel (Liu, *et al.*, 2011). This generally occurs at higher recoveries when the osmotic pressure at the exit of the membrane vessel is high (Liu, *et al.*, 2011).

For cross-flow under thermodynamic restriction, it is assumed that the driving pressure is equal to osmotic pressure at the exit of the membrane channel. The osmotic pressure (and therefore the driving pressure) will be higher at the exit of the membrane channel due to the high concentration of the remaining feed water. (Liu, *et al.*, 2011)

$$E_{s4} = 3.6 \times 10^{-6} \Delta P = 3.6 \times 10^{-6} \Delta \pi \qquad \textbf{Equation 20}$$

Valid if: $\Delta P > \Delta \pi / (1 - R)$

The calculation of the specific energy does not consider the energy in the brine stream.

For cross-flow RO systems, the osmotic pressure changes along the length of the module. This is due to the permeation of the water through the membrane. As the brine stream becomes more concentrated, the osmotic pressure will rise. The driving pressure, therefore, has to be larger than the peak value of the osmotic pressure at all times. (Liu, *et al.*, 2011)

Higher recoveries will produce brine streams with high concentrations. This will imply that for higher recoveries, higher drive pressure is required. This is visualised in Figure 16 (Liu, *et al.*, 2011).

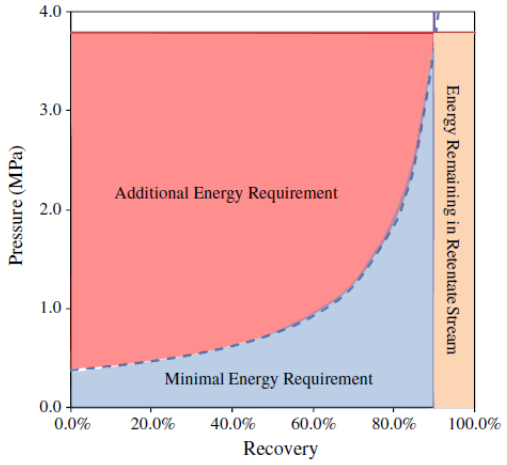

Figure 16: Energy requirements for a recovery of 90% (Liu, *et al.*, 2011)

From Figure 16 it is visible that the energy is required is divided into three categories (Liu, *et al.*, 2011).

The first (blue) is the minimal energy recovery (Liu, *et al.*, 2011). This is determined by the osmotic pressure of the concentrate stream. From Figure 16 it can be seen that the minimum energy required, rises exponentially as the recovery rises. This is attributed to the cross-flow configuration (Liu, *et al.*, 2011).

The second region (red) is the additional energy requirements. This is determined by the recovery and the drive pressure. As the recovery rises, a higher drive pressure is required and the additional energy requirement will rise (Liu, *et al.*, 2011).

The third category (orange) is the energy remaining in the brine or retentate stream. The brine stream will leave the module at the same pressure as the entrance of the feed water. The brine stream, therefore, is high in energy (Liu, *et al.*, 2011).

Osmotic pressure increases along the flow channel of the RO membrane. This increase and the heterogeneity of an RO system pose challenges in the calculation of the exact drive pressure. An accurate estimation for practical designs is provided by Liu *et al.* (2011).

$$\Delta P = \overline{\Delta\pi} + \bar{v}R_m = \Delta\pi_0 \frac{2-R}{2(1-R)} + \Delta P_{net} \qquad \textbf{Equation 21}$$

Where $\bar{v}$ = average permeate flux

R_m = Membrane resistance

$\overline{\Delta\pi}$ = Average osmotic pressure

$\Delta\pi_0$ = Osmotic pressure of the feed water

Figure 17 graphically shows the effect of the configuration associated energy and the change of the osmotic pressure over the membrane length (Liu, *et al.*, 2011).

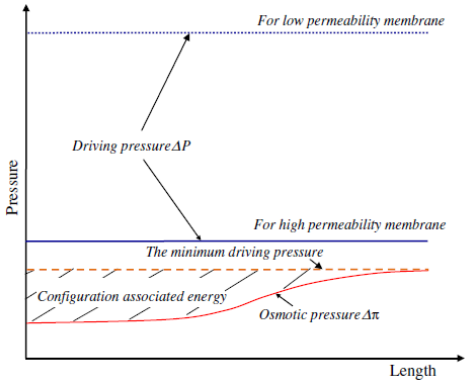

Figure 17: Osmotic pressure change over the length of an RO membrane (Liu, *et al.*, 2011)

According to Liu *et al.* (2011), the driving pressure for high recovery cross-flow RO is determined by thermodynamic restriction and not the need to maintain the required flux (Liu, *et al.*, 2011). This implies that configuration associated energy resulting from the increase of osmotic pressure is a major component in the energy requirements (Liu, *et al.*, 2011).

The thermodynamic restrictions are applicable for cross-flow recoveries higher than 45%. For these recoveries the following equations are used to determine the driving pressure and energy requirements (Liu, *et al.*, 2011).

$$\Delta P = \Delta\pi = cR_gT \qquad \textbf{Equation 22}$$

Where c is the ionic molar concentration

$$SEC = E_s = 3.6 \times 10^{-6} cR_gT \qquad \textbf{Equation 23}$$

During cross-flow RO, the majority of the energy remains either in the retentate stream (low recoveries) or in the configuration associated energy (high recoveries) (Liu, *et al.*, 2011). The energy that remains in the retentate (brine) stream can be recovered using pressure exchange systems or hydraulic turbines (Liu, *et al.*, 2011).

The limit for energy efficiency of most commercial RO systems is therefore the configuration associated energy related to recovery (Liu, *et al.*, 2011).

3.2.2 Energy destruction in a desalination plant

The energy required to desalinate water is provided largely by a high-pressure pump (Cerci, 2002). This pump supplies 80.8% of the energy to the system (Cerci, 2002). The remaining energy is supplied by a low-pressure pump.

According to Cerci (2002), the largest amount of energy loss takes place over the RO membranes. This is validated by authors including El-Emam & Dincer (2013), Nermatollahi

et al. (2013) and Romero-Ternero et al. (2005).This loss in energy amounts to 74% of the total energy input (Cerci, 2002).

The throttling of the brine to atmospheric pressure accounts for 17.1% of the total energy input (Cerci, 2002). This is an unnecessary waste of energy and can be recovered by an energy recovery system (Geisler, *et al.*, 2001).

3.2.3 Exergy Calculations

The maximum amount of work obtainable when a system is brought into equilibrium from its initial state to the environmental state is known as the exergy (Sharqawy, *et al.*, 2011). A system therefore is at zero exergy (dead state) when it reaches the environmental state (Sharqawy, *et al.*, 2011).

Exergy can be divided into three equilibria, namely mechanical, chemical and thermal. The dead state is reached when the initial temperature, pressure and concentration reach the environmental temperature, pressure and concentration (Sharqawy, *et al.*, 2011).

Flow exergy is described by Equation 24 and 25 (Cerci, 2002) (Sharqawy, *et al.*, 2011) (Macedonio & Drioli, 2010)

.

$$\Psi = (\mathrm{h} - h^*) - T_0(s - s^*) + \sum_{i=1}^{n} w_i(\mu_i^* - \mu_i^0) \qquad \textbf{Equation 24}$$

$$\mu_i = \frac{\partial G_i}{\partial w_i} \qquad \textbf{Equation 25}$$

Where h is the specific enthalpy, s is the specific entropy, μ is the chemical potential and w is the mass fraction. Properties with the superscript "*" are determined at the environmental temperature and pressure (T_0 and P_0) but at the same concentration as the initial flow stream. This is known as the restricted dead state. Properties with a "0" in the super or subscript are determined at the environmental temperature, pressure and concentration. This is known as the global dead state (Sharqawy, *et al.*, 2011).

Calculation of the chemical potential, according to Sharqawy (2011), is done using Equations 40 to 45:

$$\mu_w = \frac{\delta G_{sw}}{\delta m_w} = g_{sw} - w_s \frac{\delta g_{sw}}{\delta w_s}$$ **Equation 26**

$$\mu_s = \frac{\delta G_{sw}}{\delta m_s} = g_{sw} = (1 - w_s) \frac{\delta g_{sw}}{\delta w_s}$$ **Equation 27**

$$g_{sw} = h_{sw} - T s_{sw}$$ **Equation 28**

$$\frac{\delta g_{sw}}{\delta w_s} = \frac{\delta h_{sw}}{\delta w_s} - T \frac{\delta s_{sw}}{\delta w_s}$$ **Equation 29**

$$\frac{-\delta h_{sw}}{\delta w_s} = b_1 + 2b_2 w_s + 3b_3 w_s^2 + 4b_4 w_s^3 + b_5 T + b_6 T^2 + b_7 T^3 + 2b_8 w_s T + 3b_9 w_s^2 T + 2b_{10} w_s T^2$$ **Equation 30**

$$\frac{-\delta s_{sw}}{\delta w_s} = c_1 + 2c_2 w_s + 3c_3 w_s^2 + 4c_4 w_s^3 + c_5 T + c_6 T^2 + c_7 T^3 + 2c_8 w_s T + 3c_9 w_s^2 T + 2c_{10} w_s T^2$$ **Equation 31**

Where the subscripts sw is for seawater, s is for salt and w for water.

The values for the constants are given in Appendix H.

The chemical potential and the changes in chemical potential, however, are deemed insignificant by authors such as Cerci (2002) and MacHarg (2011) and are therefore ignored.

Exergy balances are performed similarly to the first law of thermodynamics; however, exergy is not a conserved quantity. The irreversibility of a real system causes some exergy destruction (Sharqawy, *et al.*, 2011). The exergy balance is expressed as (Cerci, 2002):

$$\sum Exergy\ inlet - \sum Exergy\ outlet = Exergy\ Destroyed$$ **Equation 32**

The exergy destruction should always be positive. A negative destruction implies entropy generation, which violates the Second Law of thermodynamics (Sharqawy, *et al.*, 2011).

The exergy destruction is an indicator where energy is lost from the system and therefore can be used to determine where energy is to be recovered (Cerci, 2002).

3.3 Energy recovery systems

According to Geisler *et al.* (2001) nearly all desalination plants tasked with producing drinking water from seawater, are equipped with an energy recovery system (ERS). The most common industrial systems are turbine based with an alternative option being a pressure exchanging system (PES) (Penate & Garcia-Rodriguez, 2010).

Typically, the Second Law efficiency of an RO desalination plant varies between 1.5% (Sharqawy, *et al.*, 2011), to 4.31% (Cerci, 2002) for plants with no ERD. This is calculated by Equation 33 (Sharqawy, *et al.*, 2011), (Kahraman, et al., 2004), (El-Emam & Dincer, 2013).

$$\eta_{II} = \frac{\dot{W}_{min}}{\dot{W}_{act}} \times 100\% \qquad \textbf{Equation 33}$$

Where η_{II} = Second Law efficiency

$\dot{W}_{min}$ = Minimum work of separation

$\dot{W}_{act}$ = Actual work

The minimum work of separation is calculated by the difference between the energy in the inlet and outlet streams (Sharqawy, *et al.*, 2011), (Kahraman, et al., 2004), (El-Emam & Dincer, 2013). This is valid for reversible process where the energy destruction is zero (Sharqawy, *et al.*, 2011).

Specific energy consumption reductions of up to 28% have been noted by Geisler *et al.* (2001) with the installation of ERDs.

Energy recovery devices in RO plants typically utilise the energy remaining in the brine stream to pump a portion of the feed stream. Figures 18 and 19 schematically show an RO process with and without an ERD system incorporation.

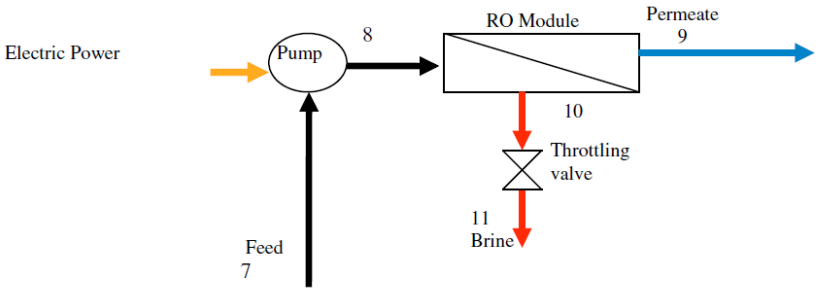

Figure 18: A RO system with no ERD (Penate & Garcia-Rodriguez, 2010)

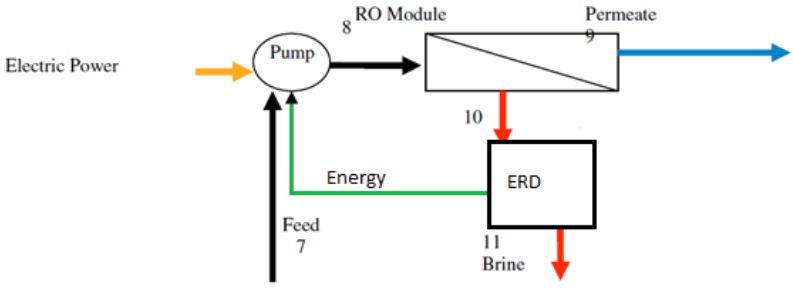

Figure 19: A RO system with an ERD (Penate & Garcia-Rodriguez, 2010)

3.3.1 Turbine based energy recovery systems

Turbines to recover the residual energy in the brine stream of RO plants have been used since the early eighties. Prior to the 1990s, the use of a Francis turbine coupled directly to the high pressure pump shaft was common (Penate & Garcia-Rodriguez, 2010).

The Francis turbine was substituted for a Pelton wheel (Penate & Garcia-Rodriguez, 2010). This technology operates at a better efficiency in high pressure applications. Efficiencies of up to 90% are obtainable in such an ERD (Penate & Garcia-Rodriguez, 2010).

These two systems are often used for large capacity reverse osmosis plants with a permeate flow rate of up to 2000 m^3/day (Geisler, *et al.*, 2001).

To establish the optimal operation point for this system is challenging. The flow rates, pressures, speed and efficiencies of all of the devices are interrelated to such an extent that operation is difficult (Penate & Garcia-Rodriguez, 2010).

The most notable problem is that when the recovery is low, the brine stream flow rate is high. This will result in the turbine rotational speed to rise and the pump to feed more water to the RO system. This will then lower the recovery even further (Penate & Garcia-Rodriguez, 2010).

Hydraulic turbochargers were used for small to medium capacity desalination plants in the 1990s. Turbochargers, in concept, are operated and installed in the same way as the Pelton turbine (Penate & Garcia-Rodriguez, 2010). They are easy to install and operate; however, a low efficiency of 70-80% has seen it replaced with pressure exchange systems (Penate & Garcia-Rodriguez, 2010).

Energy recovery turbine (ERT) systems utilise the pressure in the brine stream to rotate a hydraulic turbine (Penate & Garcia-Rodriguez, 2010). This turbine rotates a shaft, which transports the energy to the high pressure pump. This is schematically shown in Figure 20.

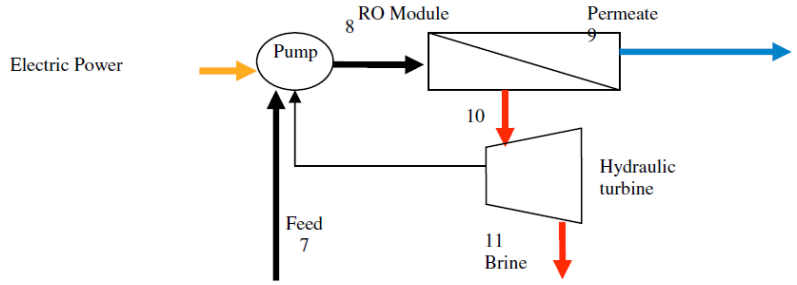

Figure 20: Energy recovery turbine system configuration (Penate & Garcia-Rodriguez, 2010)

A typical specific energy consumption of 3-4 kWh/m^3 is achievable with an energy savings rate of between 35-42% (Penate & Garcia-Rodriguez, 2010). Table 13 compares an ERT system with a PES. The figures are for SWRO systems.

The typical ERT system as used in brackish water desalination is an AT350® from Energy Recovery™. These systems typically cost R236 000 per unit (Exchange rate of R10.27 per $ as on 7 September 2014). (Energy Recovery, 26 August 2014)

3.3.2 Pressure exchange systems (PES)

PES systems, through the process of positive displacement, utilise the pressure in the reject (brine) stream to pressurise a fraction of the feed water (MacHarg, 2011).

The PES vessel consists of several ceramic ducts, encapsulated in a ceramic rotor. The rotor rotates inside a ceramic sleeve. The rotation is driven by the pressure difference between the feed water and brine (MacHarg, 2011).

Pressure transfer takes place longitudinally across each of the ceramic ducts (MacHarg, 2011). As the rotor rotates, half of the ducts are exposed to the high pressure flow and the other half to low pressure flow (Geisler, *et al.*, 2001). During rotation, each duct passes a sealing area that separates the high pressure and low pressure flows (MacHarg, 2011). This forms a liquid piston, which transfers the pressure from the high pressure to the low pressure flows (Cerci, 2002). Figure 21 illustrates the operation of a PES (MacHarg, 2011).

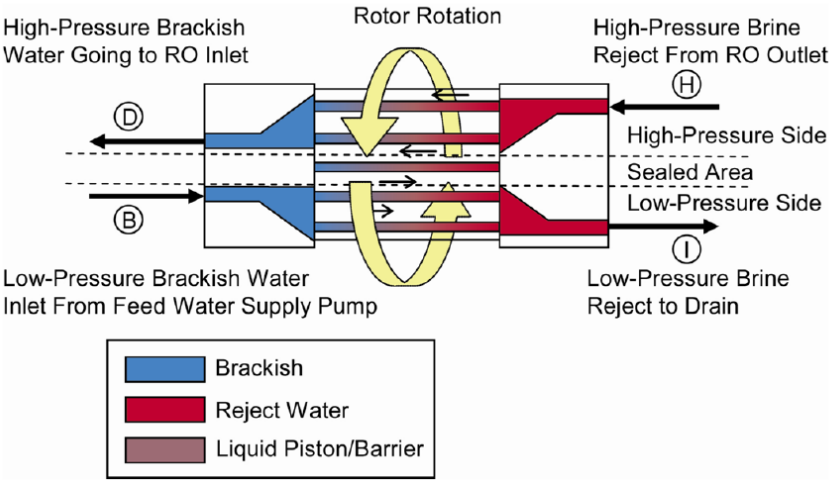

Figure 21: Operation of a pressure exchange system (MacHarg, 2011)

During each cycle, the brine and feed water are separated by a liquid piston. This piston comprises of a mixture of brine and feed water (Geisler, *et al.*, 2001).

Due to the fact that the feed water is directly in contact with this piston, some contamination may take place (Geisler, *et al.*, 2001). The volumetric ratio of brine that transfers into the feed water is known as the volumetric mixing. This is determined by a simple mass balance according to Equation 34 (MacHarg, 2011).

$$Volumetric\ Mixing = \frac{Salinity_{BO} - Salinity_{FI}}{Salinity_{BI} - Salinity_{FO}} \qquad \textbf{Equation 34}$$

Where BO is the Brine Out stream, BI is the Brine In stream, FO is the Feed Out stream and FI is the Feed In stream (MacHarg, 2011).

Volumetric mixing in a PES is 6% when the high and low pressure flow rates are equal (MacHarg, 2011). The volumetric mixing will lead to an increase in both the feed pressure and the TDS of the permeate as the salinity of the feed water increases (MacHarg, 2011).

The increase in salinity is calculated with Equation 35 (MacHarg, 2011).

$$SI = R \times VM \times 1.04$$ **Equation 35**

Where SI = Salinity Increase

R = recovery

VM = Volumetric Mixing

PES systems are typically used for plants with a water production of more than 5000m^3/day (Cerci, 2002). Industrial use of a PES has been proven for plants with a more than 2000 m^3/day capacity (Geisler, *et al.*, 2001).

By introducing a PES the thermodynamic efficiency can be increased from 4.3% to 4.9%. This amounts to energy savings of 19.8 kW on a 7250 m^3/day RO plant (Cerci, 2002). This energy is recovered from the brine stream of the RO process.

The PES system is typically used to transfer the pressure from the brine stream, to a fraction of the feed stream. Figure 22 shows the typical configuration of an RO plant with a PES.

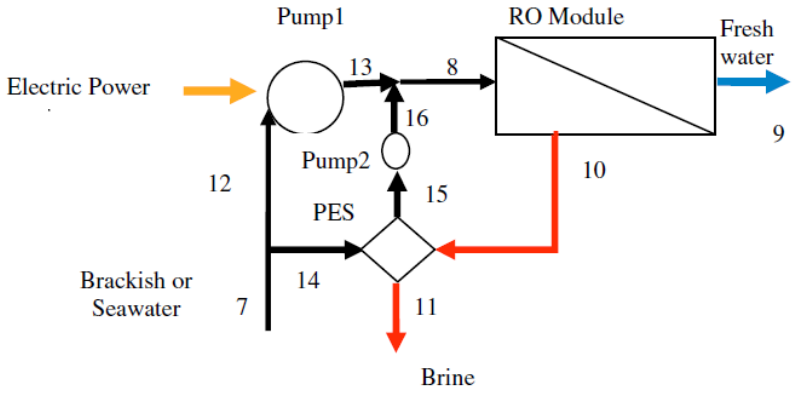

Figure 22: A RO system with a PES (Penate & Garcia-Rodriguez, 2010)

Table 13 compares the ERT and PES energy recovery systems. The ERT has one major advantage over the PES in the fact that the feed salinity is not affected. The PES is 98% efficient in exchanging energy from one stream to another (Malaeb & Ayoub, 2011). The recovery of the RO system will depend on the amount of water pumped by the HP pump.

Table 13: Comparison of ERT and PES for SWRO systems

Criteria	**Turbine**	**PES**
Capacity	Up to 5000 m^3/day	More than 5000 m^3/day
Typical recovery percentage	45-50%	37-45%

High-pressure pump	Used to pump 100% of the feed water	Used to pump 40-50% of the feed water depending on recovery
Booster pumps	No	Yes
Salinity increase before the RO membrane	No	Slight
Flow leakages for lubrication	No	Yes
Efficiency	Up to 90%	Up to 98%
Typical SEC	3-4 kWh/m^3	2-3 kWh/m^3
Energy savings rate	35-42%	55-60%

The typical PES system as used in brackish water desalination is a PX-180®. These systems typically cost R534 000 per unit (exchange rate of R10.27 per US$ as on 7 September 2014). (Energy Recovery, 26 August 2014) The payback period for these systems is in the region of 6 years (MacHarg, 2011).

Table 14 below summarises the results of the SEC from similar investigations done by various authors.

Table 14: Summary of SEC for desalination plants of varying salinities and recoveries

Author	**Year**	**Salinity (ppm)**	**R (%)**	**SEC (kWh/m^3)**	**ERD Type**	**SEC_{ERD} (kWh/m^3)**	**η_{ERD} (%)**	**Energy savings (%)**
Farooque *et al.* ¥	2008	42000	35	7	ERT	5.56	67	25.9
Farooque *et al.* ψ	2008	42000	35	9.13	ERT	7.45	81	22.6
Farooque *et al.*§	2008	42000	35	6.43	ERT	6.11	67	5.2
Farooque *et al.* ¤	2008	42000	35	6.49	ERT	6.39	67	1.5
Farooque *et al.* *	2008	41000	25	10.1	ERT	7.9	85	27.6
Liu *et al.*	2011	34500	75	2.83	N/A	N/A	N/A	N/A
Texas Water	2011	2183	80	0.52	PES	0.42	90	24

Penate & Rodriguez	2011	35000	45	3.27	PES	2.39	90	27
Geisler *et al.*	2002	Seawater	42.5	3.73	PES	2.47	98	32.7

¥ Yanbu plant
ψ Al-Jubail plant
§ Duba plant
¤ Haql plant
* Ummlujj plant

The low energy saving percentage on the Duba and Haql plants are attributed to the use of ageing reverse running pumps as an ERD (Farooque, *et al.*, 2008).

The desalination plant in Texas produces potable water from brackish water of a salinity of 2183 ppm. The SEC for this plant is 0.42 kWh/m^3.

3.4 Conclusion

The specific energy consumption of an RO desalination plant can be as high as 8 kWh/m^3 (Malaeb & Ayoub, 2011), attributing up to 50% of the product cost (Geisler, *et al.*, 2001). Of the total energy fed to the system, 17% is lost through throttling valves on the brine stream (Cerci, 2002). This energy can be recovered by using ERD such as turbines or PES systems.

The use of energy recovery systems can reduce the SEC by 25% depending on the feed salinity and recovery (Cerci, 2002).

3.5 References

Al-Zahrani, A. Orifi, J., Al-Suhaibani, B. & Al-Ansary, A. 2012, Thermodynamic analysis of a reverse osmosis desalination unit with energy recovery system. *Procedia Engineering,* 1(33):404-141.

Aljundi, I., 2009. Second-law analysis of a reverse osmoisis plant in Jordan. *Desalination,* 1(239):207-215.

Blanco-Marigorta, A., Masi, M. & Manfrida, G., 2014. Exergo-environmental analysis of a reverse osmoisis desalination palnt in Gran Canaria. *Energy,* 1(76):223-232.

Cerci, Y., 2002. Exergy analysis of a reverse osmosis desalination plant in California. *Desalination,* 3(142):257-266.

El-Emam, R. & Dincer, I., 2013. Thermodynamic and thermoeconomic analyses of seawater reverse osmosis desalination plant with energy recovery. *Energy.* 1(64):154-163.

Farooque, A. M. *et al.*, 2008. Parametric analyses of energy consumption and losses in SWCC SWRO plants utilizing energy recovery devices. *Desalination,* 1(219):137-159.

Geisler, P., Krumm, W. & Peters, T. A., 2001. Reduction of energy demand for seawater RO with the pressure exchange system PES. *Desalination,* 1(135):205-210.

Kahraman, N., Cengel, Y., Wood, B. & Cerci, Y., 2004. Exergy analysis of a combined RO, NF and EDR desalination plant. *Desalination.* 1(171):217-232.

Liu, C., Rainwater, K. & Song, L., 2011. Energy analyses and efficiency assessment of reverse osmosis desalination process. *Desalination,* 1(276):352-358.

Macedonio, F. & Drioli, E., 2010. An exergetic analysis of a membrane desalination system. *Desalination,* 1(261):293-299.

Malaeb, L. & Ayoub, G. M., 2011. Reverse osmosis technology for water treatment: State of the art review. *Desalination,* 1(267):1-8.

Mehdizadeh, H., 2006. Membrane desalination plants from an energy-exergy viewpoint. *Desalination.* 1(191):200-209.

Nermatollahi, F., Rahimi, A. & Gheinani, T., 2013. Experimental and theoretical energy and exergy analysis for a solar desalination system. *Desalination.* 1(317):23-31.

Penate, B. & Garcia-Rodriguez, L., 2010. Energy optimisation of existing SWRO (seawater reverse osmosis) plants with ERT (energy recovery turbines): Technical and thermoeconomic assessment. *Energy,* Issue 1(36):613-626.

Romero-Ternero, V., Garcia-Rodriguez, L. & Gomez-Camacho, C., 2005. Thermoeconomic analysis of wind powered seawater reverse osmosis desalination in the Canary Islands. *Desalination.* 1(186):291-298.

Sharqawy, M. H., Zubair, S. M. & Lienhard, J. H., 2011. Second Law analysis of reverse osmosis desalination plants: An alternative design using pressure retarded osmosis. *Energy,* 1(36):6617-6626.

Sorin, M., Jedrzejak, S. & Bouchard, C., 2006. On maximum power of reverse osmosis separation processes. *Desalination. 1(190):*212-220.

Texas Water Development Board, 2011. *Energy optimisation of brackish groundwater reverse osmosis desalination,* Austin: Texas Water Development Board.

Chapter 4

Plant configuration and parameters

The layout of the present industrial desalination plant is discussed. Relevant figures and operational parameters are given in order to provide the reader with adequate background to the specific plant.

4.1 Introduction

As discussed in Chapters 2 and 3, the design layout of a desalination plant is of vital importance in the overall plant performance. The investigation is done on an industrial desalination plant consisting of pretreatment, RO and polishing sections. This chapter discusses, in detail, the process used at the specific coal fired power station.

The pretreatment section consists of a coagulation vessel and 4 UF skids. This is followed by the two RO stages. After RO, the water is polished to produce demineralised water by four CEDI skids.

The design of the RO plant allows for a total demineralised water production of 240 m^3/h. This, according to Geisler *et al.* (2001), validates the incorporation of an ERD.

4.2 Pretreatment

The UF pretreatment section of the industrial desalination plant is depicted in Figure 23. For the purpose of this investigation, no cleaning procedures will be included in this section.

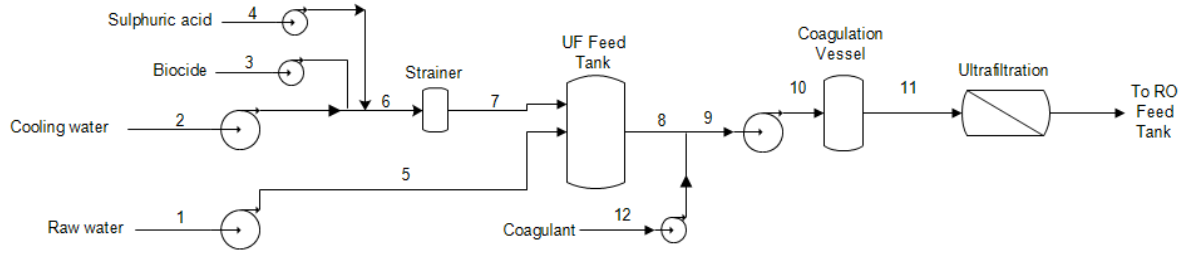

Figure 23: Pretreatment section of the industrial desalination plant

Water is fed from either a cooling water (CW) system (2) or from the raw water system (1). To reduce raw water consumption and operating cost, CW is the preferred source.

Water from the CW system is dosed with a non-oxidising biocide, isothiazolone, (3) and sulphuric acid (4) prior to entering the self-cleaning strainer. The strainer removes larger particles from the water after which it is fed to the UF Feed Tank.

From the UF Feed Tank the water is dosed with a coagulant (12) and pumped to the coagulation vessel. Aluminium chlorohydrate is used as coagulant. The pump impeller supplies the mixing required for complete coagulation. This allows pinflock formation within the 30 second retention time of the vessel. From the coagulation vessel, the water enters the UF process.

The UF system is comprised of 4 skids. Each of these skids consists of 16 modules. This dead-end filtration process has a recovery of 85% (15% of the product is used for backwashing). The microfiber membranes have a 200 kDa molecular cut-off with a nominal pore size of 25 nm and fibre opening of 0.8 mm. A maximum transmembrane pressure (TMP) of 0.5 bar is specified.

Figure 24: UF skids installed on the plant under investigation

Three pumps are used to provide the pressure for the filtration process. The pumps are 380 V, 22 kW variable speed drive (VSD) pumps with a 1.8 bar discharge pressure at 330 m^3/h. Two of these pumps are operational and one is on standby.

After UF, the pretreated water enters the RO Feed Tank. This water has a turbidity lower than 1 NTU. The turbidity analyser can be seen in Figure 74 in Appendix K. If the turbidity is not within the specification, the water is recirculated back to the CW system.

Tables 15 and 16 provide the process conditions and pumps ratings of the pretreatment plant.

Table 15: Pretreatment stream summary

Stream	Purpose	Flow Rate (m^3/h)	T (^oC)	P (kPa)	Component
1	Raw water feed	330	22.4	100	Untreated Water
2	Cooling water feed	-	-	-	Un-purified Water
3	Biocide dosing	0.008	22.4	200	Isothiazolone
4	Sulphuric acid dosing	0	22.4	200	Sulphuric acid
5	Raw water feed	330	22.4	200	Raw water
6	CW feed to strainer	0	22.4	-	Cooling water
7	CW water feed	0	22.4	-	Strained CW
8	CW feed water	-	22.4	-	Cooling water
9	UF feed pump suction	165	22.4	100	Coagulant dosed cooling water
10	Pump outlet	165	22.4	128	Coagulant dosed cooling water
11	UF feed	165	22.4	128	Coagulated cooling water
12	Coagulant dosing	0.0032	22.4	200	Aluminium chlorohydrate

Table 16: Pretreatment pump specifications

Pump	Quantity	Operational	Rating	Energy Consumption
Sulphuric acid dosing	2	1	13.2 ℓ/h @ 200 kPa	0.022 kW
Biocide dosing	2	1	5,3 ℓ/h @ 200 kPa	0.05 kW
Coagulant dosing	2	1	13.2 ℓ/h @ 200 kPa	0.022 kW
CW Booster pump	3	2	330 m^3/h @ 4 bar	75 kW
UF Feed pumps	3	2	330 m^3/h @ 200 kPa	132 kW

4.3 Reverse Osmosis

The RO feed tank serves as the suction point for the three duty and one standby high-pressure RO feed pumps. These pumps are 132 kW VSD pumps with a flow rate of 112 m^3/h at 23 bar. (Figure 75 Appendix K)

Prior to the HP pumps an antiscalant (Genesol BS™) and sulphuric acid are dosed to prevent scaling and correct the pH respectively. The chemical dosing stations can be seen in Figure 71 in Appendix K.

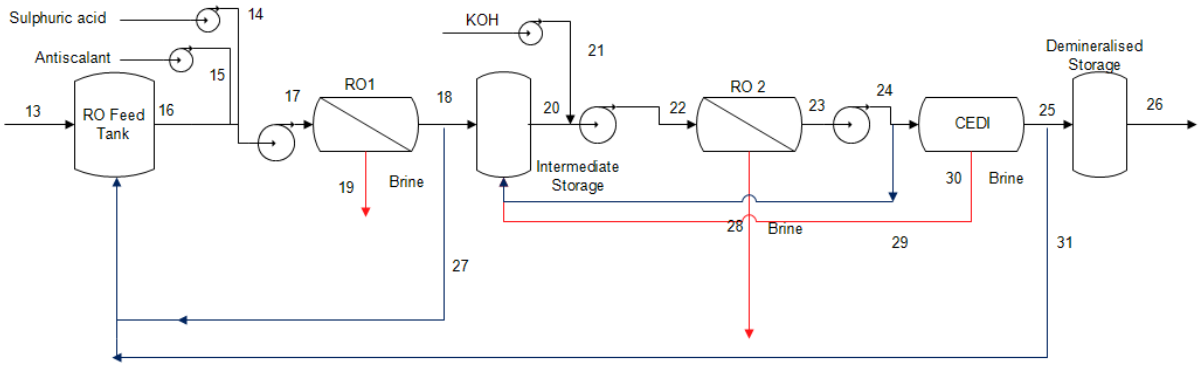

Figure 25: Reverse osmosis section of the industrial desalination plant

The HP pumps feed water to the RO stage. The two RO stages are configured in a three skid configuration. Figure 26 shows a schematic of the 3:2:1 configuration of the first stage.

The first RO stage consists of 3 skids with 18 modules each. Each module houses 6 membranes. The concentrate from the first stage feeds the second stage.

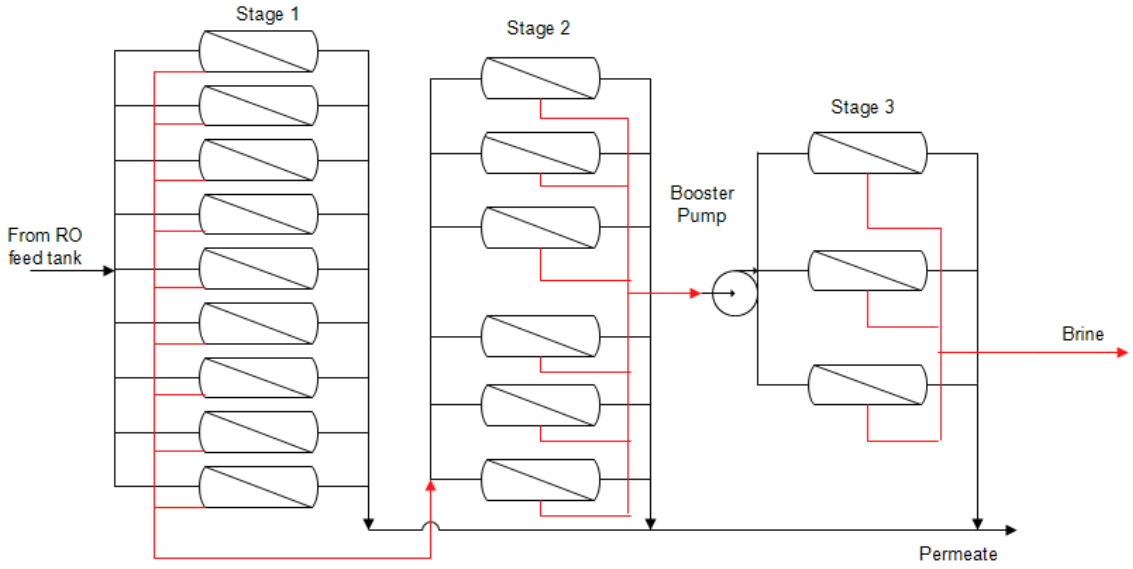

Figure 26: RO stage 1 module arrangement of an industrial desalination plant

The brine that is produced from the first RO stage (19) is passed to a neutralisation sump.

The products formed in all three of the RO skids are combined (18). If this product has a conductivity lower than 60 µS/cm it flows to an intermediate storage tank (Appendix K Figure 79). If the conductivity of this product is higher than 60 µS/cm, the permeate is recycled to the RO feed tank (27). The recovery of the RO stage is between 75% and 86%.

An inter-stage booster pump provides additional pressure to the brine from the second array. The pressure is typically increased to above 1 MPa. The booster pump as well as the pressure indicators can be seen in Appendix K, Figures 76 to 78.

Figure 27: First stage reverse osmosis skids 1, 2 and 3 in the investigated plant

The intermediate storage tank provides suction for the HP pumps (20) supplying RO stage 2. Prior to the pumps, KOH dosing is performed (21) to control the pH to 7.6.

After the pH dosing, the water is pumped to the second RO stage. Four multistage centrifugal pumps are installed with a rating of 380 V and 75 kW. Water is pumped at a pressure of 17.3 bar at 97 m^3/h. (Appendix K Figure 81)

The second RO stage also consists of three skids. Each skid consists of 12 vessels. The second stage RO has a 3:2:1 configuration and recoveries between 80% and 95% are possible.

Figure 28: Second stage RO on the plant under investigation

The permeate from the second RO stage (23) is pumped to the CEDI skids if the conductivity is lower than 3 µS/cm. If the conductivity is higher than 3 µS/cm, the water is returned to the intermediate storage tank (29).

The brine from the second RO stage is returned to the RO feed tank (28) (Flow meter and pressure indicators shown in Appendix K Figure 83 and 84).

Table 17: RO stream summary

Stream	Purpose	Flow Rate (m^3/h)	T (^oC)	P (kPa)	Component
13	Feeds RO tank	165	22.4	59	Filtered, pretreated water
14	pH control	0	22.4	200	Sulphuric acid
15	Antiscalant	0.00162	22.4	100	Genesol BS
16	HP pump suction	110	22.4	1037	Filtered, dosed water
17	RO feed	110	22.4	26	Filtered, dosed water
18	Permeate	95	22.4	1053	RO 1 permeate
19	Reject purge	15	22.4	245	Brine reject stream
20	HP pump suction	100	22.4	400	RO 1 permeate
21	pH control	0	22.4	1346	KOH
22	RO 2 inlet	100	22.4	284	RO 1 permeate
23	Pump suction	86	22.4	112	RO 2 permeate
24	CEDI inlet	86	22.4	697	RO2 permeate
27	Recycle	0	22.4	-	Out of spec RO 1 permeate
28	Reject purge	14	22.4	748	RO 2 Brine

Table 18: RO pump specifications

Pump	Quantity	Operational	Rating	Energy consumption
RO1 HP	4	3	112 m^3/h @ 23 bar	132 kW
Sulphuric acid dosing	2	1	7.2 ℓ/h @ 200 kPa	0.015 kW
Antiscalant dosing	2	1	1.6 ℓ/h @ 200 kPa	0.015 kW
KOH dosing	2	1	18 ℓ/h @ 200 kPa	0.015 kW
RO 2 HP	4	3	97 m^3/h @ 17.3 bar	75 kW
CEDI Booster	3	2	133 m^3/h @ 5 bar	30 kW
RO Booster	3	3	26 m^3/h @ 4 bar	7.5 kW

4.4 Polishing

The CEDI polishing system contains 4 CEDI skids. These skids are fed from the CEDI booster pumps (24) which can be seen in Appendix K Figure 85. If the desired feed

conductivity of 3 µS/cm is not met (Appendix K Figure 82), the water is recycled to the intermediate storage tank (29).

Figure 29: CEDI modules under investigation

The brine generated in the CEDI stage (30), is fed to the intermediate storage tank. The product, if the conductivity is lower than 0.092 µS/cm, is sent to the demineralised storage tank (25) (Flow meter in Appendix K Figure 87). If not, the water is sent to the RO feed tank (31).

Table 19: CEDI stream summary

Stream	Purpose	Flow Rate (m^3/h)	T (^oC)	P (kPa)	Component
25	Product to storage	74	22.4	112	Demineralised water
26	To units	-	22.4	-	Demineralised water
29	Recycle	-	22.4	-	High conductivity water
30	CEDI Brine	13	22.4	89	Brine
31	Reject	-	22.4	-	High conductivity water

There is a visual difference in the turbidity and colour of all the major process streams. This can be seen from Figure 36.

Figure 30: Comparison of major process stream water colour

From left to right in Figure 30 the samples are the feed water from the UF skids, the product water from the first RO stage, the product water from the second RO stage and the product water from the CEDI stage.

Figure 31 shows the feed to the first RO stage, the brine and the product water (left to right). The concentrated brine stream is visibly more concentrated than the feed to the RO stage. The permeate from the first RO stage is clear with a low turbidity.

Figure 31: First stage RO samples and colour comparison

4.5 Conclusion

The unconventional layout of the RO section which entails the brine from the first array to enter as the feed of the second array, as well as the use of two RO stages, is designed to provide ultrapure water at demineralised quality.

The three different processes, namely UF, RO and CEDI are optimised to produce a total of 240 m^3/h of demineralised water at a maximum conductivity of 0.092 µS/cm.

The flow rates, temperatures and pressures in Chapter 4 will serve as the basis on which the thermodynamic analysis is done. These values are the designed, theoretical values as obtained from the design files. All practical analyses shall be done with values obtained from the operational desalination plant. This data can be found in Appendix I and J.

Chapter 5

Thermodynamic analysis of the existing plant configuration

This chapter provides a thermodynamic analysis of the desalination plant without any energy recovery system. A complete exergy balance is conducted to determine the amount of recoverable energy as well as the ideal recovery location. The Second Law analysis and efficiencies are calculated as well as the specific energy consumption. This chapter provides the baseline to determine the feasibility of the proposed modifications.

5.1 Introduction

The thermodynamic analysis of the current desalination plant evaluates the distribution of exergy through the desalination plant. The calculations in this chapter are based on the plant configuration as described in Chapter 4. This evaluation indicates where exergy is lost or destroyed, the SEC is determined and Second Law efficiency of the plant is calculated.

The loss of exergy and the amount of exergy lost form key indicators in the process of evaluating whether an ERD can be installed. The position where the exergy is destroyed or lost indicates the location where an ERD can be installed.

The key performance indicators for the current plant are the SEC which surmounts to 353 Wh/m^3 for RO stage 1 and 13.14 Wh/m^3 for RO stage 2 respectively. 21.64 kW of the exergy is destroyed over the membranes for RO1 and for RO2 27.35 kW is destroyed over the membranes. Throttling in RO1 accounts for 4.15 kW exergy lost and for 2.42 kW exergy lost in RO2.

The loss of exergy through throttling is a waste of energy that could be recovered and therefore the ERDs will replace the throttling valves to recover this exergy.

5.2 Assumptions

The assumptions made during the thermodynamic analysis of the desalination plant are as follows:

- Temperatures stay at a constant 296 K;
- No temperature difference during throttling;
- Atmospheric pressure at sea level is 101.325 kPa;
- P_0 = 98.6 kPa;
- T_0= 295.55 K;
- $Salinity_0$ = 71.34 ppm;
- Chemical potential does not play a significant part in the exergy balance and is therefore ignored;
- The mass of the retentate on the UF filters are negligible and therefore the mass flow through the membranes remain constant;
- No change in pressure or temperature occur in the coagulation vessel;
- No change in the salinity occurs in the pretreatment section;

- The specific enthalpy and entropy for salt is h_{s0} = 12.552 kJ/kg and s_{s0} = 0.047 kJ/kg at P_0 and T_0;
- Specific heat capacity for salt is assumed to be C_p = 0.8368 kJ/kgK;
- All solutions are considered to be ideal solutions.

An uncertainty analysis was completed and is attached in Appendix L. This analysis determined the uncertainty factor of the pressure indicators on the desalination plant as well as the instrument used to determine the salinity of the water.

Two types of pressure indicators are used on the desalination plant. The first is for lower pressure applications (i.e. RO permeate). The second is for high pressure applications. The percentage offset of the pressure indicators is calculated as $\pm$0.12% and $\pm$0.15% respectively. The chlorine content measurement uncertainty analysis showed a percentage offset of $\pm$1.1%.

The values from the relevant monitoring equipment will therefore be taken as a true reflection and uncertainties will be assumed negligible.

5.3 Mass and salt balance

According to Sharqawy *et al.* (2011), the density of saline water is a function of temperature and the salt mass fraction. This relation is given as:

$$\rho_{sw} = \rho_w + mf_s(a_1 + a_2T + a_3T^2 + a_4T^3 + a_5mf_sT^2) \quad \textbf{Equation 36}$$

Where ρ_{sw} and ρ_w are the density of saline water and normal water respectively, mf_s is the salt mass fraction and T is the water temperature. The values for the constants are given in Appendix H.

The atmospheric pressure at the location of the plant was calculated using a relation to altitude (Engineering Toolbox, 2013):

$$P_{atm,h} = \frac{P_{atm,0}(1 - 0.000225577h)^{5.25588}}{1000} \quad \textbf{Equation 37}$$

The altitude of the water treatment plant is 1629 m. Therefore the atmospheric pressure is calculated to be 83.23 kPa.

The mole fraction of salt is calculated using the molecular weight of water together with the salt mass fraction (Cerci, 2002).

$$x_s = \frac{M_w}{M_w\left(\frac{1}{mf_s} - 1\right) + M_w} \quad \textbf{Equation 38}$$

$$x_w = 1 - x_s \quad \textbf{Equation 39}$$

The mass and salt balance was conducted over the three separate sections of the plant.

The pretreatment section has no change in salinity and it is assumed that the mass flow is not affected by the suspended solids removed by the UF membranes.

The mass balance was completed with samples taken from the plant and sent for analyses. The analyses resulted in the quantification of the values for the salinities of the streams.

The mass balance was completed using data taken on 19 February 2014, 24 February 2014, 11 March 2014, 17 March 2014 and 18 March 2014. The readings and samples were taken at various times to accurately estimate an average value for the flow rates of the desalination plant. The mass and salt balance for the plant is given in Table 20.

Table 20: Desalination plant mass and salt balance

Stream	Chlorine Content (ppm)	Mass Flow (kg/s)	Salinity (ppm)	Mass Fraction (salinity)	Mass flow (Salt) (kg/h)
1	39.49	91.67	71.34	7.13×10^{-5}	6.54×10^{-3}
2	39.49	0	71.34	7.13×10^{-5}	0
3	0	2.2×10^{-3}	0	0	0
4	0	0	0	0	0
5	39.49	91.67	71.34	7.13×10^{-5}	6.54×10^{-3}
6	39.49	0	71.34	7.13×10^{-5}	0
7	39.49	0	71.34	7.13×10^{-5}	0
8	39.49	45.85	71.34	7.13×10^{-5}	3.27×10^{-3}
9	39.49	45.85	71.34	7.13×10^{-5}	3.27×10^{-3}
10	39.49	45.85	71.34	7.13×10^{-5}	3.27×10^{-3}
11	39.49	45.85	71.34	7.13×10^{-5}	3.27×10^{-3}
12	0	8.89×10^{-4}	0	0	0
13	39.49	45.85	71.34	7.13×10^{-5}	3.27×10^{-3}
14	0	0	0	0	0
15	0	4.5×10^{-5}	0	0	0
16	39.49	30.72	71.34	7.13×10^{-5}	2.19×10^{-3}
17	39.49	30.72	71.34	7.13×10^{-5}	2.19×10^{-3}
18	0.10447	26.48	0.19	1.9×10^{-7}	5.00×10^{-6}

Stream	Chlorine Content (ppm)	Mass Flow (kg/s)	Salinity (ppm)	Mass Fraction (salinity)	Mass flow (Salt) (kg/h)
19	285.41	4.24	515.62	5.15×10^{-4}	2.19×10^{-3}
20	0.10	27.63	0.19	1.89×10^{-7}	5.21×10^{-6}
21	0	0	0	0	0
22	0.10	27.63	0.19	1.89×10^{-7}	5.21×10^{-6}
23	3.31×10^{-3}	24.12	5.98×10^{-3}	5.98×10^{-9}	1.44×10^{-7}
24	3.31×10^{-3}	24.12	5.98×10^{-3}	5.98×10^{-9}	1.44×10^{-7}
25	6.3×10^{-4}	20.49	1.14×10^{-3}	1.14×10^{-9}	2.33×10^{-8}
26	0	0	0	0	0
27	0	0	0	0	0
28	0.8	3.51	1.44	1.44×10^{-6}	5.07×10^{-6}
29	0	0	0	0	0
30	0.02	3.63	0.03	3.33×10^{-8}	1.21×10^{-7}
31	0	0	0	0	0

The initial salinity of the raw water entering the desalination plant is 71.34 ppm as per the samples analysed by the on-site laboratory. The salinity is calculated as $S = 1.8066\ [Cl^-]$. This relation is given by Cerci (2002).

5.4 Exergy Analysis

5.4.1 Exergy calculations

The exergy analysis was done using Equation 22 and 23.

In order to use Equation 36, the enthalpy, entropy and chemical potential have to be calculated. For an ideal solution, the enthalpy and entropy of the mixture are given by Equations 40 and 41 (Sharqawy, *et al.*, 2011).

$$h = mf_s h_s + mf_w h_w \quad \textbf{Equation 40}$$

$$s = mf_s s_s + mf_w s_w \quad \textbf{Equation 41}$$

For calculation of enthalpy (h), the enthalpy of salt and water is required at the temperature and pressure of the stream.

The enthalpy and entropy of water were calculated using the Engineering Equation Solver (EES) ™ at the specific temperature and pressure of each process stream.

The enthalpy of salt is calculated using the following equation:

$$h_s = h_{s0} + C_{ps}(T - T_0) \quad \textbf{Equation 42}$$

Where h_{s0} = 12.552 kJ/kg and C_{ps} = 0.8368 kJ/kgK.

The calculation of the entropy for salt is given in Equation 43.

$$s_s = s_{s0} + C_{ps}\ln({}^{T}/_{T_0}) \quad \textbf{Equation 43}$$

Where s_{s0} = 0.04473 kJ/kgK

Mixing is an irreversible process and therefore at a constant temperature and pressure, the entropy of the mixture should be higher than the sum of the pure components (Cerci, 2002). The entropy of the water-salt mixture is given by Equation 44 (Cerci, 2002).

$$s = mf_s s_s + mf_w s_w - R(x_s lnx_s + x_w lnx_w) \quad \textbf{Equation 44}$$

The chemical potential, according to Cerci (2002), is negligible and therefore the specific exergy is calculated using Equation 45.

$$\Psi = h - h_0 - T_0(s - s_0) \quad \textbf{Equation 45}$$

In Equation 45, h_0 and s_0 is the enthalpy and entropy of the mixtures at the reference state.

5.4.2 Pretreatment exergy analysis

For the ultrafiltration pretreatment section, an exergy analysis was performed. The exergy was calculated using Equation 45.

The exergy balance and critical parameters of the ultrafiltration pretreatment section are given by Table 21.

Table 21: Critical parameters and exergy balance for ultrafiltration pretreatment

Stream	Temp (^{0}C)	Pressure (kPa)	Mass Flow (kg/h)	Salinity (ppm)	Exergy (kJ/kg)	Exergy Flow (kW)	Change in Exergy (kW)
9	22.4	100	45.85	71.3	0	0	
							4.98
10	22.4	128.68	45.85	71.3	0.108	4.98	
							0
11	22.4	128.68	45.85	71.3	0.108	4.98	
							-2.75
13	22.4	59.2	45.85	71.3	0.049	2.23	

The temperatures, pressures and mass flows were determined from the actual water treatment plant while the salinity is a product of chemical analysis done on sampled water from the plant.

The salinity of the water is constant in the pretreatment section due to the fact that the ultrafiltration removes only suspended solids which do not affect the chlorine content or TDS.

Figure 32 shows the schematic layout of a single UF skid. The exergy flow rate is indicated for each of the process streams.

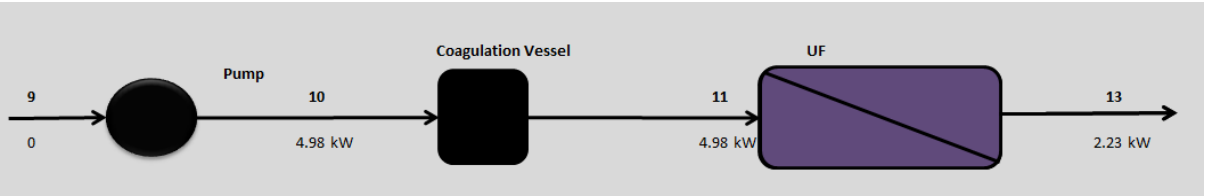

Figure 32: Schematic layout and exergy balance of a single UF skid (Exergy flow in kW)

The incoming exergy flow of 0kW before the UF feed pump is due to the fact that the water enters at its reference state.

As seen from Figure 32, UF is a dead-end filtration. The retentate on the membrane therefore is periodically backwashed. The backwash process lasts for 20 s and is done every 20 min. This process is, however, not thermodynamically analysed.

Due to the fact that both the temperature and pressure are constant over the coagulation vessel, the difference in exergy is zero.

The trans-membrane pressure over the UF membranes accounts for an exergy destruction of 2.75 kW. The exergy flows is depicted in Figure 33.

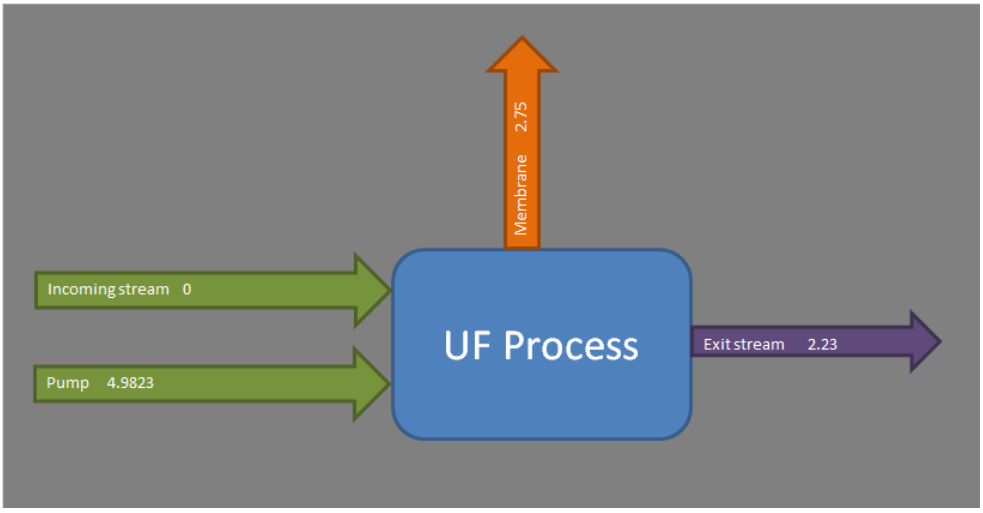

Figure 33: Exergy flow schematic flow diagram

The possibility of successfully installing an ERD in the pretreatment section is very small. This is due to the fact that there are no process streams leaving the section at high pressure that require throttling. The only stream exiting the section is the filtered water (13). This stream has an exergy flow rate of 2.23 kW. This energy is, however, not recoverable with traditional ERDs. This is due to the fact that traditional ERDs rely on the high pressure of the entering stream to provide the energy that is transferred. The pressure in the filtered water stream (13) is 52.9 kPa and it is therefore not feasible to install ERD in the pretreatment section.

The UF section of the plant is responsible for the consumption of 6.1% of the exergy added to the desalination plant.

5.4.3 RO exergy analysis

The specific exergy for the RO stages was calculated using Equation 45. The critical parameters and exergy flow for the first RO stage is given in Table 22.

Table 22: Critical parameters for RO stage 1

Stream	Temp (^{0}C)	Pressure (kPa)	Mass Flow (kg/h)	Salinity (ppm)	Specific Exergy (kJ/kg)	Exergy Flow (kW)	Change in Exergy (kW)
16	22.4	100	30.72	71.34	0	0	
							28.54
17	22.4	1037.84	30.72	71.34	0.93	28.54	
							10.95
18	22.4	25.96	26.48	0.19	1.49	39.49	
							-62.71
19	22.4	1053.9	4.24	515.62	-8.06	-34.17	
							-4.15
31	22.4	83.22602	4.24	515.62	3.85	-38.32	
34	22.4	830	5.47	293	-3.96	-21.65	
							1.56
35	22.4	1149	5.47	293	-3.67	-20.07	
36	22.4	25.96	3.23	0.19	1.55	5.01	

From Table 22 it is visible that the salinities change drastically over the RO membranes. The negative specific exergy and exergy flow rates indicate that work is required to return the fluid to its reference state. This is normal for separation processes (Cerci, 2002).

Figure 34 shows the block flow diagram of the first stage of RO as well as the exergy flow rates.

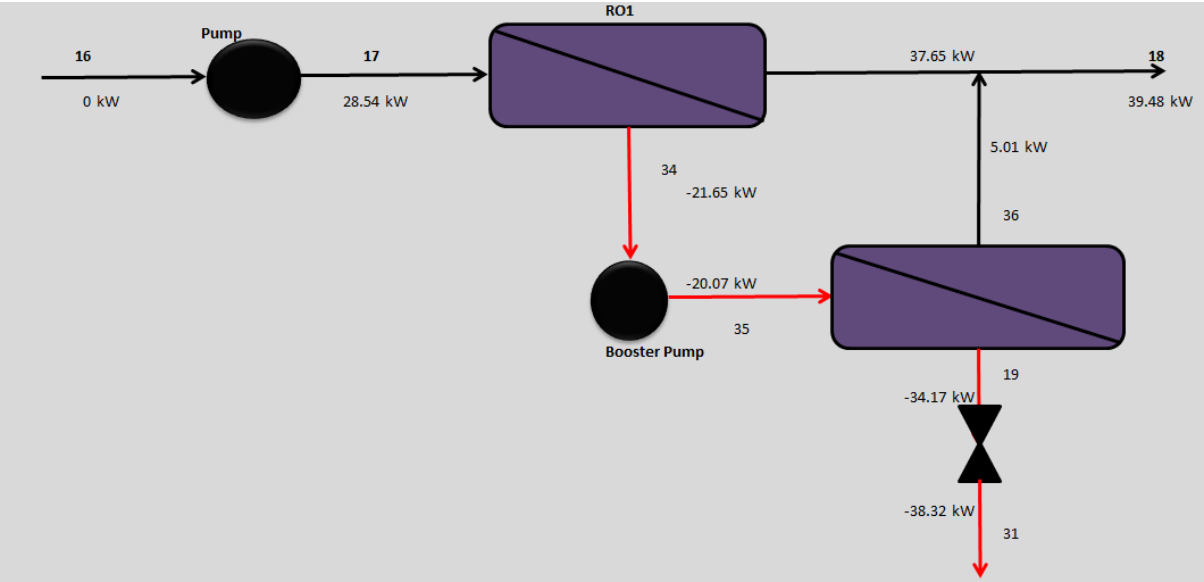

Figure 34: Schematic layout and exergy balance of a single RO stage 1 skid (Exergy flow in kW)

The red streams in Figure 34 (34, 35, 19, and 31) are brine streams and will therefore have negative exergy flow rates relative to the reference state. The first and second arrays for RO1 stage 1 are represented as a single block. The booster pump separates the second and third array.

The main pump feeding the RO membranes is responsible for adding 28.54 kW to the system. This accounts for 94% of the exergy added to RO stage 1, 46.76% of the energy added to the RO section and 35.2% of the total energy added to the desalination plant. This, according to Cerci (2002), is normal for a desalination plant.

The RO1 brine booster pumps adds 1.58 kW of exergy to the system, which in total is 1.9% of the total desalination plant energy requirements.

The RO membranes combined account for a loss of 21.64 kW of exergy. In relation to the total exergy destruction, the RO1 membranes account for 29.71% of the exergy destruction and 71% of the exergy input. A similar study done by Cerci (2002) on a brackish water desalination plant, determined the exergy destruction by the membranes to be 74% of the exergy input (Cerci, 2002).

The throttling valve separating streams 19 and 31 reduces the pressure of the brine to atmospheric pressure. This accounts for an exergy destruction of 4.15 kW and is responsible for 5.7% of the total exergy destruction of the desalination plant. The throttling destroys 13.8% of the exergy input.

Cerci (2002) found that throttling destroyed 17.12% of the exergy input in a desalination plant with a salinity of 1550 ppm and a recovery of 77.5% (Cerci, 2002). This lower recovery has the direct result that the mass flow rate of brine is higher. Therefore a larger amount of exergy is lost.

Figure 35 depicts the exergy input and destruction (in kW) for the RO1 section of the desalination plant.

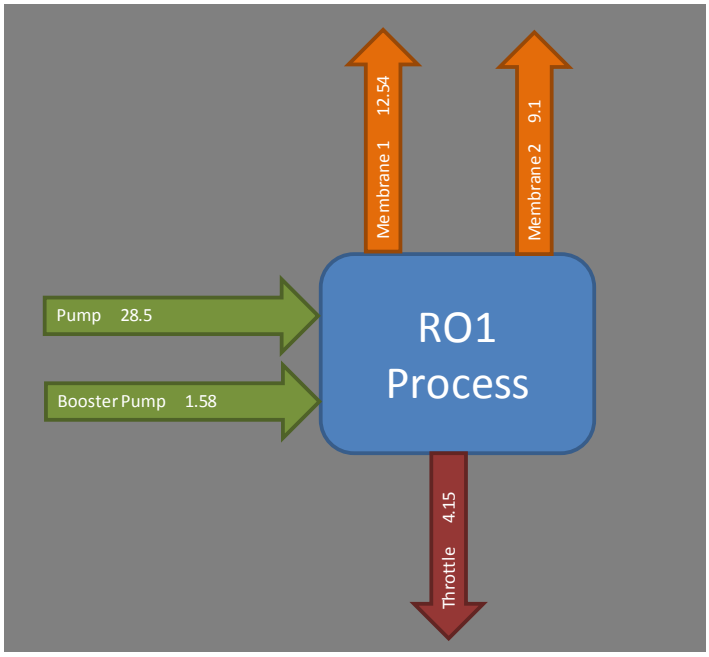

Figure 35: Exergy input and destruction diagram for RO stage 1

The exergy destruction caused by the membranes is an innate property for RO processes and is unavoidable. This exergy destruction is the main contributor to the fact that the Second Law efficiency for reverse osmosis processes is inherently low (Farooque, *et al.*, 2008).

Throttling of the brine stream from RO stage 1 accounts for the loss of 4.15 kW of exergy. This exergy is destroyed in order to return the brine to atmospheric pressure and hence deposit the brine in the UF feed tank. This loss is avoidable if the pressure from the brine stream can be transferred to the RO feed stream. The application of an ERD will be ideal in this situation.

An identical analysis was conducted for RO stage 2. Table 23 shows the critical parameters for the second RO stage.

Table 23: Critical parameters and exergy balance for RO stage 2

Stream	Temp (^{0}C)	Pressure (kPa)	Mass Flow (kg/h)	Salinity (ppm)	Specific Exergy (kJ/kg)	Exergy Flow (kW)	Change in Exergy (kW)
20	22.4	244.54	27.63	0.19	1.97	54.47	
							30.91
22	22.4	1346.36	27.63	0.19	3.09	85.38	
							-35.98
23	22.4	284.92	24.12	0.01	2.05	49.40	
							-76.75
28	22.4	748.48	3.51	1.44	2.46	8.63	
							-2.42
32	22.4	83.22	3.51	1.44	1.77	6.21	

The change in salinity between streams 22, 23 and 28 is comparable to the change in salinity seen in the first RO stage. The block diagram in Figure 36 shows the current plant layout with the exergy flow rates (kW) depicted on the process streams.

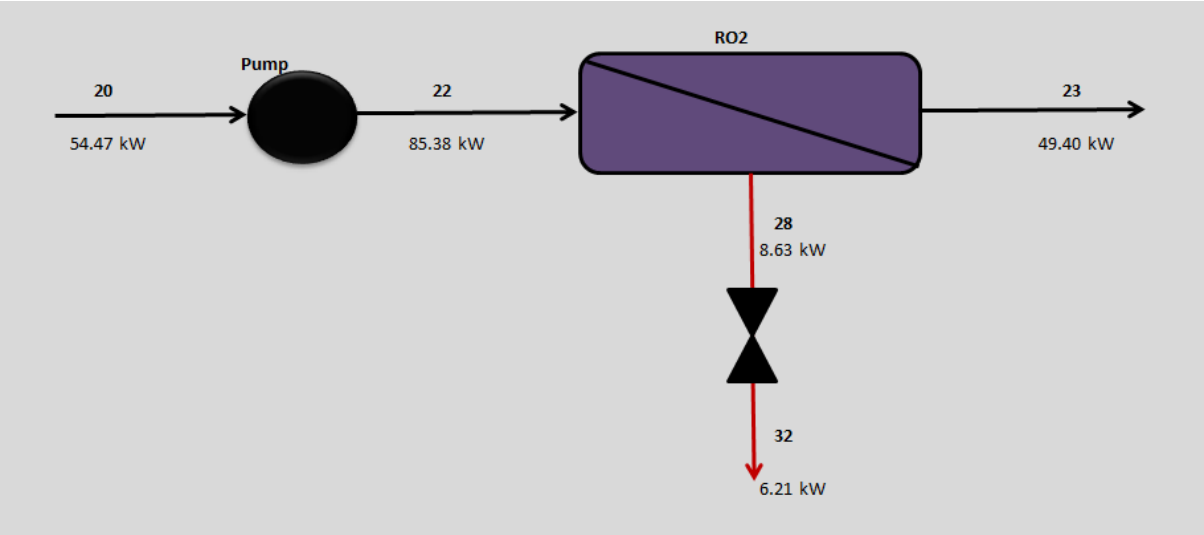

Figure 36: Schematic layout and exergy balance of a single RO stage 2 skids (Exergy flow in kW)

The feed pump for the second RO stage contributes 30.91 kW of exergy to the system. This amounts to 50.6% of the exergy added to the RO stage and 38.1% of the exergy added to the desalination process.

The exergy destruction over the three arrays for RO stage two totals to 27.35 kW. This contributes to 37.55% of the exergy destruction over the desalination plant.

In order to discharge the brine from RO stage two into the filtered water tank, stream 28 is throttled. This throttling process releases the excess pressure carried over from the RO process and therefore contributes to 2.42 kW exergy destruction. In total, the throttling of RO stage 2 surmounts to 3.32% of the exergy destroyed during the desalination process. The exergy flow rates are figuratively depicted in Figure 37.

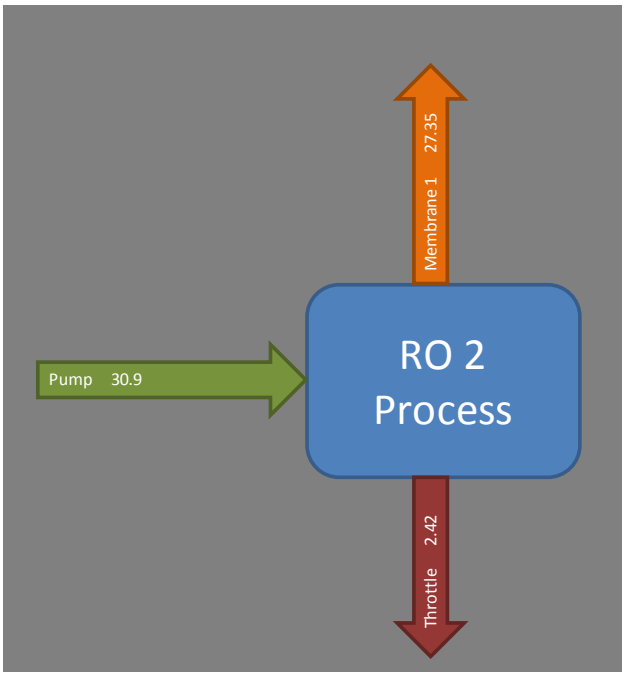

Figure 37: Exergy input and destruction diagram for RO stage 1

The lower flow rate of the brine stream in the second RO stage causes the lower amount of exergy destruction through the throttling valve than for the first RO stage. This lower mass flow is a product of a higher RO recovery. The setpoint for the first stage RO recovery was 86.2% and for the second stage it was 87.3%.

The RO section is responsible for 75.2% of the total exergy consumed by the desalination plant. This equals an exergy consumption of 61 kW when a single RO stage 1 and RO stage 2 skid is in service.

5.4.4 CEDI exergy analysis

The results of the mass and exergy balance are summarised in Table 24.

Table 24: Critical parameters for the CEDI section

Stream	Temp (^{0}C)	Pressure (kPa)	Mass Flow (kg/h)	Salinity (ppm)	Specific Exergy (kJ/kg)	Exergy Flow (kW)	Change in Exergy (kW)
23	22.4	284.92	24.12	0.006	2.048	49.40	
							9.88
24	22.4	697.68	24.12	0.006	2.458	59.28	
							-21.19
25	22.4	112.6	20.49	0.001	1.859	38.09	
							-52.60
30	22.4	89.3	3.63	0.03	1.837	6.67	

Although the feed pressure of a CEDI system is 33% (340 kPa) less than for RO, the exergy destruction over the membrane is similar to that of RO stage 1. The addition of electrical power for the electrochemical reactions, further add to the energy consumption of the CEDI systems. The electrical power added to the system is calculated by Equation 46.

$$P_{module} = \frac{VI}{1000}$$ **Equation 46**

Where P = Power in kW,

V = Voltage in Volt

I = Current (Amp)

The power is calculated for a single module and if multiplied by the number of modules, the electrical power consumed for the skid is calculated. This amounts to 5.31 kW added to the system.

The exergy balance block flow diagram is shown in Figure 38.

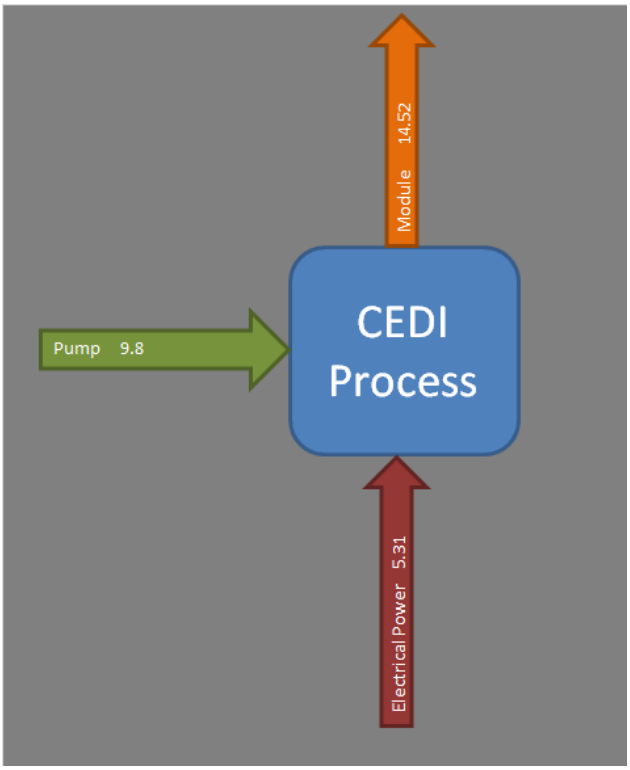

Figure 38: Exergy input and destruction diagram for the CEDI process

From this figure, it is evident that the only exergy destruction takes place over the module. There are no throttling valves in this system and the pressure of the brine and product streams (89.3 kPa and 112.6 kPa respectively) does not merit the installation of an ERD.

The pump is responsible for the addition of 9.8 kW exergy to the system. This equals 64.8% of the exergy required for the CEDI process. The remaining 35.2% is attributed to the electrical power input.

The CEDI system is accountable for 18.7% of the total exergy consumption (81.2 kW) of the desalination plant. This total is a per skid total. If the plant operates at the intended design, this value is tripled to a total of 243.6 kW.

5.5 Second Law efficiency analyses

5.5.1 Second Law efficiency calculations

The Second Law efficiency is calculated by using the minimum work required for separation and the actual work supplied to the plant.

The minimum work required is calculated with Equation 47 (Sharqawy, *et al.*, 2011).

$$\dot{W_{min}} = \sum E_{out} - \sum E_{in} \qquad \textbf{Equation 47}$$

Where W is the work required and E is the exergy flow. The exergy flow is calculated as $E = m\psi$.

The Second Law efficiency is then calculated by Equation 33.

5.5.2 Pretreatment Second Law efficiency

The ultrafiltration pretreatment section has a minimum work of separation calculated as 2.23 kW. The actual work sent to the plant by the UF feed pump is 4.98 kW. Thus the Second Law efficiency is calculated as 44.78% using Equation 33. This will be higher than for the RO stage due to the fact that it has a dead-end configuration (as seen from Section 2.4.2.6).

5.5.3 RO Second Law efficiency

The Second Law efficiency for the first stage RO was calculated using Equation 33. For the first stage, the efficiency was calculated as 3.85%. This very low efficiency is normal for RO processes. If the product and brine streams were reversibly mixed, the power production would have been equal to the minimum power input (Cerci, 2002). This indicates that the analysis performed satisfies the Second Law of thermodynamics (Cerci, 2002).

The second RO stage has a Second Law efficiency of 3.68%. This lower efficiency is due to the higher recovery of the second RO stage.

The addition of ERDs to the RO system will improve the Second Law efficiency of the RO systems.

5.6 Specific energy consumption analyses

5.6.1 Specific energy consumption calculations

The specific energy consumption for UF is calculated as the sum of the energy added by the pump to the system for every cubic meter of water (Ma, *et al.*, 2007).

The SEC for the RO skids is calculated with Equation 23 if thermodynamic restrictions do not apply. Therefore if $\Delta P < \Delta\pi/(1-R)$ the SEC is calculated as (Liu, *et al.*, 2011):

$$SEC = E_{s3} = 2.05 \times 10^{-5} C_0 \frac{2-R}{2(1-R)} + 2.78 \times 10^{-7} \Delta P_{net} \qquad \textbf{Equation 48}$$

If this condition is not met and thermodynamic restrictions do apply, the SEC is calculated as (Liu, *et al.*, 2011):

$$SEC = E_{s4} = \frac{3.6 \times 10^{-6} c_o R_g T}{1 - R}$$ **Equation 49**

For the CEDI process, the SEC is calculated using the equations P=VI to calculate the electrical power required to produce a cubic meter of water. This is added to the energy added by the pump.

5.6.2 RO SEC

Thermodynamic restrictions apply for RO stage 1. This is proved by the fact that

$$\Delta P < \Delta\pi/(1 - R)$$

$$\Delta P < 9198\ kPa$$

Therefore the SEC for the first RO stage is calculated from Equation 49 as:

$$SEC = E_{s4} = \frac{3.6 \times 10^{-6} c_o R_g T}{1 - R} = 353\ Wh/m^3$$

For the second RO stage, thermodynamic restrictions do not apply. The SEC, therefore, is calculated with Equation 48 as 307 Wh/m^3. (See Appendix F)

The SEC increases as the recovery of the membrane process increases. This relationship is shown in Figure 39.

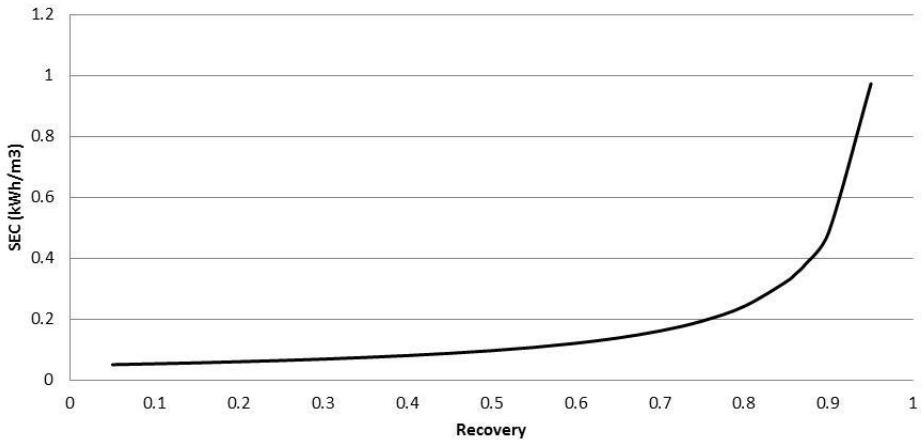

Figure 39: Effect a change in recovery has on the SEC

Figure 39 shows that, as expected, the SEC increases exponentially as the recovery increases. This data was calculated using an initial salinity of 71 ppm. This increase is due to the fact that the high salinity at the end of the membrane channel causes the osmotic pressure to rise. This in turn results in a higher required driving pressure.

Figure 40 shows the energy requirement regimes as defined by Figure 16 in Chapter3.

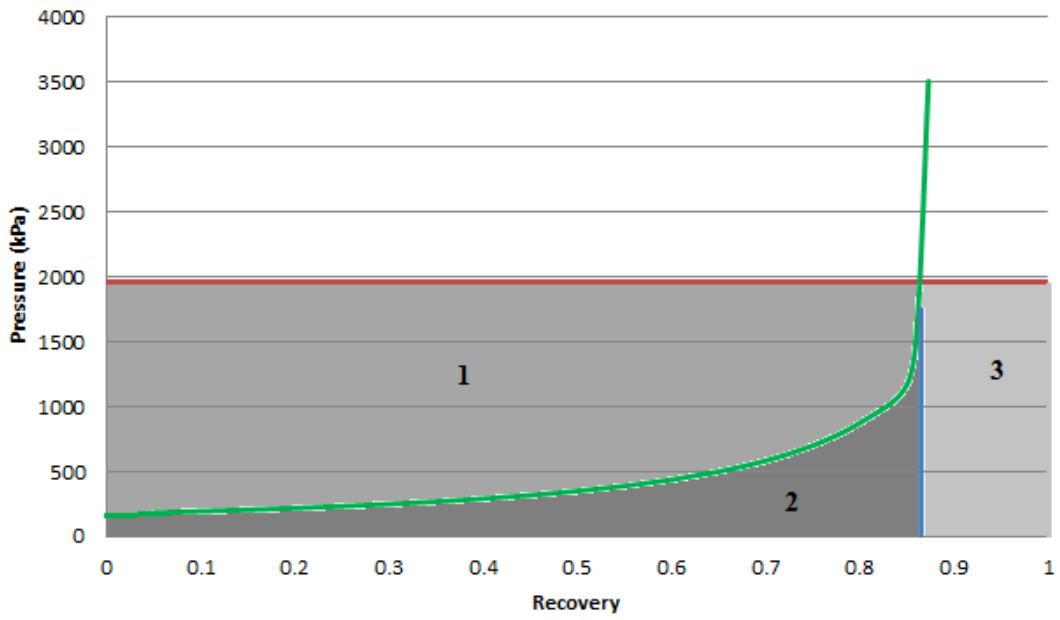

Figure 40: Energy requirement regimes for RO stage 1

For the 85% recovery shown in Figure 39, the minimum energy requirement is depicted by the area under the osmotic pressure (green) curve. Region 1 on the graph shows the additional energy requirements, region 2 the minimum energy requirement and region 3 the energy remaining in the brine stream which is recoverable.

5.6.3 CEDI SEC

The minimum work of separation was calculated with the use of Equation 50.

$$\dot{W_{min}} = \sum E_{out} - \sum E_{in} + VI \qquad \textbf{Equation 50}$$

Where V is the potential difference over the modules and I is the electrical current sent to the modules.

This equation incorporates the electrical work added to the system for the electrochemistry section of the CEDI module.

Using Equation 33, the Second Law efficiency was calculated as 4.38%. This low efficiency is indicative of membrane processes with large differential pressure over the membranes (Farooque, *et al.*, 2008).

5.7 Conclusion

The UF pretreatment section of the desalination plant is only accountable for the use of 6.1% of the total exergy input. The UF membranes destroy 3.8% of the total exergy destroyed in the desalination process.

The lack of throttling valves and the fact that the filtered water leaves the section at a pressure of 59.2 kPa inhibits the use of ERDs in this section.

The UF Second Law efficiency is 44.78%.

The first RO stage is responsible for 37.1% of the total exergy input to the system. The membranes destroy 29.7% of the total exergy destroyed during desalination. The throttling valve destroys 4.15 kW of exergy, which is 5.7% of the total exergy destroyed.

The exergy destroyed by throttling may be recovered by using ERDs. This will improve the SEC of 353 Wh/m^3 and Second Law efficiency of 3.85%.

The second RO stage is accountable for 38.1% of the total exergy input to the system. The destruction of exergy over the second RO stage membranes is 37.6% of the total exergy destruction. The throttling of the brine destroys 2.42 kW, which is 3.3% of the total exergy destruction.

The exergy lost during throttling can be recaptured with the use of an ERD. This will increase the Second Law efficiency of 3.7% and decrease the SEC of 307 Wh/m^3.

The CEDI stage is responsible for 18.7% of the exergy consumed by the desalination process. The modules destroy 19% of the total exergy destroyed by the process. The low pressure of the product and brine streams does not allow for ERD incorporation.

Figure 41 shows the specific exergy inputs as a percentage of total input. The destruction of exergy as a percentage of total exergy destruction is also given in this figure.

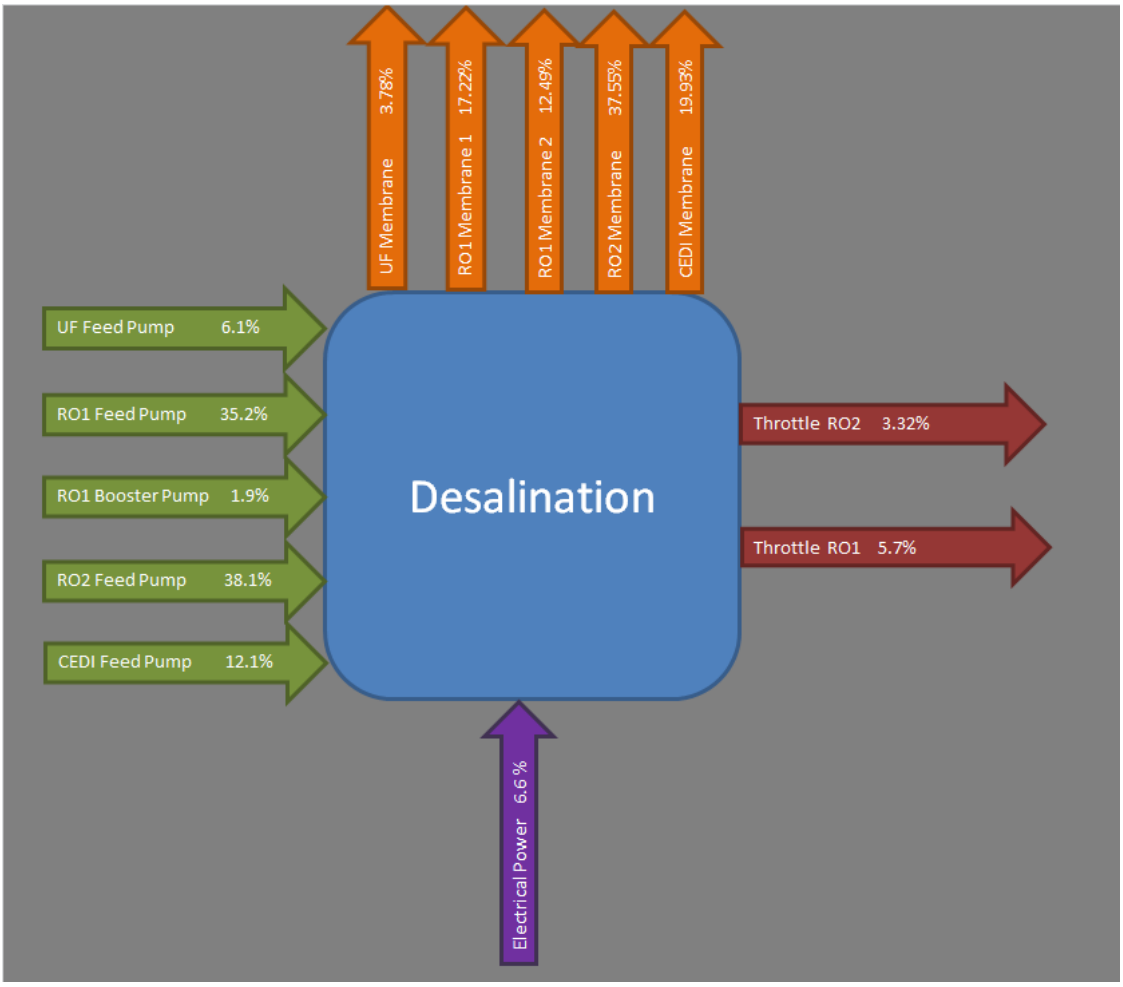

Figure 41: Percentage exergy contribution and destruction of the desalination process

Two possible process streams have been identified for the installation of ERDs. The ERDs will replace the throttling valves on both the first and second stage reverse osmosis systems. This is a common practice for reverse osmosis desalination plants (Cerci, 2002) (Flynn, 2009) (Kucera, 2010) (Sharqawy, *et al.*, 2011) (MacHarg, 2011).

5.8 References

Cerci, Y., 2002. Exergy analysis of a reverse osmosis desalination plant in California. *Desalination*, 3(142):257-266.

Farooque, A. M. *et al.*, 2008. Parametric analyses of energy consumption and losses in SWCC SWRO plants utilizing energy recovery devices. *Desalination*, Issue 1(219):137-159.

Kucera, J., 2010. *Reverse Osmosis: Design, Processes and Application for Engineers.* Hoboken: Wiley and Sons.

Sharqawy, M. H., Zubair, S. M. & Lienhard, J. H., 2011. Second Law analysis of reverse osmosis desalination plants: An alternative design using pressure retarded osmosis. *Energy*, 1(36):6617-6626.

Chapter 6

Thermodynamic analysis of the proposed design

This chapter proposes the incorporation of specific ERDs at specific locations. These proposed changes are then thermodynamically analysed to determine if the amount of energy recovered validates the installation of these devices. An exergy balance is conducted and compared with the original plant. The Second Law efficiency is calculated as well as the specific energy consumption and a comparison between the proposed and original plant is made.

6.1 Introduction

Energy recovery devices have successfully been incorporated on industrial desalination plants that produce potable water from saltwater at a rate in excess of 2000 m^3/day (MacHarg, 2011). The investigated desalination plant is capable of producing 5760 m^3/day from three separate skids. Each skid therefore produces water at a rate of 1920 m^3/day.

The ERDs most commonly used in industry are either a turbine based device or pressure exchanging device (Penate & Garcia-Rodriguez, 2010).

Turbine based devices have an energy recovery efficiency of up to 90%. From Table 14, the average, however, is 65%. This is 30% lower than the 95% achievable efficiency from PES devices.

Due to the fact that the high pressure brine is in direct contact with the low pressure feed water, volumetric mixing does occur in the PES. This volumetric mixing does have an effect on the initial salinity of the RO feed water.

Energy recovery devices may lead to an up to 28% reduction in the energy consumption of a desalination plant, according to Cerci (2002).

In Chapter 5 two locations have been identified where ERDs can be installed. The high pressure brine from both the first and second RO stages is ideal for the installation of an ERD.

All calculations discussed in Chapter 5 will be applicable for this section with the additions mentioned below.

The following additional assumptions were made in order to complete the calculations for Chapter 6:

- No change in temperature over any ERD;
- PES efficiency of 95%;
- ERT efficiency of 65%;
- Volumetric mixing of 6%;
- Average molecular weight of salt is 58.8 mol/kg;
- No frictional losses in pressure vessels or membrane chambers;
- The uncertainties calculated on the pressure indicators and salinity measurements (Appendix L) are not significant and will be ignored for Chapter 6.

This chapter discusses the effect an energy recovery device would have on the SEC as well as the Second Law efficiency of the two RO stages. An optimal process recovery is determined in order to maximise the energy recovered by the ERD. Included in this chapter is a financial analysis that establishes the financial feasibility of the proposed installation.

6.2 First pass reverse osmosis

The installation of an ERD in the first pass reverse osmosis, as per calculations in Chapter 5, will be installed in the high pressure brine discharge section. These ERDs will replace the throttling valves currently used to return the brine to atmospheric pressure. This is the preferred position for the installation of ERDs across the desalination industry (Al-Zahrani, *et al.*, 2012), (Cerci, 2002), (Flynn, 2009), (Kremser, *et al.*, 2006), (MacHarg, 2011), (Penate & Garcia-Rodriguez, 2010), (Sharqawy, *et al.*, 2011).

The installation of two types of ERD, namely an energy recovery turbine (ERT) and a pressure exchanger system (PES) will be investigated. The ERT efficiencies are assumed to be in the region of 65% (from Table 14) whereas the efficiency for the PES systems is assumed to be 95% (Table 14).

The PES, however, does cause some salinity increase in the feed water to the RO system. This is due to the direct contact of the brine and the feed water. The salinity increase of the feed water is calculated using Equation 35 and the volumetric mixing is assumed as 6% (MacHarg, 2011) (Liu, *et al.*, 2011).

The increase in salinity of the feed water will lead to an increase in the SEC of the RO unit; however, the high efficiency of the PES with regards to the ERT may render this increase in SEC negligible.

Figure 42 shows the block flow diagram of the first pass RO stage with a PES incorporated. The brine stream (stream 19), leaves the system at a pressure of 1053 kPa with a flow rate of 4.2 kg/s at a recovery of 86.2%. This residual energy that is captured in the high pressure brine can be recovered using an ERD.

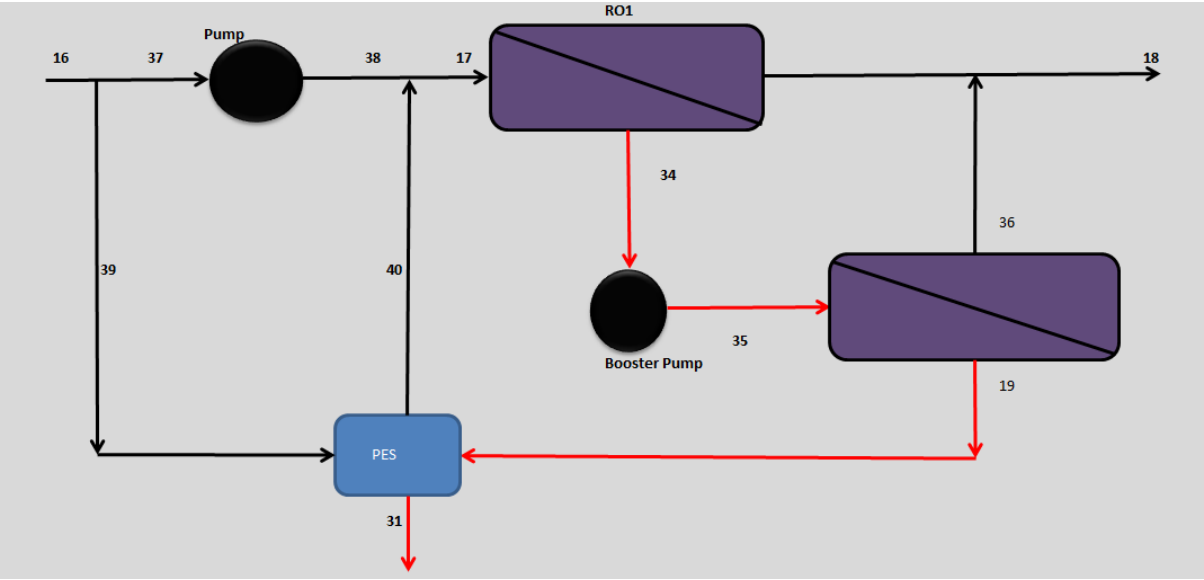

Figure 42: First pass RO with PES incorporation

From Figure 42 it can be seen that a fraction of the feed water to the RO feed pumped is removed and sent to the PES. The pressure in the RO brine stream (stream 19) is then transferred by the PES to the feed water stream. The mass flow of stream 39 is equal to that of stream 19 (4.24 kg/s); therefore, the larger the brine flow, the higher the mass flow through the PES will be.

The salinity increase is calculated at 0.05% at a recovery of 86.2% with an assumed volumetric mixing of 6% (Geisler, *et al.*, 2001). Therefore the initial salinity of the feed water will increase from 71.343 ppm to 71.348 ppm. The critical parameters of the system as shown in Figure 42 are given by Table 25.

Table 25: Critical parameters for RO first stage with PES

Stream	Temp (°C)	Pressure (kPa)	Mass Flow (kg/s)	Salinity (ppm)	Specific Exergy (kJ/kg)	Exergy Flow (kW)	Change in Exergy (kW)
16	22.4	100	30.72	71.35	0	0	
17	22.4	1037.84	30.72	71.35	0.93	28.54	
18	22.4	25.96	26.48	0.19	1.49	39.48	
19	22.4	1053.9	4.24	515.6227	-8.06	-34.17	
							-4.10
31	22.4	83.22602	4.24	515.59	-9.03	-38.28	
34	22.4	830	5.47	293.0	-3.96	-21.65	
							1.59
35	22.4	1149	5.47	293.0	-3.67	-20.07	
36	22.4	25.96	3.23	0.19	1.55	5.01	
37	22.4	100	26.48	71.34	0	0	
							24.60
38	22.4	1037.84	26.48	71.34	0.93	24.60	
39	22.4	100	4.24	71.34	0	0	
							4.02
40	22.4	1053.9	4.24	71.38	0.95	4.02	

The temperature of 22.4°C is constant through the first RO pass. An initial mass flow of 30.7 kg/s is split into two streams, stream 37 and 39. The process stream 37 passes through the HP pump and is discharged at a pressure of 1037kPa with a flow of 26.48 kg/s. The other 4.24 kg/s passes through the PES where the pressure is exchanged with the high pressure of the brine. This increases the salinity with 0.002 ppm.

The salinity changes from 71.3 ppm to 0.19 ppm. This calculates to a salt passage of 0.27%.

The zero inlet specific exergy to the system is due to the fact that the pressure, temperature and salinity of this stream are identical to the reference state.

The negative change in exergy flow on the brine stream before and after the PES shows that 4.1 kW of exergy is transferred from the brine to the feed. The feed then accumulates this

4.02 kW. The 0.08 kW difference is due to the volumetric mixing. The feed pump adds 24.6 kW exergy to the system while the booster pump adds 1.58 kW of exergy.

The membranes for the first two arrays destroy 12.54 kW of exergy while the membranes for the third array destroy 9.1 kW. This is identical to the original design.

The minimum work required in order to complete the separation process is calculated as 1.2 kW. This increase from 1.16 kW is due to the salinity increase caused by the installation of the PES.

The Second Law efficiency, as calculated by Equation 33, is 4.88%. This is an improvement of 25.6% from the original 3.85%.

The SEC improves by 12.2% from 0.353 kWh/m^3 to 0.31 kWh/m^3.

The block diagram in Figure 43 shows the process flow of a system with an incorporated ERT.

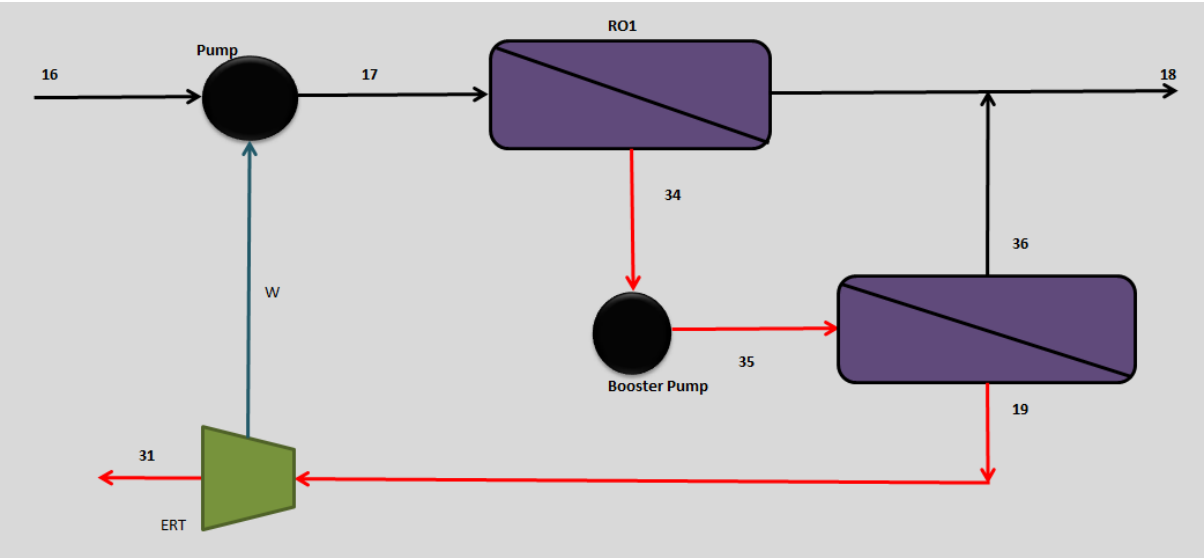

Figure 43: First pass RO with ERT incorporation

The incorporation of an ERT does not necessitate the division of the feed stream to the feed pump. Instead the work gained from the ERT is sent to the RO feed pump. This system is, however, not as direct; therefore more energy losses occur. The fact that the brine and feed streams never come directly into contact with each other does mean that no salinity increase is possible. The critical parameters for the system with the ERT are given in Table 26.

Table 26: Critical parameters for RO first stage with ERT

Stream	Temp (°C)	Pressure (kPa)	Mass Flow (kg/s)	Salinity (ppm)	Exergy (kJ/kg)	Exergy Flow (kW)	Change in Exergy (kW)
16	22.4	100	30.72	71.34	0	0	
							28.54
17	22.4	1037.84	30.72	71.34	0.93	28.54	
18	22.4	25.96	26.48	0.19	1.49	39.48	
							-62.71
19	22.4	1053.9	4.24	515.62	-8.06	-34.17	
							-4.15
31	22.4	83.22602	4.24	515.62	3.85	-38.32	
34	22.4	830	5.47	293	-3.96	-21.65	
							1.59
35	22.4	1149	5.47	293	-3.67	-20.07	
36	22.4	25.96	3.23	0.19	1.55	5.01	

The temperature and feed pressure is identical to that of the original system. The unaltered mass flow to the HP pump is 30.72 kg/s and no salinity increase exists in this configuration. The feed pressure to the RO system is 1037.84 kPa, identical to the original system.

The salt passage is 0.27%. This is identical to the original system and the system with the PES. The difference between the initial salinity (stream 17 in Table 25 and stream 17 in Table 26) is due to the fact that some volumetric mixing takes place when a PES is installed.

Exergy destruction over the membranes of the first two arrays amount to 12.5 kW whereas the third array destruction is lower at 9.1 kW. As expected, this is identical to the original system and the PES incorporated system.

High pressure pumping adds 28.53 kW exergy to the system. This is 3.8% higher than the 24.6 kW added by the system with the PES and identical to the original system. This is due to the fact that the same mass flow of water is pumped in this configuration as opposed to the original layout. The booster pump adds the same 1.58 kW than with the previous two configurations.

The minimum work required is 1.16 kW which is 3.3% lower than the minimum work required for the system with the PES. This lower work required is due to the fact that the initial salinity is lower for the ERT system than for the PES.

The Second Law efficiency for the process with the ERT is 4.23%, which is an improvement of 9.9% from the original system. It is, however, not as good as the efficiency of the process with the PES.

The SEC of the first pass RO with the ERT is calculated as 0.323 kWh/m^3. This is an improvement of 8.4% on the original plant.

The results for the first pass RO are summarised in Table 27.

Table 27: Summary of energy consumption for first stage RO

	Original	PES	ERT
Minimum work (kW)	1.16	1.2	1.16
Second Law efficiency (%)	3.85	4.88	4.23
SEC (Wh/m^3)	352.74	309.7	323.17

From Table 27 it is clear that the Second Law efficiency and the SEC are improved by the installation of an ERD. The minimum work required for the process with the PES is higher due to the volumetric mixing; however, this configuration is also the most efficient system with the lowest SEC.

The SEC rises exponentially as the recovery rises. This is due to the increase in pressure required in the RO process. The relationship between recovery and SEC is shown in Figure 44.

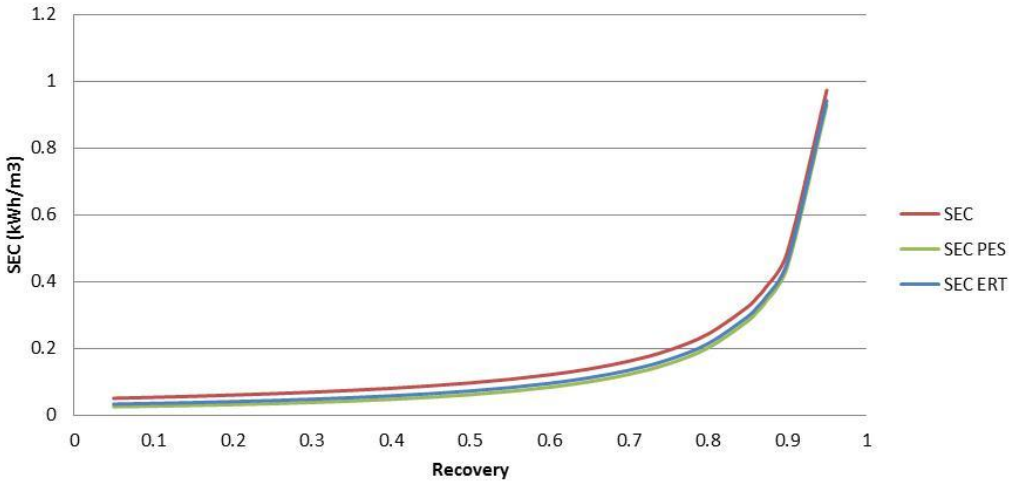

Figure 44: SEC as a function of recovery for the first RO stage

From Figure 44 it is visible that the SEC for the first RO stage is constantly lower with the ERDs. At lower recoveries, the difference between the original configuration and any of the ERDs is not as large as for the recoveries ranging between 50% and 90%. This is due to the fact that the brine pressure is not excessively high and therefore the energy flow through the ERD is not as high. Between the recoveries of 50% and 90%, as shown in Figure 44, a definite difference is visible between the original configuration, the ERT and PES. The difference between the PES and ERT is also visible. This difference is due to the higher efficiency of the PES with regards to the ERT.

At recoveries higher than 90%, the difference is not as prominent as at the lower recoveries (As seen in Figure 45). This is a direct result of the lower brine flow at high recoveries. The lower brine flow does mean that less energy is available for the ERD to recover.

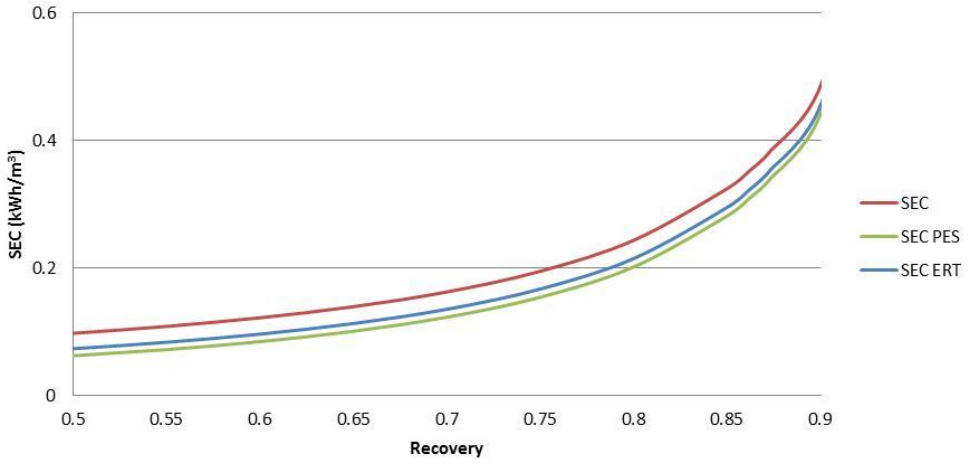

Figure 45: SEC as a function of recovery for the first RO stage between 50% and 90%

The brine stream has a high salinity and the salinity of the brine stream increases as the recovery increases. This causes the salinity of the feed to increase even further due to volumetric mixing when a PES is used. This increase in feed salinity causes the SEC to rise and therefore the difference between the ERT and PES is not as visible at high recoveries.

The installation of an ERD on the brine stream of the first RO pass proves to be technically feasible and effective. From Chapter 5, a second possible position was identified namely the brine stream on the second RO pass.

6.3 Second pass reverse osmosis

The brine stream from the second stage RO exits the system at 750 kPa with a flow rate of only 3.5 kg/s at a recovery of 87.3%. This stream is then throttled in the original configuration to atmospheric pressure. The energy in the high pressure brine is therefore lost and can be utilised by the installation of an ERD. Figure 46 schematically depicts the layout of the process with a PES incorporated.

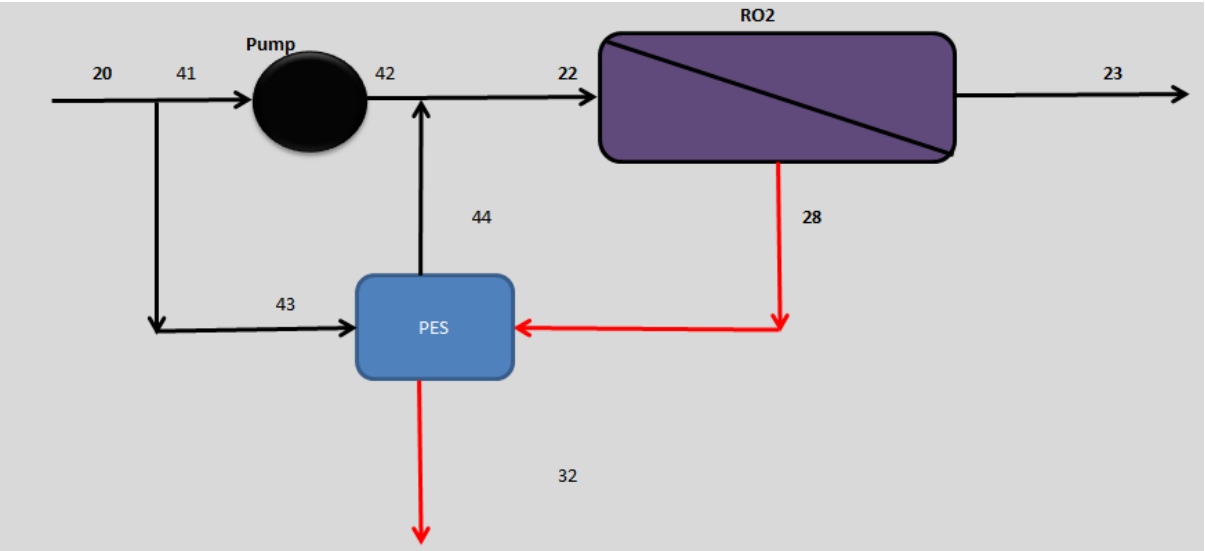

Figure 46: Schematic layout of RO stage 2 with a PES

The incorporation of a PES does necessitate the division of the feed stream to the RO feed pump. This will in effect mean that a smaller amount of water is pumped and therefore less energy is required. The direct contact between the high salinity brine stream (1.44 ppm) and the feed water (0.189 ppm) does encourage some volumetric mixing. Table 28 gives the results of the critical parameters calculated for the installation of a PES. The effect of the volumetric mixing will increase the initial feed salinity from 0.18874 ppm to 0.18875 ppm. This is a minute increase in salinity and it is not expected that this will hamper the

performance of the RO system. The salinity increase does cause a 3% increase in the minimum work required from 1.14 kW to 1.175 kW.

Table 28: Critical parameters of the second RO stage with a PES

Stream	Temp (^{o}C)	Pressure (kPa)	Mass Flow (kg/s)	Salinity (ppm)	Exergy (kJ/kg)	Exergy Flow (kW)	Change in Exergy (kW)
20	22.4	244.54	27.63	0.19	1.97	54.47	
22	22.4	1346.36	27.63	0.19	3.09	85.38	
							-35.98
23	22.4	284.92	24.12	0.01	2.05	49.40	
28	22.4	748.48	3.51	1.44	2.46	8.63	
							-2.38
32	22.4	83.22602	3.51	1.44	1.78	6.24	
41	22.4	244.54	25.63	0.1887	1.97	50.52	
							28.67
42	22.4	1346.36	25.63	0.1887	3.09	79.20	
43	22.4	244.54	2.00	0.1887	1.97	3.94	
							2.27
44	22.4	1346.36	2.00	0.1889	3.09	6.21	

The mass flow of the feed water through the PES is 2.00 kg/s. This is calculated according to the exergy available to be recovered. The assumed 95% efficiency of the PES is the same as for the PES in the previous section.

The feed pressure to the second RO stage is 1346 kPa. This high pressure is due to the high recovery and the fact that no brine booster pumps are used. The driving force applied by the pumps should therefore supply sufficient pressure to all three RO arrays.

Salt passage for the second RO stage with a PES is calculated as 3.1%. This is the same as for the original design.

26.98 kW of exergy is added to the system by the RO feed pumps. This is 12.7% less than for the original design.

Exergy destruction due to the membrane is 27.35 kW. This is identical to the original system, as expected.

The Second Law efficiency improves with 18.1% to 4.36% while the SEC improves with 7.7% to 283 Wh/m^3.

Installing an ERT does not influence the minimum work required for the separation process due to the fact that no volumetric mixing takes place. The efficiency of the ERT, however, is considerably lower at 65% (MacHarg, 2011). This installation is shown in Figure 47.

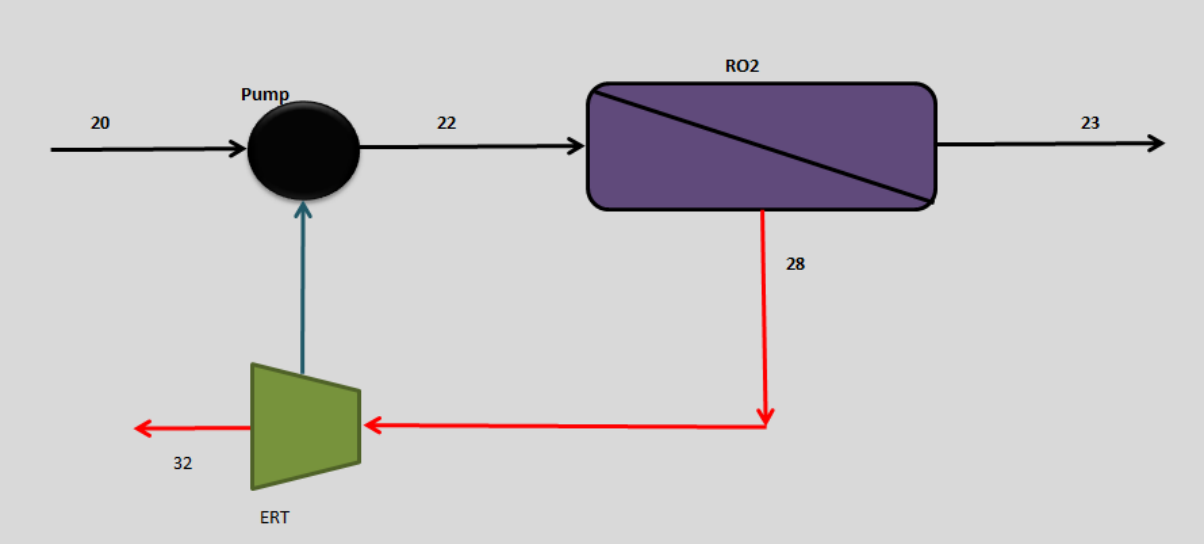

Figure 47: Second stage RO with ERT installation

The incorporation of the ERT does not necessitate the alteration of the feed stream to the pump. The entire brine stream flows through the ERT and the energy recovered is sent to the high pressure pump. Table 29 shows the critical parameters for this configuration.

Table 29: Critical parameters of the second RO stage with an ERT

Stream	Temp (°C)	Pressure (kPa)	Mass Flow (kg/s)	Salinity (ppm)	Exergy (kJ/kg)	Exergy Flow (kW)	Change in Exergy (kW)
20	22.4	244.54	27.63	0.189	1.97	54.47	
							30.91
22	22.4	1346.36	27.63	0.189	3.09	85.38	
							-35.98
23	22.4	284.92	24.12	0.006	2.05	49.40	
							-76.75
28	22.4	748.48	3.51	1.44	2.46	8.63	
							-2.42
32	22.4	83.23	3.51	1.44	1.77	6.21	

The feed pressure of 1346 kPa is identical to the previous two configurations and the high pressure pump is responsible for 30.9 kW exergy added to the process. This is 12.7% more than for the PES configuration.

3.1% of the salt passes through the membrane. This number is significantly higher than for the first RO stage (0.27%). The higher percentage can be attributed to the fact that the ions that do pass through the first stage RO membrane, will be sufficiently small enough to pass through the second RO stage. The lower concentration gradient, however, does mean that the majority of the salts will be rejected.

Exergy destruction over the membrane amounts to 27.35 kW, identical to the previous configurations.

The ERT does recover 1.57 kW exergy, which is 30.6% less than the PES recovers.

The Second Law efficiency improves by 5.37% to 3.89% while the SEC improves by 5.36% to 290 Wh/m^3.

The results are summarised in Table 30.

Table 30: Summary of energy consumption for second stage RO

	Original	PES	ERT
Minimum work (kW)	1.14	1.18	1.14
Second Law efficiency (%)	3.688	4.355	3.886
SEC (Wh/m^3)	307	283	290

From Table 30 it is clear that the use of a PES will yield better results in both the efficiency and the SEC of the system.

6.4 Recovery and energy consumption

The SEC is directly proportionate to the amount of energy recovered by the device. The amount of energy recovered by the device is dependent on the amount of energy flow through the device. For a constant pressure, this energy flow grows as the mass flow of brine increases. The lower the recovery of the system, the larger the difference between the original SEC and the SEC with an ERD installed.

The SEC for a system without an ERD installed is shown in Figure 48.

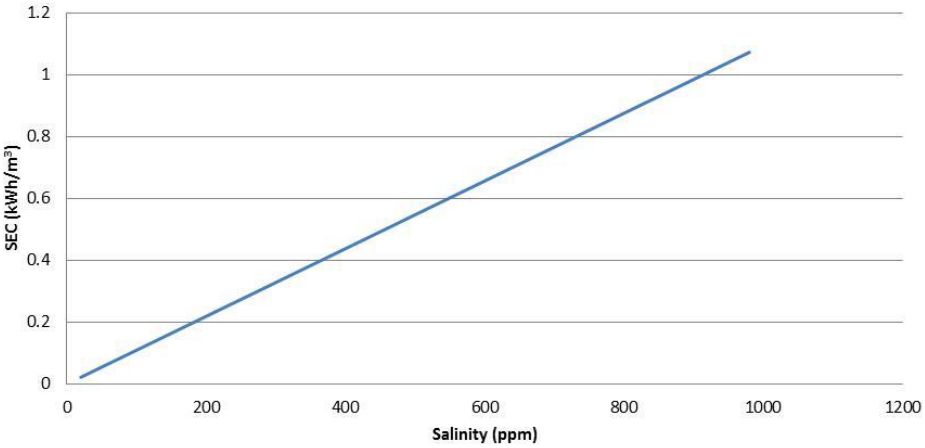

Figure 48: Relationship between SEC and salinity

This shows the direct correlation between the salinity of the feed water and the SEC. The SEC rises as the salinity increases due to the fact that the driving pressure requirements increase.

The recovery has an adverse effect on the flow through the ERD as shown in Figure 49.

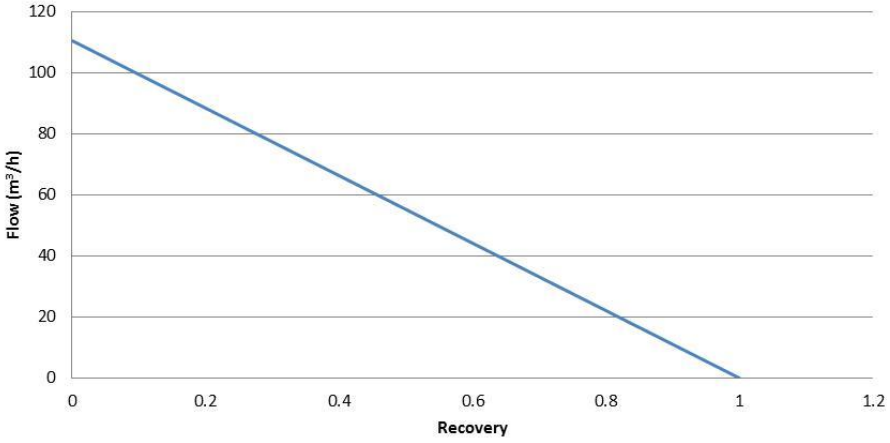

Figure 49: Flow rate through the ERD as a function of recovery

The brine flow rate decreases as the recovery increases. Therefore, the mass flow of brine through the ERD declines. In the case of a PES, the flow of feed water through the PES will decline accordingly. This decrease in brine flow causes less recoverable energy to flow through the ERD.

As the recovery increases, the driving pressure increases as well. This causes exponential growth in the brine pressure as the recovery increases. This can be seen from Figure 50.

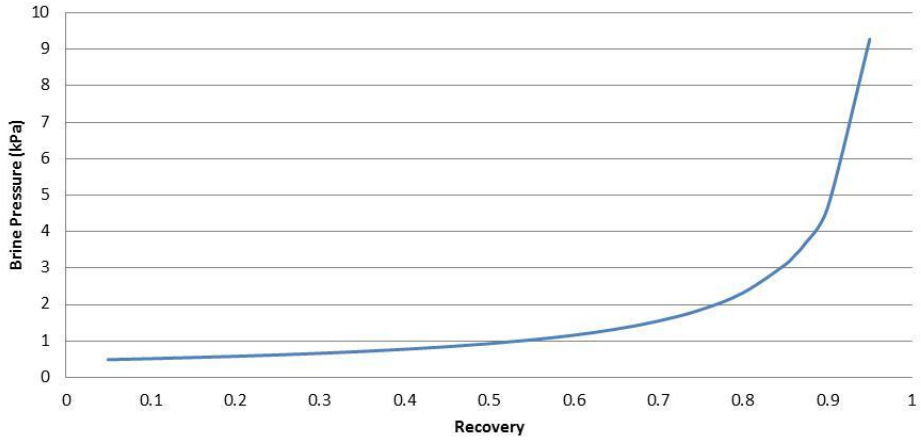

Figure 50: RO brine pressure relationship with recovery

The higher brine pressure has the direct effect that more exergy is stored in the brine and therefore more exergy can be recovered. The pressure difference between the high pressure brine feed to the ERD and the discharge at atmospheric pressure increases exponentially as the recovery rises. This differential pressure directly translates to recoverable energy (Figure 51).

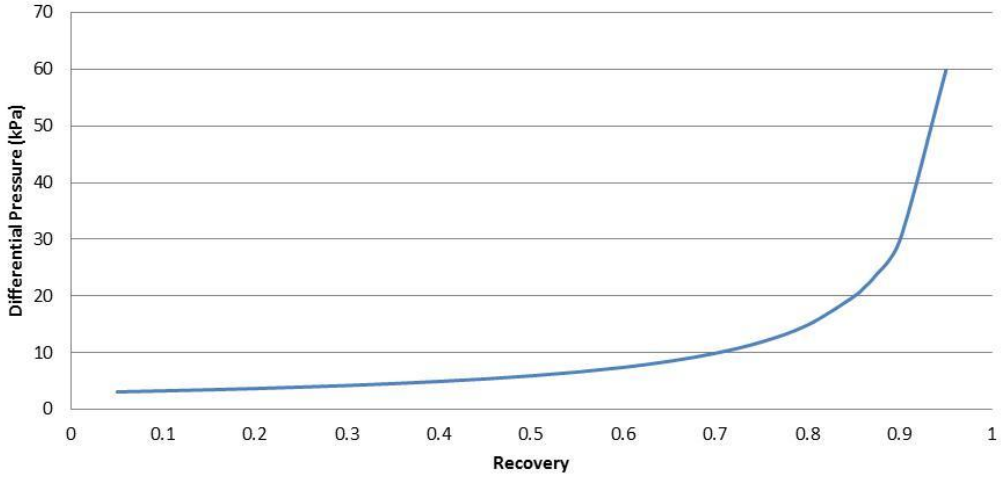

Figure 51: Pressure difference over the ERD as the recovery of the RO changes

As the recovery of the RO process increases, the SEC will increase. The differential pressure over the ERD will increase as well, however the mass flow through the ERD will decrease.

The relationship between a system with and without an ERD is given as:

$$SEC_{original} = (\frac{R_{gas}c_0T}{1-R})/3.6 \times 10^{-6} \quad \textbf{Equation 51}$$

$$SEC_{PES} = \frac{\frac{R_{gas}c_0T}{1-R}(1+SI) - \eta_{PES}W_{throttle}}{3.6 \times 10^6} \quad \textbf{Equation 52}$$

$$SEC_{original} - SEC_{PES} = \frac{\frac{-R_{gas}c_0T}{1-R}SI - \eta_{PES}(1-R)(P_{atm} - \frac{c_0R_{gas}T}{1-R})}{3.6 \times 10^6} \quad \textbf{Equation 53}$$

Figure 52 visually depicts the relationship between this difference and recovery in order to establish an optimal point.

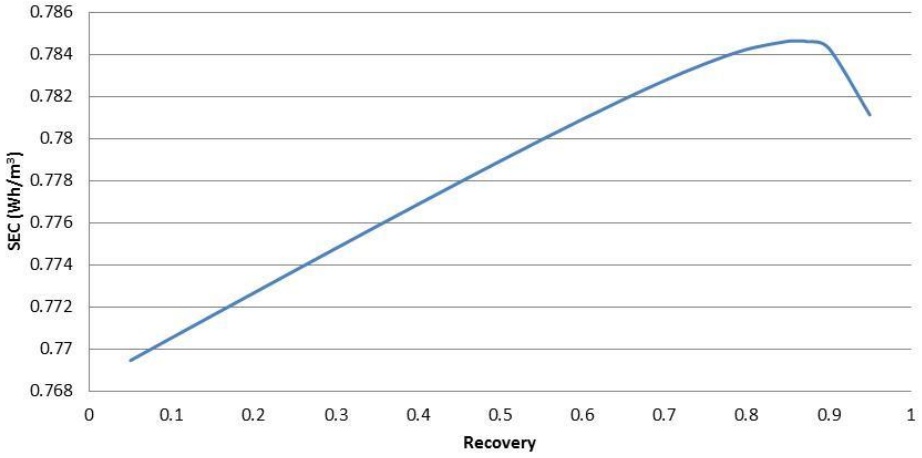

Figure 52: SEC difference between original design and an installed ERD as a function of recovery

From Figure 52 it is clearly visible that the advantages of installing an ERD diminish at recoveries higher than 90%. Between the recoveries of 80% and 90%, however, the mass flow through the ERD is sufficient to deliver maximum exergy through the high pressure brine to the ERD. Below 80%, the pressure in the brine stream drops dramatically and even though the mass flow is high, the process stream does not have sufficient exergy to be transferred.

In order to maximise the benefits of this plant, the recoveries of the RO sections should therefore be between 80% and 90%.

6.5 Financial Benefits

With the installation of a PES to both first stage RO and second stage RO, a total of 0.201 kWh is saved for every cubic metre of water produced. The plant is designed to produce 240 m^3/h, which amounts to 2 102 400 m^3/year.

The total amount of energy saved with the installation of a PES will then amount to 422 244 kWh per annum.

The power station sells each kilowatt hour of electricity at a price of R0.351 to the parent company. This parent company then sells the electricity at average price of R1.3/kWh to the end users.

If a PES is installed, the power station could save up to R148 000 per year and the parent company can save R549 000 every year.

The future value is calculated using Equation 54 (MacHarg, 2011):

$$FV = PV(1 + i)^n \qquad \textbf{Equation 54}$$

Where FV is the future value

PV is the present value

i is the interest rate and

n is the term in years

Over the 20 year life span of the plant, assuming 5% inflation, the power station will save R5.45 million and the company will save R16.52 million. The payback period for the capital investment is calculated at 7 years.

Table 31: Financial benefits summary for the installation of a PES

Economic Considerations (PES)	
Energy Price (R/kWh)	0.351
Average selling price for Eskom (R/kWh)	1.3
Cost of PES (R)	534040
Amount of PES installed	6
Energy saved RO 1 (kWh/m^3)	0.129
Energy saved RO 2 (kWh/m^3)	0.072
Total energy saved (kWh/m^3)	0.201
Capital Investment	3204240
Water produced (m^3/h)	240
Water produced per year (m^3/year)	2102400
kWh saved	422244
R/year saved by Power Station	148 207.58
R/year saved by Company	548 917
R/year saved on RO1 by Company	352 964
R/year saved on RO2 by Company	195 953
Inflation on Energy (%)	6
Life of plant savings (Station-20years)	R 5 451 903
Net financial gain (Company-20years)	R 16 519 798
Payback period (years)	7

The study done by Cerci (2002), shows that R150 000 per year can be saved with the addition of a PES which is identical to the current study. MacHarg (2011) determined a payback period of 5 years.

For the ERT, the yearly savings by the station decline to R34 000 whereas the company stands to benefit R126 000. The capital investment on an ERT is, however, much lower than for a PES. The six ERTs will amount to R1.4mil. The payback period for such an investment is in the region of 12 years.

Table 32: Financial benefits summary for the installation of an ERT

Economic Considerations (ERT)	
Energy Price (R/kWh)	0.351
Average selling price for Eskom (R/kWh)	1.3
Cost of ERT (ZAR)	236210
Amount of ERTs installed	6
Energy saved RO 1 (kWh/m^3)	0.0296
Energy saved RO 2 (kWh/m^3)	0.0165
Total energy saved (kWh/m^3)	0.046
Capital Investment	R 1 417 260.00
Water produced (m^3/h)	240
(m^3/year)	2102400
kWh saved	96788.30
R/year saved by Station	33 972.69
R/year saved by Company	125 825
R/year saved on RO1 by Company	80 839
R/year saved on RO2 by Company	44 986
Inflation on Energy (%)	6
Life of plant savings (Station-20years)	R 1 249 706
Net financial gain (Company-20years)	R 3 586 184
Payback period (years)	12

6.6 Conclusion

The installation of the ERDs on the brine stream of the RO systems improves the efficiency and SEC of the system.

A PES on the first RO stage will improve the Second Law efficiency by 25.6% to 4.88% while the SEC improves by 12.2% to 309.7 Wh/m^3.

An ERT on the first RO stage will improve the Second Law efficiency with 9.9% to 4.23% while the SEC will improve by 8.4% to 323.17 Wh/m^3.

A PES system on the second RO pass will improve the Second Law efficiency by 18.1% to 4.355% while the SEC will improve by 7.78% to 283 Wh/m^3.

An ERT on the second RO pass will improve the Second Law efficiency by 5.4% to 3.89% while the SEC will improve by 5.35% to 290 Wh/m^3.

The RO stages should optimally be run at a recovery between 80% and 90% in order to maximise the energy recovery.

Installing a PES system can save the power station in excess of R5.45mil over the 20 year life span of the plant while the company can benefit as much as R16.5mil over the same period.

6.7 References

Al-Zahrani, A. Orifi, J., Al-Suhaibani, B. & Al-Ansary, A. 2012, Thermodynamic analysis of a reverse osmosis desalination unit with energy recovery system. *Procedia Engineering,* 1(33):404-141.

Cerci, Y., 2002. Exergy analysis of a reverse osmosis desalination plant in California. *Desalination,* 3(142):257-266.

Farooque, A. M. *et al.*, 2008. Parametric analyses of energy consumption and losses in SWCC SWRO plants utilizing energy recovery devices. *Desalination,* Issue 1(219):137-159.

Kremser, U., Drescher, G., Otto, S. & Recknagel, V., 2006. First operating experience with the treatment of 3100m3/day of Elbe river water by means of reverse osmosis to produce process water and demineralised water for use in the industry. *Desalination,* 1(189):53-58.

Penate, B. & Garcia-Rodriguez, L., 2010. Energy optimisation of existing SWRO (seawater reverse osmosis) plants with ERT (energy recovery turbines): Technical and thermoeconomic assessment. *Energy,* (36):613-626.

Sharqawy, M. H., Zubair, S. M. & Lienhard, J. H., 2011. Second Law analysis of reverse osmosis desalination plants: An alternative design using pressure retarded osmosis. *Energy,* 1(36):6617-6626.

Singh, R., 2006. *Hybrid membrane systems for water purification.* 1 ed. Amsterdam: Elsevier.

Texas Water Development Board, 2011. *Energy optimisation of brackish groundwater reverse osmosis desalination,* Austin: Texas Water Development Board.

Chapter 7

Research Validation

This chapter helps validate the research findings presented in previous chapters and substantiates the results from the analyses.

7.1 Introduction

Due to the capital expenditure required in order to implement either the PES or ERT systems, the company will not install these systems within the next five years. This has resulted in the fact that no experimental results are available on this freshwater desalination plant to validate the calculations.

The validation of this research relies on experimental data from previous work by other authors. Although the water chemistry, especially the salinity of the feed water, differs from the investigated plant, a definite correlation is possible.

To supplement the validation from literature, a simulation with WinFlows® was completed and the results from the simulation are provided in order to validate the calculations done in Chapters 5 and 6.

7.2 Results from literature

The critical parameters that determine the success or failure of this investigation is the Second Law efficiency, specific energy consumption and the percentage difference between a system with an ERD and without an ERD. As seen in Figure 48, SEC rises as the salinity increases. Therefore, it is expected that all results where seawater or brackish water is desalinated the SEC will be higher than for the freshwater desalination. Table 33 provides a summary of results from different authors.

Table 33: Comparison of results from literature and this work

			No ERD	ERD		
Author	**Year**	**Salinity (ppm)**	**SEC (kWh/m^3)**	**Type**	**SEC (kWh/m^3)**	**E_{save} (%)**
Farooque	2008	42000	7	ERT	5.56	25.9
Farooque	2008	42000	9.13	ERT	7.45	22.6
Farooque	2008	42000	6.43	ERT	6.11	5.2
Farooque	2008	42000	6.49	ERT	6.39	1.5
Farooque	2008	41000	10.1	ERT	7.9	27.6
MacHarg	2011	2183	0.52	PES	0.42	24
Penate*	2011	35000	3.27	PES	2.39	27
Geisler	2002	Sea	3.73	PES	2.47	32.7
Geisler	1999	Sea	3.7	ERT	2.52	31.8
Geisler	1999	Sea	3.7	PES	2.34	36.8
Geisler	1999	Sea	5.9	ERT	4.3	27.1
Geisler	1999	Sea	5.9	PES	2.85	51
Mohamed	2005	Sea	10	PES	3.7	63
Gilau	2006	Sea	3.92	ERT	2.33	40.6
This Work	2014	71.1	0.353	PES	0.31	12.2
Average						29.77
Std Dev						15.25

* Calculated with the amount of throttled exergy recovered

The minimum energy required in order to produce water at a potable quality from brackish water, as calculated by MacHarg (2011) is 0.52 kWh/m^3 without the use of an ERD. This is 47% higher than the 0.353 kWh/m^3 as calculated in this work. This 47% increase is due to the 2112 ppm higher salinity of the brackish feed water. The specific configuration and membrane types will also play a role in the specific energy consumption.

The respective SECs from Table 33 improve between 1.5% and 63%. This work proposes a 12.2% improvement for the first RO stage and 12.1% for the second RO stage. On average, the installation of an ERD according to Table 33 has reduced the SEC with 28.6% with a standard deviation of 15.37%. This work has reduced the SEC with 12.2%, which is one percentage point from being within one standard deviation from the mean value.

Cerci (2002) calculated the Second Law efficiency of a brackish water RO system as 4.3% for a system without an ERD. In this work the Second Law efficiency was calculated as 3.85% for a system with no ERD.

The improvement of 25.6% for the first RO pass efficiency as calculated from this work is higher than the 14% improvement calculated by Cerci (2002). The second stage RO efficiency improves with 18.1% in this work which is 22% more of an improvement than Cerci (2002) calculates.

The installation of ERDs has in all previous cases proven to be advantageous. All the plants investigated by previous authors and this work have shown improvements in both the SEC and Second Law efficiencies.

7.3 Simulation with WinFlows®

WinFlows® was developed by GE Power and Water in 2003 (General Electric, 2003). It is a simulation package that has the ability to calculate the performance, energy consumption and effect of energy recovery devices on an RO system (General Electric, 2003). The simulation program models the behaviour of the plant based on theoretical calculations (General Electric, 2003). The membrane specific information required for the calculations (membrane resistance, membrane flux and scaling potential) are acquired from a database supplied by the membrane manufacturer (Texas Water Development Board, 2014). This specific simulation package was chosen due to the fact that it allows the simulation of three stage RO where the permeate from one array is used as the feed for the next array (as in the plant under investigation).

The Texas Water Development Board completed a study on the accuracy of computer based simulations. Brackish water desalination models done on simulation programs, including WinFlows®, had the following accuracies (Texas Water Development Board, 2014):

- Pressure was accurate within $\pm 6.5\%$;
- Energy consumption within $\pm 12\%$; and
- Salt passage within $\pm 5\%$.

A simulation was carried out on each of the two RO stages in order to determine the SEC and energy savings with the use of an ERD.

7.3.1 RO stage 1 simulation

The simulation for RO stage 1 was carried out by completing the feed water quality as per Table 20. The total alkalinity is only used to calculate fouling potential and antiscalant dosing. For the purpose of this analysis it was not included.

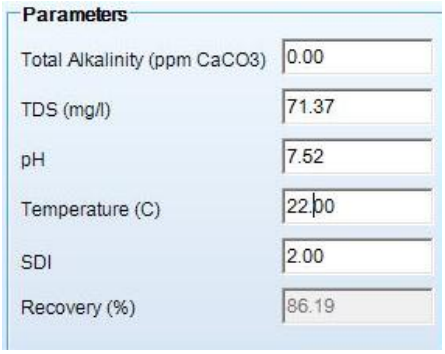

Figure 53: Feed water parameters for the first RO stage

The results from the simulation without an ERD are as shown in Figure 54.

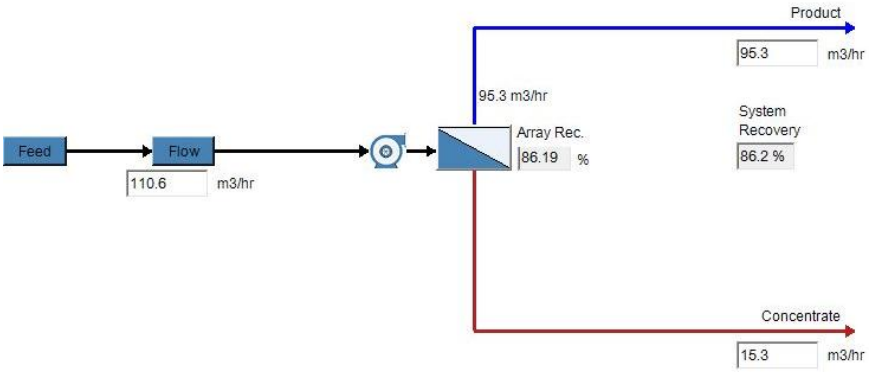

Figure 54: RO1 first stage simulation diagram

Figure 54 shows the volumetric flows as simulated by WinFlows®. The flows of each of the streams are identical with the 86.19% recovery for the first RO stage. The three RO arrays and the inter-stage booster pump are incorporated in the block depicting the RO system. WinFlows® does not visually show the booster pump or the three arrays, although it is incorporated. The water quality results are shown in Figure 55.

	Feed	Product	Concentrate
Alkalinity, ppm CaCO3	0.03	0.00	0.16
TDS, mg/l	71.34	0.18	517.61
pH	7.00	7.24	6.84
LSI	-43.00	-42.76	-43.16

Figure 55: Results from the RO first stage simulation with no ERD installed

The salinity (TDS) from the actual plant is 0.18 ppm for the product stream and 518 ppm for the concentrate stream. This is identical to the simulated values.

Figure 56 gives the results from the feed pump and energy analysis.

Figure 56: Pump specification and energy consumption for the first RO stage with no ERD

The feed pressure for RO stage 1 was simulated at 1135 kPa. This is 100 kPa higher than the actual plant data. The higher feed pressure is attributed to the fact that the membrane resistance and system resistance on the plant are not the same as for the simulation.

The SEC is calculated by the simulation as 0.4 kWh/m^3. This is 0.05 kWh/m^3 higher than the calculated value from Chapter 5. The slightly higher SEC is due to the 100 kPa difference in the simulated feed pressure.

The feed water quality and the RO array configuration for the simulation with the PES incorporation are identical to the system with no PES. This scenario is simulated as in Figure 57.

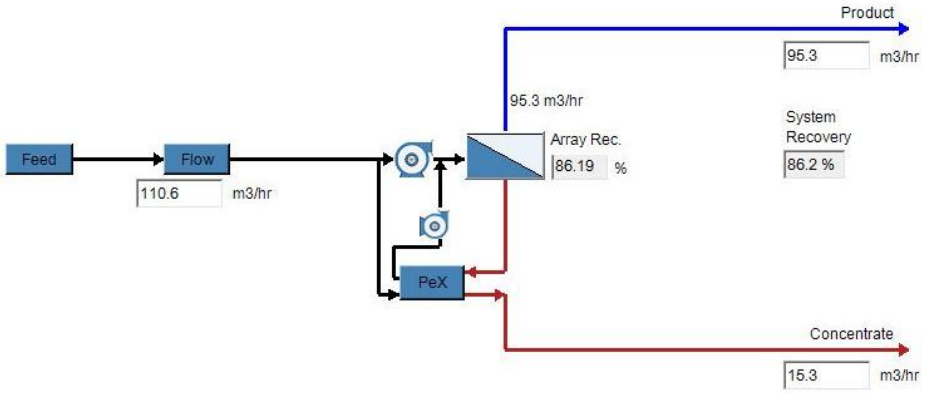

Figure 57: RO stage 1 simulation with a PES incorporated

Figure 57 above shows the PES that is simulated on the brine stream from the RO stage. The pump that is shown on the high pressure feed outlet of the PES is a booster pump that, if needed, supplies added pressure to the feed stream.

The energy consumption results from this system are shown in Figure 58 below.

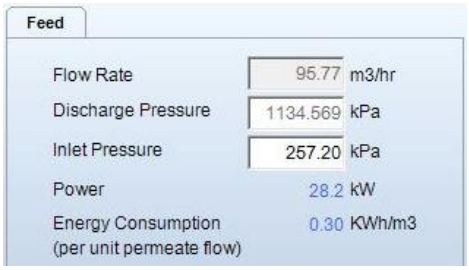

Figure 58: Pump specification and energy consumption of RO stage 1 with a PES

The feed pressure to the RO stage is 100 kPa higher than the feed pressure on the plant. The SEC of the simulation is 0.294 kWh/m^3. The calculated value from Chapter 6 is 0.309 kWh/m^3 which is 4% higher than for the simulated value.

The results from the PES and the financial benefit are shown in Figures 59 and 60 below.

Input Parameters

Parameter	Unit	Value
Manual or Auto Efficiencies		Auto
LP Discharge Pressure	kPa	202.600
Leakage (reject in HP out stream)	%	6.000
Cost of Power	$/kWh	0.120
Circulation Pump Efficiency	%	55.929
Circulation Pump Motor Efficiency	%	89.431
Circulation Pump VFD Efficiency	%	97.000
RO Permeate Flow	m3/hr	95.314
RO Recovery Rate	%	86.190
RO Feed Pressure	kPa	1134.569
Membrane Differential Pressure	kPa	245.803
Feedwater Salinity	mg/l	71.343

Pressure Exchanger Performance

Parameter	Unit	Value
Model		EX-45S
Number of Units	Number	2.000
Unit Flow	m3/hr	7.633
Lubrication Per Array	m3/hr	0.455
Lubrication Flow	%	2.978
Dfferential Pressure HP Side	kPa	54.619
Dfferential Pressure LP Side	kPa	54.619
Efficiency	%	90.680
Mixing at Membrane Feed	%	5.314
Power Savings	kW	4.513
HP Pump Efficiency	%	89.000
HP Pump Motor Efficiency	%	96.000
HP Power Consumed	kW	28.162

Figure 59: Simulated results for the PES on RO stage 1

Pressure Exchanger Power Results

Parameter	Unit	Value
Total Power Consumption	kW	28.005
Specific Power Consumption	kWh/m3	0.294
Specific Power Consumption	kWh/kgal	1.112

Figure 60: Simulated energy consumption results for the PES on RO stage 1

A PES efficiency of 90% is assumed by WinFlows® and cannot be changed by the user.

The installation of a Pelton wheel type ERT is the only turbine based ERD that can be simulated with WinFlows®. The configuration is shown in Figure 61 below.

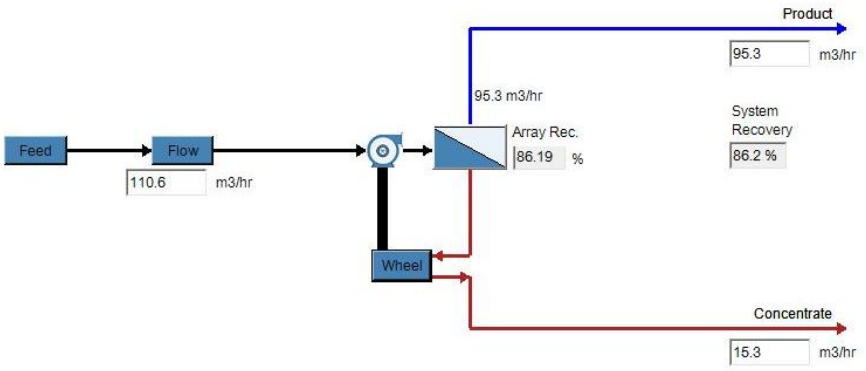

Figure 61: Simulation of ERT on RO stage 1

The results, feed pump results and energy consumption of this system is shown in Figure 62.

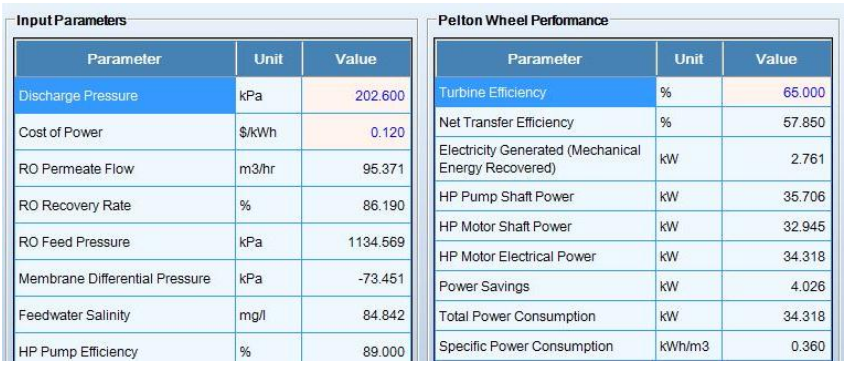

Input Parameters

Parameter	Unit	Value
Discharge Pressure	kPa	202.600
Cost of Power	$/kWh	0.120
RO Permeate Flow	m3/hr	95.371
RO Recovery Rate	%	86.190
RO Feed Pressure	kPa	1134.569
Membrane Differential Pressure	kPa	-73.451
Feedwater Salinity	mg/l	84.842
HP Pump Efficiency	%	89.000

Pelton Wheel Performance

Parameter	Unit	Value
Turbine Efficiency	%	65.000
Net Transfer Efficiency	%	57.850
Electricity Generated (Mechanical Energy Recovered)	kW	2.761
HP Pump Shaft Power	kW	35.706
HP Motor Shaft Power	kW	32.945
HP Motor Electrical Power	kW	34.318
Power Savings	kW	4.026
Total Power Consumption	kW	34.318
Specific Power Consumption	kWh/m3	0.360

Figure 62: ERT simulation results of RO stage 1

The efficiency of the turbine is set at 65%. This gives a SEC of 0.36 kWh/m^3 which is 0.037 kWh/m^3 higher than the calculated 0.323 kW/m^3.

Table 34: Comparison between the simulated and calculated results for the first RO stage

	Calculations			Simulation		
	No ERD	PES	ERT	No ERD	PES	ERT
SEC (kWh/m^3)	0.352	0.309	0.323	0.4	0.294	0.360

The results from the simulations are within the accuracy boundaries as discussed in Section 7.3.

7.3.2 RO stage 2 simulation

The second RO skid was simulated in WinFlows® with the inlet feed water quality specified as per the samples taken from the plant (Appendix J). The salinity and pH were inserted as shown in Figure 63 below.

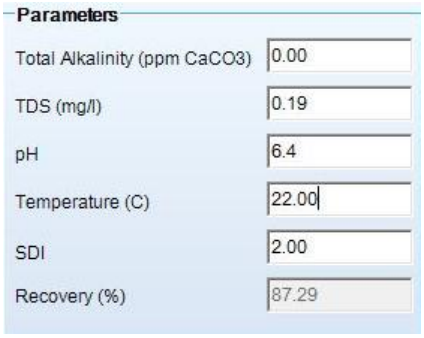

Figure 63: RO stage 2 simulation feed water quality

The second RO skid was simulated without the use of an ERD. The flow of all process streams and the recovery was simulated as per the plant in operation. All RO arrays are simulated without an inter-stage booster pump.

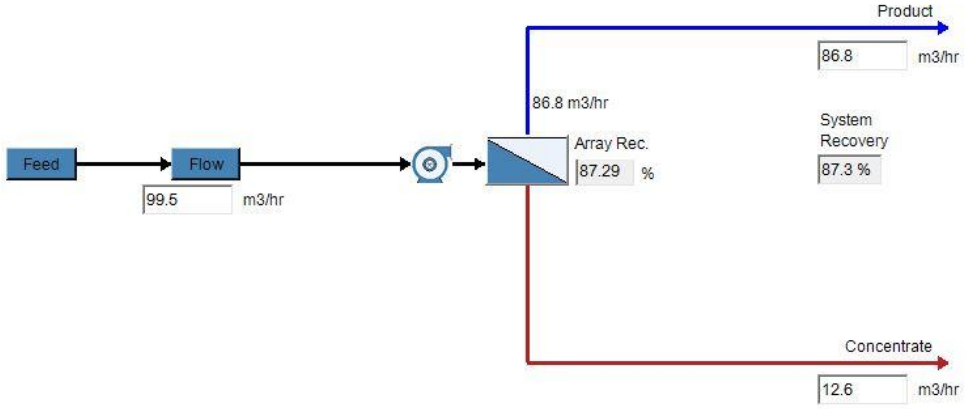

Figure 64: RO stage 2 simulation with no ERD

The energy consumption for the second RO system was simulated as per Figure 65 below.

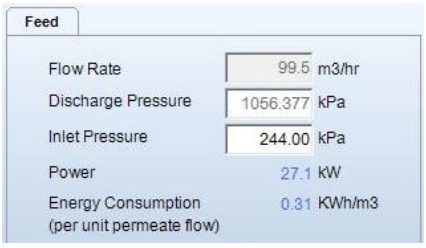

Figure 65: Simulated feed pump specification for RO stage 2 with SEC

The feed pump energy consumption was calculated as 27.1 kW. The SEC for the second RO stage was calculated as 0.31 kWh/m^3. This is 0.003 kWh/m^3 more than for the calculated 0.307 kWh/m^3.

The plant was simulated with the proposed PES installed on the brine stream from the RO modules. This is shown in Figure 66.

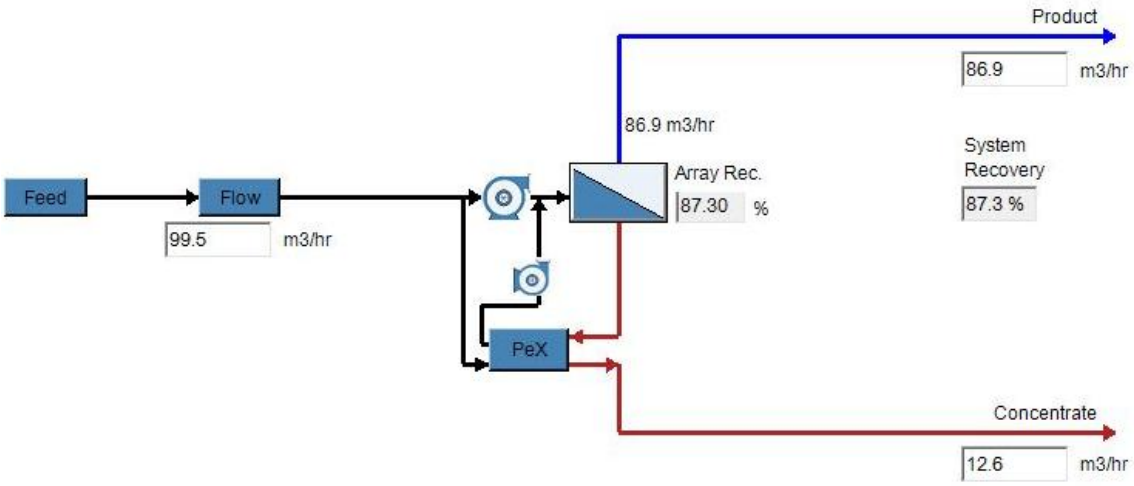

Figure 66: Simulation of second RO stage with PES

The results from the PES are shown in the figures below.

Input Parameters

Parameter	Unit	Value
Manual or Auto Efficiencies		Auto
LP Discharge Pressure	kPa	202.600
Leakage (reject in HP out stream)	%	6.000
Cost of Power	$/kWh	0.120
Circulation Pump Efficiency	%	55.331
Circulation Pump Motor Efficiency	%	89.323
Circulation Pump VFD Efficiency	%	97.000
RO Permeate Flow	m3/hr	85.870
RO Recovery Rate	%	86.300
RO Feed Pressure	kPa	1046.156
Membrane Differential Pressure	kPa	199.914
Feedwater Salinity	mg/l	0.191

Pressure Exchanger Performance

Parameter	Unit	Value
Model		EX-45S
Number of Units	Number	2.000
Unit Flow	m3/hr	6.815
Lubrication Per Array	m3/hr	0.455
Lubrication Flow	%	3.335
Dfferential Pressure HP Side	kPa	47.582
Dfferential Pressure LP Side	kPa	47.582
Efficiency	%	89.578
Mixing at Membrane Feed	%	5.282
Power Savings	kW	1.595
HP Pump Efficiency	%	89.000
HP Pump Motor Efficiency	%	96.000
HP Power Consumed	kW	22.827

Figure 67: PES simulated results from second RO stage

Pressure Exchanger Power Results

Parameter	Unit	Value
Total Power Consumption	kW	24.717
Specific Power Consumption	kWh/m3	0.288
Specific Power Consumption	kWh/kgal	1.090

Figure 68: PES simulated energy consumption results from second RO stage

A PES efficiency of 90% is assumed by WinFlows® and cannot be changed by the user. The PES on RO stage 2 improves the SEC to 0.288 kWh/m^3 as simulated. This is 0.005 kWh/m^3 higher than the calculated 0.283 kWh/m^3.

The installation of a Pelton wheel type ERT is the only turbine based ERD that can be simulated with WinFlows®. The configuration is shown in Figure 69 below.

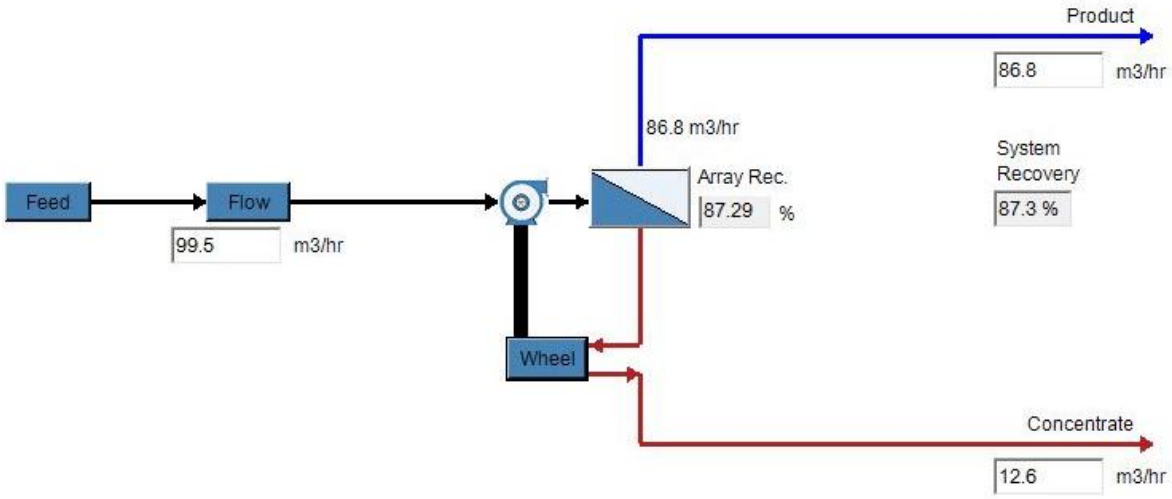

Figure 69: Second RO stage simulation with ERT installed

The results from the Pelton wheel turbine are shown below in Figure 70.

Input Parameters

Parameter	Unit	Value
Discharge Pressure	kPa	202.600
Cost of Power	$/kWh	0.130
RO Permeate Flow	m3/hr	86.883
RO Recovery Rate	%	87.300
RO Feed Pressure	kPa	1115.509
Membrane Differential Pressure	kPa	175.544
Feedwater Salinity	mg/l	0.231
HP Pump Efficiency	%	89.000

Pelton Wheel Performance

Parameter	Unit	Value
Turbine Efficiency	%	65.000
Net Transfer Efficiency	%	57.850
Electricity Generated (Mechanical Energy Recovered)	kW	1.680
HP Pump Shaft Power	kW	26.655
HP Motor Shaft Power	kW	24.975
HP Motor Electrical Power	kW	26.016
Power Savings	kW	2.608
Total Power Consumption	kW	26.016
Specific Power Consumption	kWh/m3	0.299

Figure 70: Simulated results from second RO stage with ERT

The efficiency of the turbine is set at 65%. This gives a SEC of 0.299 kWh/m^3 which is 0.009 kWh/m^3 higher than the calculated 0.290 kW/m^3.

The comparison between the simulation results and calculations done in Chapters 5, 6 and 7 is summarised in Table 35.

Table 35: Comparison between the simulated and calculated results for the second RO stage

	Calculations			Simulation		
	No ERD	PES	ERT	No ERD	PES	ERT
SEC (kWh/m^3)	0.307	0.283	0.290	0.31	0.288	0.299

The results from the simulations are within the accuracy boundaries as discussed in Section 7.3.

7.4 Conclusion

The results from literature and the simulated results from WinFlows® are within the specification (as discussed in Section 7.3) with regards to the calculated results.

The difference between the calculated and simulated results was within the accuracy limits as stated by the Texas Water Development Board (2014) for computer models for all the calculated values.

The installation of an ERD does improve the SEC in both the first and the second RO stages. A PES installation proves to be more efficient in the reduction of the SEC than an ERT.

Chapter 8

Conclusion and Recommendations

This chapter concludes the research and according to the findings presents recommendations. These changes include the installation of a PES on the brine stream of each of the RO skids.

8.1 Consolidation of the work done

The relevance of the research is exaggerated by the fact that water is available for use in a finite amount. The water used today is the same water consumed throughout history. It is not replenished, it is merely recycled.

In the process of electricity generation, water is used as the working fluid to transport energy from the fuel to the turbine. This water has to be ultrapure in order to reduce maintenance cost on the boilers. Different methods have been used to produce demineralised water. Desalination through RO offers an environmentally friendly design with low operating cost compared to traditional methods such as ion exchange.

The low efficiency and high energy consumption of RO desalination plants can be improved with the use of energy recovery devices (ERDs).

Due to the current energy crisis and the drive to conserve natural resourses through energy management, ERDs have been used successfully in seawater desalination plants to reduce the energy demands of membrane based desalination plants.

This research postulates the novelty to include ERDs in fresh water applications even though these plants operate at lower pressures and at higher recoveries than its seawater counterparts. This reduces the energy flow in the brine stream of the RO plant and may prevent the use of energy recovery devices for fresh water applications. This contribution could transform the ultrapure water production industry.

The results of the mathematical formalisation and modelling was an exergy analysis that determined throttling valves on the brine stream of both RO stages can be replaced with a PES to recover the energy in the high pressure stream.

The two types of ERDs most commonly used in industry are ERTs and PESs. These are usually installed on the brine streams of an RO plant, replacing the throttling valve.

A PES has a higher efficiency of 95% as opposed to the 65% of the ERTs.

Installing a PES will improve the Second Law efficiency of the first stage RO to 4.88%. This is an improvement of 25.6%. The Second Law efficiency is improved by 12.2% to 309.7 Wh/m^3.

For the second RO stage, the PES improves the Second Law efficiency with 18.1% to 4.355% whereas the SEC is improved with 7.7% to 283 Wh/m^3.

Through the design search process the installation of a PES was preferred over an ERT due to the fact that an ERT does not improve the SEC or Second Law efficiency as dramatically as the PES does. For the first RO stage, the Second Law efficiency is improved by 9.9% whereas the SEC is improved by 8.4% with the installation of an ERT and the second stage RO efficiency is improved with 5.4% and the SEC is improved with 5.35%.

The recovery set-point of the RO skids will play a major part in the amount of energy that can be recovered by the ERD. If the recovery is below 80%, the pressure in the brine stream is low, causing less energy to be transferred by the ERD.

For recoveries above 90%, the specific exergy will be high due to the high brine pressure. The exergy flow, however, will be low due to the low mass flow rate. This low exergy flow causes less energy to be transferred by the ERD.

In order to maximise the benefits of this plant, the recoveries of the RO sections should therefore be between 80% and 90%.

Financially, the power station can save up to R5.45 million over the 20 year life span of the plant from the installation of a PES on both the RO stage brine streams. The company can save in excess of R20.19 million over the same 20 year period. The payback period for the initial capital investment of R3.2 million is calculated to be 7 years.

By simulating the results on WinFlows® and making an informed argument from literature, the results were evaluated.

8.2 Aspects meriting further investigation

It is recommended that a PES be installed on all the first and second stage RO skids. These PES's are to be installed on the brine stream of the process and should substitute the throttling valve. The process should also be optimised to operate at a recovery between 80% and 90% in order to maximise the energy recovered by the PES's.

8.3 Validation in terms of objectives

The work presented here satisfies the objectives that were set in paragraph 1.2. These objectives can be aligned with the seven guidelines for a design based research as stated in paragraph 1.3:

1. Establish the design as an artefact

   The feasibility of the design was proven in Chapter 6 where it was determined that the installation of a PES on the brine stream of both the first and second RO stages will improve the SEC and Second Law efficiency of the desalination plant.

2. Problem relevance

   Throughout Chapters 1 and 2 the criticality of water conservation as well as the significance of the energy efficiency of desalination plants was emphasised. Water is a finite resource that will grow in scarcity over the coming generations. This, coupled with the high energy consumption of desalination plants ensures that the problem statement is relevant to an ever expanding industry.

3. Design evaluation

   The proposed designs were evaluated with the use of mathematical modelling in Chapters 5 and 6. An informed argument was made through correlations with previous studies in Chapter 7. This chapter also contained simulation results which validated the design.

4. Research contribution

   The novelty of installing ERDs on fresh water desalination plants was evaluated in this study. This is of significant value to the desalination and demineralised water production industries. The study proved that the inherently inefficient design of membrane based demineralisation plants can be improved by installing ERDs on high recovery desalination plants.

5. Rigorous method application

   The design method implemented was rigorous to the extent that results from previous research were utilised (Chapters 2 and 3) together with intensive mathematical modelling (Chapters 5 and 6) and simulations using WinFlows® (Chapter 7).

6. Design search process

   The feasibility of the design was tested through not only the installation of a PES but also ERTs (Chapter 6). These two designs were evaluated and through the design search process, the PES was chosen as the most efficient design that satisfies all process variables.

7. Communication

   The results from the investigation are unambiguously presented in a scientific report.

Simulation is indeed a powerful technique for deriving, from our knowledge of the mechanisms governing the behaviour of ERDs in fresh water applications, a theory for reducing energy consumption.

References

Al-Shammiri, M., Safar, M. & Al-Dawas, M., 2000. Evaluation of two different antiscalant in real operation at the Doha research plant. *Desalination,* 1(128):1-16.

Al-Zahrani, A., Orifi, J., Al-Suhaibani, B. & Al-Ansary, A. 2012, Thermodynamic analysis of a reverse osmosis desalination unit with energy recovery system. *Procedia Engineering,* 1(33):404-141.

Aljundi, I., 2009. Second-law analysis of a reverse osmoisis plant in Jordan. *Desalination,* 1(239):207-215.

American Water Works Association, 1999. *Water Quality and Treatment.* 5 ed. New York: McGraw-Hill.

Arar, O., Yuksel, U., Kabay, N. & Yuksel, M., 2013. Demineralisation of geothermal water reverse osmosis permeate by electrodeionisation with layerd bed configuration. *Desalination,* 1(317):48-45.

Bae, H., Kim, H., Jeong, S. & Lee, S., 2011. Changes in the relative abundace of biofilm-forming bacteria by conventional sand-filtration and microfiltration as pretreatments for seawater reverse osmosis desalination. *Desalination,* 1(273):258-266.

Bartels, C., Franks, R., Rykbar, R., Schierach, M. & Wilf, M., 2005. The effect of feed ionic strength on salt passage through reverse osmosis membranes. *Desalination,* 1(184):185-195.

Blanco-Marigorta, A., Masi, M. & Manfrida, G., 2014. Exergo-environmental analysis of a reverse osmoisis desalination palnt in Gran Canaria. *Energy,* 1(76):223-232.

Betz Inc., 1991. *Industrial water conditioning.* 9th ed. Trevose: Betz Laboratories Inc..

Cerci, Y., 2002. Exergy analysis of a reverse osmosis desalination plant in California. *Desalination,* 3(142):257-266.

Munir, C., 1998. *Ultrafiltration and Microfiltration Handbook.* 2 ed. Boca Raton: CRC Press.

Clifford, D. A. & Letterman, R. D., 1999. *Water quality and treatment: A handbook of community water supplies.* New York: McGraw-Hill.

Cuda, P., Pospisil, P. & Tenglerova, J., 2006. Reverse osmosis in water treatment for boilers. *Desalination,* 1(198):41-46.

Dey, A. & Thomas, G., 2003. *Electronics grade water preparation.* 1 ed. Littleton: Tall Oaks Publishing Co.

Doulton USA, 2008. *Activated carbon for drinking water.* [Online]
Available at: http://doultonusa.com/HTML%20pages/activated_carbon_water_filtration.htm
[Accessed 1 October 2013].

DOW Chemical Company, 2004. *Water chemistry and pretreatment: Biological fouling prevention of FilmTec elements and DBNPA.* s.l.:DOW Chemical Co.

DOW Chemical Company, 2007. *FilmTec reverse osmosis technical manual.* s.l.:DOW liquid separations.

DOW Chemical Company, 2013. *DOWEX Marathon Anion Exchange resin,* Product Information: DOW Chemical company.

DOW Chemical Company, 2013. *DOWEX Marathon Cation Exchange resin,* Product information: Strong acid cation exchange resin.

El-Emam, R. & Dincer, I., 2013. Thermodynamic and thermoeconomic analyses of seawater reverse osmosis desalination plant with energy recovery. *Energy.* 1(64):154-163.

Engineering Toolbox, 2013. *The Engineering Toolbox.* [Online]
Available at: http://www.engineeringtoolbox.com/air-altitude-pressure-d_462.html
[Accessed 5 May 2014].

Farooque, A. M. *et al.*, 2008. Parametric analyses of energy consumption and losses in SWCC SWRO plants utilizing energy recovery devices. *Desalination,* 1(219):137-159.

Flynn, D. J., 2009. *The Nalco Water Handbook.* 3 ed. New York: McGraw Hill.

Fues, P. & Kucera, J., 2007. *High-efficiency filtration for membrane pretreatment.* s.l., 68th International Water Conference.

Geisler, P., Krumm, W. & Peters, T. A., 2001. Reduction of energy demand for seawater RO with the pressure exchange system PES. *Desalination,* 1(135):205-210.

General Electric, 2003. *Winflows.* [Online]
Available at: http://www.gewater.com/winflows.jsp
[Accessed 31 August 2014].

Glater, J., 1998. The early history of reverse osmosis membrane development. *Desalination,* 1(117).

Greenlee, L., Lawler, D., Freeman, D., Marriot, B. & Moulin, P., 2009. Reverse osmosis desalination: Water sources, technology and today's challenges. *Water research,* 1(43):2317-2348.

Henver, A., March, S., Park, J. & Ram, S., 2004. Design Science in information systems research. *MIS Quarterly,* 1(28):75-105.

Huang, H., Cho, H., Schwab, K. & Jacangelo, J., 2011. Effects of feedwater pretreatment on the removal of organic microconstituents by a low fouling reverse osmosis membrane. *Desalination,* 1(281):446-454.

Hwang, S. & Kammermeyer, K., 1984. *Membrane Separations.* 1 ed. Malabar: Robert E. Krieger Publishing Co.

Kahraman, N., Cengel, Y., Wood, B. & Cerci, Y., 2004. Exergy analysis of a combined RO, NF and EDR desalination plant. *Desalination.* 1(171):217-232.

Kremser, U., Drescher, G., Otto, S. & Recknagel, V., 2006. First operating experience with the treatment of 3100m3/day of Elbe river water by means of reverse osmosis to produce process water and demineralised water for use in the industry. *Desalination,* 1(189):53-58.

Kucera, J., 2010. *Reverse Osmosis: Design, Processes and Application for Engineers.* Hoboken: Wiley and Sons.

Le Gouellec, Y. & Elimelech, M., 2002. Calcium Sulfate (gypsum) scaling in nanofiltration of agricultural drainage water. *Journal of Membrane Science,* 1(205):279-291.

Liu, C., Rainwater, K. & Song, L., 2011. Energy analyses and efficiency assessment of reverse osmosis desalination process. *Desalination,* 1(276):352-358.

Lonsdale, H., Merten, U. & Riley, R., 1965. Transport properties of cellulose acetate osmotic membranes. *Journal of applied polymer science,* Volume 9.

Macedonio, F. & Drioli, E., 2010. An exergetic analysis of a membrane desalination system. *Desalination,* 1(261):293-299.

Malaeb, L. & Ayoub, G. M., 2011. Reverse osmosis technology for water treatment: State of the art review. *Desalination,* 1(267):1-8.

Ma, W., Zhao, Y. & Wang, L., 2007. The pretreatment with enhanced coagulation and UF membrane for seawater desalination with reverse osmosis. *Desalination,* 1(203):256-259.

Mehdizadeh, H., 2006. Membrane desalination plants from an energy-exergy viewpoint. *Desalination.* 1(191):200-209.

Meltzer, T. H., 1992. *High-Purity Water Preparation.* 1 ed. Littleton: Tall Oaks Publishing Company.

Morelli, C., 1996. *Basic principles of water treatment.* 1 ed. Littleton,CO: Tall Oaks Publishing Co.

Nermatollahi, F., Rahimi, A. & Gheinani, T., 2013. Experimental and theoretical energy and exergy analysis for a solar desalination system. *Desalination.* 1(317):23-31.

NIST, 2014. *The NIST reference on constants, units, measurements and uncertainty.* [Online] Available at: http://physics.nist.gov/cuu/Uncertainty/basic.html
[Accessed 27 August 2014].

Penate, B. & Garcia-Rodriguez, L., 2010. Energy optimisation of existing SWRO (seawater reverse osmosis) plants with ERT (energy recovery turbines): Technical and thermoeconomic assessment. *Energy*,1(36):613-626.

Perry, R. & Green, D., 1997. *Perry's Chemical Engineers' Handbook.* New York: McGraw Hill.

Pororov, A. & Kornilova, N., 2011. Intensive demineralisation through ion exchange. *Filtration and Separation,* 48(2):36-40.

Rautenbach, R., Linn, T. & Al-Gobaisi, D. M. K., 1997. Present and future pretreatment concepts - Strategies for reliable and low maintenance reverse osmosis seawater desalination. *Desalination,* 1(110):97-106.

Romero-Ternero, V., Garcia-Rodriguez, L. & Gomez-Camacho, C., 2005. Thermoeconomic analysis of wind powered seawater reverse osmosis desalination in the Canary Islands. *Desalination.* 1(186):291-298.

Rosberg, R., 1997. Ultrafiltration, a viable cost-saving pretreatment for reverse osmosis and nanofiltration- A new approach to reduce cost. *Desalination,* 1(110):107-114.

Sagle, A. & Freeman, B., 2004. *Fundamentals of membranes for water treatment.* The future of desalination in Texas, Texas water development board, Austin.

Sharqawy, M. H., Zubair, S. M. & Lienhard, J. H., 2011. Second Law analysis of reverse osmosis desalination plants: An alternative design using pressure retarded osmosis. *Energy,* 1(36):6617-6626.

Singh, R., 2006. *Hybrid membrane systems for water purification.* 1 ed. Amsterdam: Elsevier.

Sorin, M., Jedrzejak, S. & Bouchard, C., 2006. On maximum power of reverse osmosis separation processes. *Desalination. 1(190):*212-220.

Texas Water Development Board, 2011. *Energy optimisation of brackish groundwater reverse osmosis desalination,* Austin: Texas Water Development Board.

Texas Water Development Board, 2014. *Texas water development board.* [Online]
Available at:
https://www.twdb.state.tx.us/publications/reports/contracted_reports/doc/1148321310_Part%20II_Performance%20Evaluation.pdf
[Accessed 2 September 2014].

United Nations, 2012. *Water resources.* [Online]
Available at: http://www.unwater.org/statistics_res.html
[Accessed 16 September 2013].

US Geological Survey, 2004. *Estimated use of water in the United States in 2000,* s.l.: USGS Circular 1268.

Vidojkovic, S. *et al.*, 2013. Extensive feedwater quality control and monitoring concept for preventing chemistry-related failures of boiler tubes in a subcritical thermal power plant. *Applied Thermal Engineering,* 1(59):683-694.

Wenten, I., Khoiruddin, Arfianto & Zudiharto, 2013. Bench scale electrodeionisation for high pressure boiler feed water. *Desalination,* 1(314):109-114.

Wijmans, J. & Baker, R., 1995. The solution-diffusion model: A review. *Journal of Membrane Science,* 1(107):1-21.

Wood, J. & Gifford, J., 2004. *Process and systems design for reliable operations of RO/CEDI systems.* Pittsburgh, Proceedings of the 65th annual inernational water conference.

Wood, J., Gifford, J., Arba, J. & Shaw, M., 2009. Production of ultrapure water by continuous electrodeionisation. *Desalination,* 1(250):973-976.

Yokogama, 2014. *Yokogama.* [Online]
Available at: http://cdn2.us.yokogawa.com/EJX630A_GS__08_.pdf
[Accessed 27 August 2014].

Appendices

The following sections will serve as supplementary reading to the previous chapters.

Appendix A: Ion Exchange

A.1 Ion exchange process

Ion exchange is the process where an ion in a mixture, is exchanged for an ion in either an aqueous form or on a resin (Flynn, 2009). For the production of demineralised water, this process usually consists of cation filters, degassers, anion filters and mixed bed filters (Clifford & Letterman, 1999). If raw water is used to produce demineralised water, pretreatment is a necessity.

A.1.2 Ion exchange filters

The earliest methods to prohibit or reduce scaling of heat exchange equipment that utilises water, was done with ion exchange through sodium aluminosilicates (Kucera, 2010). The advances in polymeric science introduced the industry to polymeric ion exchange resins. These polymers were produced at lower cost and the regenerative capabilities of the resin made it an attractive option for ion exchange processes (Kucera, 2010).

The ion exchange process for demineralised water production consists of a cation filter, degasser, anion filter and mixed bed filters. This configuration is the most commonly used due to the higher exchange efficiency and lower capital cost (Kucera, 2010).

A.1.2.1 Cation exchange

Cation exchange is the process where cations from water, for example sodium, potassium and calcium, are exchanged for hydrogen ions from a polymeric resin (Flynn, 2009). The cation exchange vessel is a stainless steel tank containing the strong acid resins (Kucera, 2010). The water from the sand filters is pumped to the top of this vessel and the water is evenly distributed with a set of sprayers (Flynn, 2009). This allows an even flow of water through all parts of the resin bed (Flynn, 2009).

The resins consist of long chain polymers with a hydrogen functional group (Flynn, 2009). The affinity of the resin for the cation is higher than for the hydrogen, as seen in Table 36 (Flynn, 2009). The higher affinity cations, displace the hydrogen in the resin and attach to the polymer (Flynn, 2009). The hydrogen is then released into solution with the water (Flynn, 2009).

Table 36: Affinity of normal cations and ions towards resins (Flynn, 2009)

Cations	Anions	Affinity
Fe^{3+}	CrO_4^{2-}	Highest

Pb^{3+}	SO_4^{2-}	
Cu^{2+}	NO_3^-	
Ca^{2+}	NO_2^-	
Mg^{2+}	Br^-	
K^+	Cl^-	
Na^+	HCO_3^-	
H^+	OH^-	
Li^+	F^-	Lowest

According to this, the cations with the highest affinity will attach to the resin first and displace the cations with the lowest affinity (Flynn, 2009). Lithium ions are not removed by the cation filter as the affinity for lithium is lower than the affinity for hydrogen (Flynn, 2009).

The exchange reaction is as follows (Clifford & Letterman, 1999):

$$(R)H + Na^+ \rightarrow (R)Na + H^+$$ **Equation 55**

Where R is the polymeric resin matrix

Each resin has a set number of hydrogen ions that are able to be substituted. Therefore the resin can be exhausted. The volume of water purified by the cation filter before exhaustion will vary according to the quality of the water (Clifford & Letterman, 1999).

The capacity of a resin is expressed as equivalents per litre (eq/ℓ). To calculate the ionic load for a resin, the individual ions have to be expressed as their calcium carbonate equivalents in terms of milligrams per litre (mg/ℓ as $CaCO_3$). Applicable ions are then totalled and converted to grams per litre (g/ℓ). The total exchangeable cations (TEC) is the sum of all cations removed by the resin (Flynn, 2009).

Typical strong acid cation exchange resins have a sulfonic acid functional group with a styrene gel matrix. The total exchange capacity is typically 1.8eq/ℓ. A bed depth of 800mm is advisable (DOW Chemical Company, 2013).

To calculate the volume of water to be cleaned by a resin before regeneration, Equation 57 is used.(Flynn, 2009)

$$V = \frac{Exchange\ Capacity}{ionic\ load}$$ **Equation 56**

Or

$$V = \frac{(resin\ capacity)(resin\ volume)}{ionic\ load}$$ **Equation 57**

Where V = the volume water that can theoretically be treated (l)

Exchange capacity = resin ion exchange capacity (g/ℓ as $CaCO_3$)

Ionic load = ions equivalents to be exchanged (g/ℓ as $CaCO_3$)

Resin capacity = resin ion exchange ability (g $CaCO_3$/ℓ)

Resin volume = Volume of the resin bed (ℓ)

After the theoretical volume has been treated, a regeneration process is required to reinstate the exchange capacity of the cation resin. This is generally done by flushing the resin with 5 times the resin volume of an 8% sulphuric acid solution (DOW Chemical Company, 2013). This can either be done co-currently or counter-currently.

The resins can be regenerated until the end of its lifetime, which is between 10 to 15 years (Flynn, 2009).

The first signs that regeneration is necessary will be the inability to remove the cations with the lowest affinity. From Table 36 it is visible that if sodium and potassium concentrations in the product streams rise, regeneration is required (Flynn, 2009).

The regeneration process consumes large amounts of strong acids, which is costly and poses environmental risks (Flynn, 2009).

In the presence of calcium carbonate ($CaCO_3$), carbon dioxide will form as a product of cation exchange (American Water Works Association, 1999).

$$(R)H + CaCO_3 \rightarrow (R)Ca + 2H^+ + {CO_3}^{2-}$$ **Equation 58**

This forms carbon dioxide which needs to be removed. The removal of carbon dioxide is done using a degasser or decarboniser (Pororov & Kornilova, 2011).

A.1.2.2 Degasser

The degasser atomises the water through sprayers at the top. The water comes into contact with a packing layer. Air is forced through the vessel from the bottom by a blower. This removes the carbon dioxide and other gases trapped in the water (Flynn, 2009).

The water from the degasser is high in unwanted anions with a pH of 3 (Flynn, 2009). As demineralised water has a neutral pH, the unwanted anions need to be removed and replaced by hydroxide ions, which will restore the pH (Meltzer, 1992).

Water from the degasser is fed to the anion exchange unit (Pororov & Kornilova, 2011). This process will remove all unwanted anions and replace it with hydroxide ions (Flynn, 2009). This will restore the pH that was lowered in the cation exchange process.

A.1.2.3 Anion exchange

The anion exchange process is divided into two sub-processes, weak base anion (WBA) and strong base anion (SBA) (Pororov & Kornilova, 2011).

The SBA unit removes both strong mineral acids and weak acids produced by the cation exchange process. This includes carbonic and silicic acid. The ion exchange reaction is as follows (Flynn, 2009):

$$Cl^- + (R)OH \rightarrow (R)Cl + OH^-$$ **Equation 59**

The hydroxide ion that is released into solution will then react with the hydrogen ion released by the cation exchange resin the produce water (American Water Works Association, 1999).

$$2H^+ + OH^- \rightarrow H_2O$$ **Equation 60**

The resins typically consist of a styrene gel matrix with a quaternary amine functional group. The exchange capacity is 1 eq/ℓ (DOW Chemical Company, 2013).

Regeneration is done with a 5% sodium hydroxide concentration at a volume of 6 bed volumes. The typical bed depth used is 800mm (DOW Chemical Company, 2013).

During regeneration, the ion exchange process is reversed and the product water is high in unwanted anions. This process uses large amounts of chemicals (Flynn, 2009).

From Table 36 it is evident that the need for regeneration will be determined by the concentration of HCO_3^- and Cl^- in the product stream (Flynn, 2009). These ions have a lower affinity for the resin and will therefore be readily displaced by ions such as SO_4^-. Fluoride ions will not be removed by the anion exchange process (Flynn, 2009).

The quality of the raw water will determine if SBA or WBA or both processes are used. (Flynn, 2009)

A.1.2.4 Mixed bed filters

Mixed Bed filters form the final stage in the demineralisation process. This stage is a combination of cation and anion exchange. It serves as a polishing plant to produce ultrapure water (Meltzer, 1992).

The resins, made up of strong acid cation and SBA resins, are homogeneously mixed. Regeneration of the mixed bed is always preceded by backwashing. Due to the difference in density between the cation and anion exchange resins, separation is possible during backwashing. The cation resin will remain on the bottom of the vessel while the SBA resin will collect at the top. The resins are then manually separated and separately regenerated (Meltzer, 1992).

The particle size distribution of the resin is crucial in effective polishing. The resin beads should have the same size to prevent separation during normal operation. The backwash stage will fluidise the resin bed to allow particle separation (Flynn, 2009).

The ion exchange process is systematically replaced by reverse osmosis. The reverse osmosis is regarded as a process that poses less environmental risks and has less effluent discharge than the older ion exchange process (Kucera, 2010).

Appendix B: Exergy Balance Calculations

Appendix B shows the spreadsheets and gives some sample calculations from the exergy balance. A list of symbols is included. The sample calculations are done for the values encircled in red on the spreadsheet.

Table 37: List of symbols for calculations in Appendix B

Symbol	Description	Unit
P	Density	kg/m^3
η	Efficiency	%
π	Osmotic Pressure	kPa
ψ	Specific Exergy	kJ/kg
x	Mole Fraction	Fraction
mf	Mass fraction	Fraction
h	Specific Enthalpy	kJ/kg
s	Specific Entropy	kJ/KgK
T	Temperature	K
P	Pressure	kPa
¥	Exergy flow	kW
F	Volumetric Flow	m^3/s
m	Mass Flow	kg/s
SEC	Specific energy consumption	kW/m^3
W	Work	kW
S	Salinity	Ppm
R_g	Universal gas constant	J/molK
c	Concentration	mg/ℓ
R	Recovery	%

The following subscripts were used in the calculations:

Table 38: List of subscripts used in the calculations

Subscript	Description
sw	Salt water – Water with a high salinity
w	Water
s	Salt
0	Initial state
Brine	Brine stream conditions
Feed	Feed stream conditions
Permeate	Permeate stream conditions
atm	Atmospheric conditions
ERD	Energy recovery device
Original	Original design conditions
PES	Design with the PES incorporated

Table 39: Exergy balance calculations

Stream	Temperature (^{0}C)	Temperature (K)	Pressure (Pa)	Flow rate (m^3/h)	ρ_{sw}	Mass flow (kg/s)	Chlorine Content	Salinity (ppm)	mfs	mfw	xs	xw	hs	ss	hw	sw	h	s	Exergy	Exergy Flow
1	22.4	295.55	98600	330	1000.05	91.67167119	39.49	71.342634	7.13426E-05	0.99992866	7.1343E-05	0.99992866	12.552	0.04473	93.97	0.3303	93.9641914	0.33653608	0	0
2	22.4	295.55	0	0	1000.05	0	39.49	71.342634	7.13426E-05	0.99992866	7.1343E-05	0.99992866	12.552	0.04473	93.97	0.3303	93.9641914	0.33653608	0	0
3	22.4	295.55	400000	0.008	1000.00	0.002222222	0	0	0	1	#DIV/0!	#DIV/0!	12.552	0.04473	94.25	0.3302	94.25	#DIV/0!	#DIV/0!	#DIV/0!
4	22.4	295.55	400000	0	1000.00	0	0	0	0	1	#DIV/0!	#DIV/0!	12.552	0.04473	94.25	0.3302	94.25	#DIV/0!	#DIV/0!	#DIV/0!
5	22.4	295.55	400760	330	1000.05	91.67167119	39.49	71.342634	7.13426E-05	0.99992866	7.1343E-05	0.99992866	12.552	0.04473	94.25	0.3302	94.2441714	0.33643609	0.30953292	28.3753997
6	22.4	295.55	0	0	1000.05	0	39.49	71.342634	7.13426E-05	0.99992866	7.1343E-05	0.99992866	12.552	0.04473	93.97	0.3303	93.9641914	0.33653608	0	0
7	22.4	295.55	0	0	1000.05	0	39.49	71.342634	7.13426E-05	0.99992866	7.1343E-05	0.99992866	12.552	0.04473	93.97	0.3303	93.9641914	0.33653608	0	0
8	22.4	295.55	100000	165.06	1000.05	45.85250317	39.49	71.342634	7.13426E-05	0.99992866	7.1343E-05	0.99992866	12.552	0.04473	93.97	0.3303	93.9641914	0.33653608	0	0
9	22.4	295.55	100000	165.0632	1000.05	45.85339211	39.49	71.342634	7.13426E-05	0.99992866	7.1343E-05	0.99992866	12.552	0.04473	93.97	0.3303	93.9641914	0.33653608	0	0
10	22.4	295.55	128680	165.0632	1000.05	45.85339211	39.49	71.342634	7.13426E-05	0.99992866	7.1343E-05	0.99992866	12.552	0.04473	93.99	0.33	93.98419	0.33623611	0.10865725	4.98230338
11	22.4	295.55	128680	165.0632	1000.05	45.85339211	39.49	71.342634	7.13426E-05	0.99992866	7.1343E-05	0.99992866	12.552	0.04473	93.99	0.33	93.98419	0.33623611	0.10865725	4.98230338
12	22.4	295.55	200000	0.0032	1000.00	0.000888889	0	0	0	1	#DIV/0!	#DIV/0!	12.552	0.04473	94.06	0.3303	94.06	#DIV/0!	#DIV/0!	#DIV/0!
13	22.4	295.55	59200	165.0632	1000.05	45.85339211	39.49	71.342634	7.13426E-05	0.99992866	7.1343E-05	0.99992866	12.552	0.04473	93.93	0.33	93.9241943	0.33623611	0.04866153	2.23129613
14	22.4	295.55	0	0	1000.00	0	0	0	0	1	#DIV/0!	#DIV/0!	12.552	0.04473	93.97	0.3272	93.97	#DIV/0!	#DIV/0!	#DIV/0!
15	22.4	295.55	200000	0.000162	1000.00	0.000045	0	0	0	1	#DIV/0!	#DIV/0!	12.552	0.04473	94.06	0.3302	94.06	#DIV/0!	#DIV/0!	#DIV/0!
16	22.4	295.55	100000	110.58	1000.05	30.71834364	39.49	71.342634	7.13426E-05	0.99992866	7.1343E-05	0.99992866	12.552	0.04473	93.97	0.3303	93.9641914	0.33653608	0	0
17	22.4	295.55	1037840	110.58	1000.05	30.71834364	39.49	71.342634	7.13426E-05	0.99992866	7.1343E-05	0.99992866	12.552	0.04473	94.84	0.3301	94.8341294	0.3363361	0.92904371	28.5386841
18	22.4	295.55	25960	95.32	1000.00	26.4777816	0.10447	0.188735502	1.88736E-07	0.99999981	1.8874E-07	0.99999981	12.552	0.04473	93.62	0.3303	93.6199847	0.33032581	1.4912397	39.4847192
19	22.4	295.55	1053900	15.26	1000.39	4.240542056	285.4105768	515.622748	0.000515623	0.99948438	0.00051562	0.99948438	12.552	0.04473	94.86	0.3301	94.8175601	0.36669096	-8.05890397	-34.1741212
20	22.4	295.55	244540	99.472	1000.00	27.63111111	0.10447	0.188735502	1.88736E-07	0.99999981	1.8874E-07	0.99999981	12.552	0.04473	94.1	0.3303	94.0999846	0.33032581	1.97123961	54.4675408
21	22.4	295.55	400000	0	1000.00	0	0	0	0	1	#DIV/0!	#DIV/0!	12.552	0.04473	94.25	0.3302	94.25	#DIV/0!	#DIV/0!	#DIV/0!
22	22.4	295.55	1346360	99.472	1000.00	27.63111111	0.10447	0.188735502	1.88736E-07	0.99999981	1.8874E-07	0.99999981	12.552	0.04473	95.13	0.33	95.1299844	0.33002581	3.0899044	85.3774919
23	22.4	295.55	284920	86.832	1000.00	24.12	0.00331	0.005979846	5.97985E-09	0.99999999	5.9798E-09	0.99999999	12.552	0.04473	94.14	0.3302	94.1399995	0.33020099	2.04814532	49.401265
24	22.4	295.55	697680	86.832	1000.00	24.12	0.00331	0.005979846	5.97985E-09	0.99999999	5.9798E-09	0.99999999	12.552	0.04473	94.52	0.3301	94.5199995	0.33010099	2.45770031	59.2797316
25	22.4	295.55	112600	73.76	1000.00	20.48888889	0.00063	0.001138158	1.13816E-09	1	1.1382E-09	1	12.552	0.04473	93.98	0.3303	93.9799999	0.3303002	1.85882283	38.0852144
26	22.4	295.55	0	0	1000.00	0	0	0	0	1	#DIV/0!	#DIV/0!	12.552	0.04473	93.97	0.3303	93.97	#DIV/0!	#DIV/0!	#DIV/0!
27	20	293.15	0	0	1000.00	0	0	0	0	1	#DIV/0!	#DIV/0!	10.54368	0.03790706	93.97	0.3303	93.97	#DIV/0!	#DIV/0!	#DIV/0!
28	22.4	295.55	748480	12.64	1000.00	3.511111111	0.799400785	1.444197458	1.4442E-06	0.99999856	1.4442E-06	0.99999856	12.552	0.04473	94.57	0.3301	94.5698815	0.33027307	2.45672531	8.62583555
29	20	293.15	0	0	1000.00	0	0	0	0	1	#DIV/0!	#DIV/0!	10.54368	0.03790706	93.97	0.3303	93.97	#DIV/0!	#DIV/0!	#DIV/0!
30	22.4	295.55	89300	13.072	1000.00	3.631111111	0.018432154	0.03329953	3.32995E-08	0.99999997	3.33E-08	0.99999997	12.552	0.04473	93.96	0.3303	93.9599973	0.33030503	1.83739268	6.67177696
34	22.4	295.55	830000	19.692	1000.22	5.47	39	2.93E+02	2.93E-04	0.999707	0.000293	0.999707	12.552	0.04473	94.65	0.33	94.6259453	0.35216976	-3.95877921	-21.6545223
35	22.4	295.55	1149000	19.692	1000.22	5.47	39	2.93E+02	2.93E-04	0.999707	0.000293	0.999707	12.552	0.04473	94.94	0.33	94.9158603	0.35216976	-3.66886418	-20.0686871
36	22.4	295.55	25960		1000.00	3.2298	39	0.188735502	1.88736E-07	0.99999981	1.8874E-07	0.99999981	12.552	0.04473	93.62	0.3301	93.6199847	0.33012581	1.55034969	5.00731944

Density calculation

$$\rho_{sw} = \rho_w + mf_s(a_1 + a_2T + a_3T^2 + a_4T^3 + a_5mf_sT^2)$$

$$\rho_{sw} = 1000 + 7.13462 \times 10^{-5}((82.02) + (-2.001).4 + (0.01677)22.4^2 + (-3.06 \times 10 - 5)(22.4)^3 + (-1.613 \times 10^{-5})(7.13462 \times 10^{-5})(22.4^2))$$

$$\rho_{sw} = 1000.05 kg/m^3$$

Salinity calculation

$$S = 1.8066 [Cl^-]$$

$$S = 1.8066(39.49)$$

$$S = 71.34 \text{ ppm}$$

Mole fraction Salt

$$x_s = \frac{M_w}{M_w\left(\frac{1}{mf_s} - 1\right) + M_w}$$

$$x_s = \frac{18.02}{18.02\left(\frac{1}{7.1343\times10^{-5}} - 1\right) + 18.02}$$

$$x_s = \frac{18.02}{18.02\left(\frac{1}{7.3426\times10^{-5}} - 1\right) + 18.02}$$

$$x_s = 7.1314 \times 10^{-5}$$

Mole fraction Water

$$x_w = 1 - x_s$$

$$x_w = 1 - 7.1314 \times 10^{-5} = 0.99992864$$

Enthalpy of salt in water

$$h_s = h_{s0} + C_{ps}(T - T_0)$$

$$h_s = 12.552 + 0.8368(295.55 - 295.55)$$

$$h_s = 12.552\ kJ/kg$$

Entropy of salt in water

$$s_s = s_{s0} + C_{ps}\ln(^{T}/_{T_0})$$

$$s_s = 0.0447 + 0.8368\ln(^{295.55}/_{295.55})$$

$$s_s = 0.0447\ kJ/kgK$$

Enthalpy of solution

$$h = mf_s h_s + mf_w h_w$$

$$h = 7.13462 \times 10^{-5}\ (12.552) + (0.99992866\ )93.99$$

$$h = 93.9841\ kJ/kg$$

Entropy of solution

$$s = mf_s s_s + mf_w s_w - R(x_s lnx_s + x_w lnx_w)$$

$$s = 7.13462 \times 10^{-5}(0.0447) + 0.99992866(0.33) - 8.314((7.1314 \times 10^{-5})\ln(7.1314 \times 10^{-5}) + 0.99992864ln0.99992864)$$

$$s = 0.336236\ kJ/kgK$$

Specific Exergy

$$\Psi = h - h_0 - T_0(s - s_0)$$

$$\Psi = 93.9841 - 93.9641 - 295.55(0.336236 - 0.33653608)$$

$$\Psi = 0.10865\ kJ/kg$$

Exergy flow

$$¥ = m\Psi$$

$$¥ = 45.85\ \times 0.10865 = 4.9823\ kW$$

Appendix C: Mass Balance

Table 40: Mass balance

	Average		
Stream	Temperature (°C)	Pressure (kPa)	Flow rate (m^3/h)
1	22.36	98.6	330
2	22.44	0	0
3	22.36	400	0.008
4	22.4	400	0
5	22.36	400.76	330
6	22.6	0	0
7	22.5	0	0
8	22.38	100	165.06
9	22.38	100	165.0632
10	22.38	128.68	165.0632
11	22.38	128.68	165.0632
12	22.48	200	0.0032
13	22.38	59.2	165.0632
14	22.18	0	0
15	22.5	200	0.000162
16	22.4	100	110.58
17	22.4	1037.84	110.58
18	22.4	25.96	95.32
19	22.4	1053.9	15.26
20	22.4	244.54	99.472
21	22.4	400	0
22	22.4	1346.36	99.472
23	22.4	284.92	86.832
24	22.4	697.68	86.832
25	22.4	112.6	73.76
26	22.4	0	0
27	22.4	0	0
28	22.4	748.48	12.64
29	22.4	0	0
30	22.4	89.3	13.072
31	22.4	0	0

A sample from the mass balance over the first RO stage is given below.

$$F_{feed} = F_{permeate} + F_{brine}$$

$$110.58 = 95.32 + F_{brine}$$

$$F_{brine} = 15.26\, m^3/h$$

Appendix D: Salt Balance

Table 41: Salt balance

Stream	Chlorine Content	Mass Flow (kg/s)	Salinity (ppm)	mfs	Mass flow (Salt) (kg/h)
1	39.49	91.671671	71.342634	7.1343E-05	0.006540098
2	39.49	0	71.342634	7.1343E-05	0
3		0.0022222	0	0	0
4		0	0	0	0
5	39.49	91.671671	71.342634	7.1343E-05	0.006540098
6	39.49	0	71.342634	7.1343E-05	0
7	39.49	0	71.342634	7.1343E-05	0
8	39.49	45.852503	71.342634	7.1343E-05	0.003271238
9	39.49	45.853392	71.342634	7.1343E-05	0.003271302
10	39.49	45.853392	71.342634	7.1343E-05	0.003271302
11	39.49	45.853392	71.342634	7.1343E-05	0.003271302
12		0.0008889	0	0	0
13	39.49	45.853392	71.342634	7.1343E-05	0.003271302
14		0	0	0	0
15		0.000045	0	0	0
16	39.49	30.718344	71.342634	7.1343E-05	0.002191528
17	39.49	30.718344	71.342634	7.1343E-05	0.002191528
18	0.10447	26.477782	0.1887355	1.8874E-07	4.9973E-06
19	285.4105768	4.240562	515.622718	0.00051562	0.00218653
20	0.10447	27.631111	0.1887355	1.8874E-07	5.21497E-06
21		0	0		
22	0.10447	27.631111	0.1887355	1.8874E-07	5.21497E-06
23	0.00331	24.12	0.00597985	5.9798E-09	1.44234E-07
24	0.00331	24.12	0.00597985	5.9798E-09	1.44234E-07
25	0.00063	20.488889	0.00113816	1.1382E-09	2.33196E-08
26		0	0		
27		0	0		
28	0.799400785	3.5111111	1.44419746	1.4442E-06	5.07074E-06
29		0	0		
30	0.018432154	3.6311111	0.03329953	3.33E-08	1.20914E-07
31		0	0		

A sample from the mass balance over the first RO stage is given below.

$$m_{salt\ (feed)} = m_{salt(permeate)} + m_{salt\ (brine)}$$

$$mf_{s\ feed} m_{feed} = mf_{s\ perm} m_{perm} + mf_{s\ brine} m_{brine}$$

$$mf_{s\ brine} m_{brine} = (7.13 \times 10^{-5}) \times 30.718 - 1.887 \times 10^{-7} \times 26.47$$

$$mf_{s\ brine} = \frac{(7.13 \times 10^{-5}) \times 30.718 - 1.887 \times 10^{-7} \times 26.47}{m_{brine}}$$

$$mf_{s\ brine} = \frac{(7.13 \times 10^{-5}) \times 30.718 - 1.887 \times 10^{-7} \times 26.47}{4.24}$$

$$mf_{s\ brine} = 0.000515$$

Appendix E: Specific Energy Consumption RO1

Table 42: Specific energy consumption calculations for RO stage 1

R	V deur ERD	Pbrine	Energy	W	SEC PES	SEC ERT	SEC
0	110.58	2996.638	80229.39	0.022285941	0.021171644	0.014486	
0.05	105.051	184529.8	-96238.6	-0.02673294	0.02588828	0.033882	0.051258
0.1	99.522	194781.5	-100400	-0.02788886	0.027639302	0.035978	0.054106
0.15	93.993	206239.2	-104561	-0.02904478	0.029725517	0.03841	0.057289
0.2	88.464	219129.1	-108722	-0.03020069	0.032209775	0.041239	0.060869
0.25	82.935	233737.8	-112884	-0.03135661	0.035171682	0.044545	0.064927
0.3	77.406	250433.3	-117045	-0.03251253	0.038713594	0.048432	0.069565
0.35	71.877	269697.4	-121206	-0.03366844	0.042969357	0.053031	0.074916
0.4	66.348	292172.2	-125368	-0.03482436	0.048117434	0.058523	0.081159
0.45	60.819	318733.3	-129529	-0.03598028	0.054401184	0.06515	0.088537
0.5	55.29	350606.6	-133690	-0.03713619	0.062161307	0.073252	0.097391
0.55	49.761	389562.9	-137852	-0.03829211	0.07188993	0.083322	0.108212
0.6	44.232	438258.3	-142013	-0.03944803	0.084325238	0.096097	0.121738
0.65	38.703	500866.6	-146174	-0.04060395	0.100627241	0.112737	0.13913
0.7	33.174	584344.4	-150336	-0.04175986	0.122729284	0.135174	0.162318
0.75	27.645	701213.3	-154497	-0.04291578	0.154111394	0.166886	0.194781
0.8	22.116	876516.6	-158658	-0.0440717	0.201733619	0.21483	0.243477
0.85	16.587	1168689	-162819	-0.04522761	0.281836075	0.295238	0.324636
0.861953	15.26518995	1269885	-163814	-0.04550396	0.309698122	0.323168	0.352746
0.872929	14.05150394	1379571	-164728	-0.0457577	0.339940812	0.353472	0.383214
0.9	11.058	1753033	-166981	-0.04638353	0.443139107	0.456804	0.486954
0.95	5.529	3506066	-171142	-0.04753945	0.929244447	0.943007	0.973907
1	0	#DIV/0!	#DIV/0!	#DIV/0!	#DIV/0!	#DIV/0!	

The calculation for the SEC and SEC PES is done using Equation 47.

$$P_{Brine} = \Delta\pi = \frac{cR_gT}{1-R} \qquad (Thermodynamic\ Restriction)$$

$$= \frac{71.34 \times 8.314 \times 295.55}{1 - 0.861953}$$

$$= 1269885Pa$$

$$SEC = P_{Brine} \div 3.6 \times 10^6$$

$$= 0.352746\ kWh/m^3$$

The work recovered by the ERD is calculated using the following equation:

$$W = \frac{(P_{atm} - P_{Brine})F_{ERD}}{F_{feed} \times 3.6 \times 10^6}$$

$$= \frac{(83226 - 1269885)15.26518}{110.58 \times 3.6 \times 10^6}$$

$$= -0.0455\ \mathrm{kWh}/m^3$$

This is then used to calculate the SEC with the ERD. The SEC for the PES system is calculated using the following equation:

$$SEC\ PES = W \times \eta_{PES} + (1 + SI)SEC = -0.0455 \times 0.95 + (1 + 0.000513)0.352746$$

$$= 0.30969\ kWh/m^3$$

Appendix F: Specific Energy Consumption RO2

Table 43: Specific energy consumption calculations for RO stage 2

R	Δπ	ΔP_{net}	Δπ	ΔP	SEC	W4	ERT	PES
0	5272.221	NA	2996.638				2996.638	0
0.05	14.68164	1101805	488.1699	1102293	0.306438	0.000136	0.007662	-0.13008
0.1	15.49728	1101805	515.2904	1102320	0.306445	0.000143	0.157106	0.088338
0.15	16.40889	1101804	545.6016	1102349	0.306453	0.000152	0.20693	0.161154
0.2	17.43444	1101803	579.7017	1102382	0.306462	0.000161	0.231851	0.197572
0.25	18.59674	1101801	618.3485	1102420	0.306473	0.000172	0.246812	0.219433
0.3	19.92508	1101800	662.5163	1102463	0.306485	0.000184	0.256794	0.234017
0.35	21.45777	1101799	713.4791	1102512	0.306498	0.000198	0.263932	0.244444
0.4	23.24592	1101797	772.9356	1102570	0.306514	0.000215	0.269296	0.252275
0.45	25.35919	1101795	843.2025	1102638	0.306533	0.000234	0.273478	0.25838
0.5	27.89511	1101792	927.5228	1102720	0.306556	0.000258	0.276837	0.263278
0.55	30.99456	1101789	1030.581	1102820	0.306584	0.000286	0.2796	0.267304
0.6	34.86888	1101785	1159.403	1102945	0.306619	0.000322	0.281923	0.270682
0.65	39.85015	1101780	1325.033	1103105	0.306663	0.000368	0.283913	0.27357
0.7	46.49185	1101774	1545.871	1103319	0.306723	0.000429	0.285654	0.276088
0.75	55.79021	1101764	1855.046	1103619	0.306806	0.000515	0.287217	0.278333
0.8	69.73777	1101750	2318.807	1104069	0.306931	0.000644	0.288671	0.280401
0.85	92.98369	1101727	3091.743	1104819	0.30714	0.000859	0.290118	0.282419
0.861953	101.0351	1101719	3359.456	1105078	0.307212	0.000933	0.290482	0.282918
0.872929	109.762	1101710	3649.626	1105360	0.30729	0.001014	0.29083	0.283392
0.9	139.4755	1101681	4637.614	1106318	0.307556	0.001288	0.29179	0.284671
0.95	278.9511	1101541	9275.228	1110816	0.308807	0.002576	0.294752	0.288423
1	#DIV/0!	#DIV/0!	#DIV/0!	#DIV/0!	#DIV/0!	#DIV/0!	#DIV/0!	#DIV/0!

The calculation for the SEC and SEC PES is done using Equation 48

$$E_{s3} = 2.05 \times 10^{-5} C_0 \frac{2 - R}{2(1 - R)} + 2.78 \times 10^{-7} \Delta P_{net}$$

$$E_{s3} = 2.05 \times 10^{-5} (0.188) \frac{2 - 0.8729}{2(1 - 0.8729)} + 2.78 \times 10^{-7} (1105360)$$

$$SEC = 0.307\ kWh/m^3$$

The work recovered by the ERD is calculated using the following equation:

$$W = \frac{(P_{atm} - P_{Brine})}{R \times 3.6 \times 10^6}$$

$$= \frac{(83226 - 4637000)12.64}{99.47 \times 3.6 \times 10^6}$$

$$= -0.024\ \text{kWh}/m^3$$

This is then used to calculate the SEC with the ERD. The SEC for the PES system is calculated using the following equation:

$$SEC\ PES = W \times \eta_{PES} + (1 + SI)SEC = -0.024 \times 0.95 + (1 + 0.000513)0.307$$

$$= 0.284\ kWh/m^3$$

Appendix G: Difference between original SEC and SEC with ERD

Table 44: Difference in SEC for a system with and without an ERD

SEC-SECPES	Diff pres
0.000769466	3071.13
0.000770539	3246.372
0.000771609	3442.23
0.000772676	3662.571
0.000773738	3912.291
0.000774796	4197.685
0.000775847	4526.986
0.00077689	4911.17
0.000777924	5365.206
0.000778944	5910.05
0.000779947	6575.969
0.000780927	7408.369
0.000781872	8478.596
0.000782767	9905.567
0.000783581	11903.33
0.000784252	14899.96
0.000784638	19894.36
0.000784654	21624.22
0.000784628	23499.18
0.000784313	29883.15
0.000781141	59849.53

From Equation 53 the following sample calculation is done:

$$SEC_{original} - SEC_{PES} = \frac{\frac{-R_{gas}c_0T}{1-R}SI - \eta_{PES}(1-R)\left(P_{atm} - \frac{c_0R_{gas}T}{1-R}\right)}{-3.6\times10^6}$$

$$= \frac{\frac{-8.314\times1.212\times295.55}{1-0.05}0.000513 - 0.95(1-0.05)(83.226 - \frac{1.212\times8.314\times295.55}{1-0.05})}{-3.6\times10^6}$$

$$= \left(\frac{-1.52778}{0.95} - 0.9025(83.226 - 3134.873)\right)\times(-3.6\times10^{-6})$$

$$= (-1.608189 - 2754.111)\times(-3.6\times10^{-6})$$

$$= 0.0007694\ kWh/m^3$$

Appendix H: Values for constants

Table 45: Values for constants from calculations

Constant	Value	Constant	Value
a_1	802	b_9	2.778×10^{4}
a_2	-2.001	b_{10}	97.28
a_3	0.01677	c_1	-4.231×10^{2}
a_4	-3.06×10^{-5}	c_2	1.463×10^{4}
a_5	-1.613×10^{-5}	c_3	-9.880×10^{4}
b_1	-2.348×10^{4}	c_4	3.095×10^{5}
b_2	3.152×10^{5}	c_5	2.562×10^{1}
b_3	2.803×10^{6}	c_6	-1.443×10^{-1}
b_4	-1.446×10^{7}	c_7	5.879×10^{-4}
b_5	7.826×10^{3}	c_8	-6.111×10^{1}
b_6	-44.17	c_9	8.041×10^{1}
b_7	0.2139	c_{10}	3.035×10^{-1}
b_8	-1.991×10^{4}		

Appendix I: Monitoring sheets

The following monitoring sheets are compiled on a two-hourly basis by the operators. The data gathered from this was used to compile the practical data from the desalination plant.

Eskom — Monitoring Sheet — Doc No: — Rev:

DATE: 18 March 2014

SHIFT:C

Biocide Dosing — Coagulant dosing — GenesysBS

UF SKID IN OPERATION		1				
Time		08:00	10:00	12:00	14:00	16:00
P/P A/B/C discharge pressure	kPa	184				
P/P A/B/C Speed	%	90.0				
Common Inlet Pressure	kPa	120.7				
Skid inlet Pressure	kPa	49.4				
Skid out let Pressure	kPa	65.8				
Trans Membrain Pressure		32.6				
Permeate Flow	m3/hr	165.4				
Common Permeate Flow	m3/hr	329.6				
Permeate Trubidity	NTU	0.207				
Common permeate Turb	NTU	0.260				
Inlet Vave position	%	47.3				
	°C	30.6				

UF SKID IN OPERATION		2				
Time		08:00	10:00	12:00	14:00	16:00
P/P A/B/C discharge pressure	kPa	182				
P/P A/B/C Speed	%	90.0				
Common Inlet Pressure	kPa	120.7				
Skid inlet Pressure	kPa	58.6				
Skid out let Pressure	kPa	60.9				
Trans Membrain Pressure		28.27				
Permeate Flow	m3/hr	165.3				
Common Permeate Flow	m3/hr	329.6				
Permeate Trubidity	NTU	0.207				
Common permeate Turb	NTU	0.260				
Inlet Vave position	%	27.1				
Feed Temperature	°C	30.6				

RO1 SKID IN OPERATION		3				
Time		08:00	10:00	12:00	14:00	16:00
Feed Press	kPa	1028.10				
Feed Cond	µS/cm	1761.1				
Feed pH		7.2				
Permeate Flow	m3/hr	952.2				
Common Permeate Press	kPa	29.6				
Concentrate Flow	m3/hr	1547				
Concentrate Pressure	kPa	1033.9				
Permeate Conductivity	µS/cm	3.657				
Permeate Temperature	°C	20.8				
Common Permeate Conductivity	µS/cm	2.657				
Common Permeate Temperature	°C	20.4				
Booster p/p in Pressure	kPa	821.3				
Booster p/p out Pressure	kPa	1133				
Concentrate Conductvity	µS/cm	1.268				
Brine v/v Position	%	25.0				
Recovery s.p	%	88.9				
Feed p/p Speed	%	73.8				

RO1 SKID IN OPERATION						
Time		08:00	10:00	12:00	14:00	16:00
Feed Press	kPa					
Feed Cond	µS/cm					
Feed pH						
Permeate Flow	m3/hr					
Common Permeate Press	kPa					
Concentrate Flow	m3/hr					
Concentrate Pressure	kPa					
Permeate Conductivity	µS/cm					
Permeate Temperature	°C					
Common Permeate Conductivity	µS/cm					
Common Permeate Temperature	°C					
Booster p/p in Pressure	kPa					
Booster p/p out Pressure	kPa					
Concentrate Conductvity	µS/cm					
Brine v/v Position	%					
Recovery s.p	%					
Feed p/p Speed	%					

COMMENTS:

Assistant Shift Supervisor Signature:

Shift Supervisor Signature:

Eskom	Komati Power Station Desalination Plant Monitoring Sheet	Doc No:
		Rev:

24/02/2014
SHIFT:A

Time		20:00	22:00	00:00	02:00	04:00	06:00
Feed Press	kPa						
Feed Cond	µS/cm						
Feed pH							
Permeate Flow	m3/hr						
Common Permeate Press	kPa						
Concentrate Flow	m3/hr						
Concentrate Pressure	kPa						
Permeate Conductivity	µS/cm						
Permeate Temperature	°C						
Common Permeate Conductivity	µS/cm						
Common Permeate Temperature	°C						
Concentrate Conductvity	µS/cm						
Brine v/v Position	%						
Recovery s.p	%						
Feed p/p Speed	%						

RO2 SKIDS IN OPERATION		3	3	3	3	3	
Time		20:00	22:00	00:00	02:00	04:00	06:00
Feed Press	kPa	1559,8	1534,1	1580,5	1580,6	1584,3	
Feed Cond	µS/cm	8,7	8,1	9,3	9,3	10,1	
Feed pH		7,358	7,208	7,243	7,240	7,243	
Permeate Flow	m3/hr	86,2	86,2	86,0	86,0	86,0	
Common Permeate Press	kPa	338,9	338,0	338,1	337,7	340,8	
Concentrate Flow	m3/hr	13,0	13,0	12,9	12,4	12,3	
Concentrate Pressure	kPa	729,1	729,4	729,4	729,1	729,6	
Permeate Conductivity	µS/cm	0,739	0,871	0,9118	0,935	0,961	
Permeate Temperature	°C	22,5	22,4	22,0	22,4	22,6	
Common Permeate Conductivity	µS/cm	0,733	0,863	0,901	0,940	0,946	
Common Permeate Temperature	°C	22,6	22,5	22,6	22,1	22,3	
Concentrate Conductvity	µS/cm	62,0	68,9	69,1	68,4	64,2	
Brine v/v Position	%	61,5	61,5	61,5	61,5	61,5	
Recovery s.p	%	87,5	87,5	87,5	87,5	87,4	
Feed p/p Speed	%	94,1	94,1	94,0	93,1	96,1	

CEDI IN OPERATION							
		20:00	22:00	00:00	02:00	04:00	06:00
Common Inlet Pressure	kPa						
Permeate Feed Pressure	kPa						
Concentrate Feed Pressure	kPa						
Permeate Out pressure	kPa						
Concentrate Out Pressure	kPa						
Permeate Flow	m3/hr						
Concentrated Flow	m3/hr						
Permeate Conductivity	µS/cm						
Permeate Temperature	°C						
Common Permeate Conductivity	µS/cm						
Common Permeate Temperature	°C						
Common Permeate SiO2	ppb						
Common Permeate Sodiums	ppb						
Concentrate Conductivity	µS/cm						
Skid Current	Amps						

CEDI OPERATION		1	1	1	1	1	
Time		20:00	22:00	00:00	02:00	04:00	06:00
Common Inlet Pressure	kPa	350,1	349,0	346,9	350,1	351,3	
Permeate Feed Pressure	kPa	268,3	268,3	271	324,1	319,4	
Concentrate Feed Pressure	kPa	105,6	97,3	152,5	155,1	155,1	
Permeate Out pressure	kPa	97,2	104,3	154,2	134,7	136,9	
Concentrate Out Pressure	kPa	78,5	78,5	130,9	132,9	134,9	
Permeate Flow	m3/hr	82,6	82,9	81,3	81,8	82,1	
Concentrated Flow	m3/hr	5,0	5,0	5,0	5,2	5,2	
Permeate Conductivity	µS/cm	0,055	0,057	0,055	0,055	0,056	
Permeate Temperature	°C	22,0	22,0	22,0	22,0	22,0	
Common Permeate Conductivity	µS/cm	1,007	0,056	0,056	0,056	0,056	
Common Permeate Temperature	°C	22,0	22,1	22,0	22,0	22,0	
Common Permeate SiO2	ppb	3,7	3,6	3,6	3,8	4,0	
Common Permeate Sodiums	ppb	0,141	0,135	0,141	0,174	0,150	
Concentrate Conductivity	µS/cm	8,12	4,96	4,94	6,80	8,05	
Skid Current	Amps	6	6	6,0	6,0	6,0	

COMMENTS: * Kas high - Sample valve closed so that the CEDI can dive to fill up the UF Filtered Tank.

Assistant Shift Supervisor Signature:
Shift Supervisor Signature:

24/02/2014

SHIFT:A

CEDI in Operation 1

		20:00	22:00	00:00	02:00	04:00
Skid Current	Amps	6	6	6	6	6
Module 1 Amps	Amps	6	6	6	6	6
Module 2 Amps	Amps	6	6	6	6	6
Module 3 Amps	Amps	6	6	6	6	6
Module 4 Amps	Amps	5	5	5	5	5
Module 5 Amps	Amps	3	3	3	3	3
Module 6 Amps	Amps	6	6	6	6	6
Module Voltage 1	Volts	380	380	380	380	380
Module Voltage 2	Volts	240	240	240	240	240
Module Voltage 3	Volts	360	360	360	360	360
Module Voltage 4	Volts	400	400	400	400	400
Module Voltage 5	Volts	260	260	260	260	260
Module Voltage 6	Volts	380	380	380	380	380

Appendix J: Chemical analyses results

From the samples taken, the following results were obtained by the on-site laboratory. The samples were taken on three separate dates and analysed accordingly.

Table 46: Results from the sample analysis on 7 February 2014

Parameter	Unit	UF feed	UF perm	RO1 Brine	Unit	RO1 Perm	RO2 Brine	RO2 Perm	CEDI Brine	Demin
pH_{25}		7.78	7.44	7.51		6.26	7.51	6.98	7.08	7.43
Conductivity (K_{25})	$\mu S.cm^{-1}$	187.4	183.4	1050	$\mu S.cm^{-1}$	4.7	35	2.2	2.2	1.2
Sodium (Na^+)	$mg.kg^{-1}$				$mg.kg^{-1}$					
Potassium (K^+)	$mg.kg^{-1}$				$mg.kg^{-1}$					
Calcium Hardness	$mg.kg^{-1}$ as $CaCO_3$	34.9	33.4	106.8	$mg.kg^{-1}$ as $CaCO_3$	0	0.75	0	0	0
Magnesium Hardness	$mg.kg^{-1}$	31.8	32.3	111.5	$mg.kg^{-1}$	0	1.91	0	0	0
Total Hardness	$mg.kg^{-1}$	66.7	65.7	218.3	$mg.kg^{-1}$	0	2.66	0	0	0
M-Alkalinity	$mg.kg^{-1}$	50.4	43.1	264.6	$mg.kg^{-1}$	3.7	15.7	3.8	3.8	2.8
P-Alkalinity	$mg.kg^{-1}$	0	0	0	$mg.kg^{-1}$	0	0	0	0	0
Chloride (Cl^-)	$mg.kg^{-1}$	14.12	12.84	58.25	$\mu g.kg^{-1}$	96.9	775.7	3.96	14.2	0.67
Sulphate ($SO4^-$)	$mg.kg^{-1}$	37.92	33.38	148.5	$\mu g.kg^{-1}$	93.9	596.5	7.15	0.43	<0.2
Silica (SiO_2)	$mg.kg^{-1}$	8	4	47	$\mu g.kg^{-1}$	164	1088	11	56	3
Iron (Fe)	ppb	0			ppb					
Oil	ppb	0	0	0	ppb	0	0	0	0	0
Turbidity	NTU	7.88	0.688	1.17	NTU	0.698	0.805	0.798	0.888	0.868
Copper	$mg.L^{-1}$				$mg.L^{-1}$					
TOC	ppm				ppm					
Flow	m^3/h			15.25	m^3/h	94.98	13.06	84.6	4.73	81.32
T	^0C			25.9	^0C	25.9		24.2		24
P	kPa			980	kPa	730	720	400	129	155
Conductivity Analyser	$\mu S.cm^{-1}$				$\mu S.cm^{-1}$	3.77		1.76		0.055

Table 47: Results from the sample analysis on 10 February 2014

Parameter	Unit	UF feed	UF perm	RO1 Brine	Unit	RO1 Perm	RO2 Brine	RO2 Perm	CEDI Brine	Demin
pH_{25}		7.63	7.56	8.11		6.21	7.85	7.29	6.39	7.28
Conductivity (K_{25})	$\mu S.cm^{-1}$	190.2	191.2	1038	$\mu S.cm^{-1}$	3.5	38.2	1.7	4.3	1.1
Sodium (Na^+)	$mg.kg^{-1}$				$mg.kg^{-1}$					
Potassium (K^+)	$mg.kg^{-1}$				$mg.kg^{-1}$					
Calcium Hardness	$mg.kg^{-1}$ as $CaCO_3$	35	31	228	$mg.kg^{-1}$ as $CaCO_3$	0	0	0	0	0
Magnesium Hardness	$mg.kg^{-1}$	35	32	229	$mg.kg^{-1}$	0	0	0	0	0
Total Hardness	$mg.kg^{-1}$	70	63	457	$mg.kg^{-1}$	0	0	0	0	0
M-Alkalinity	$mg.kg^{-1}$	41.9	44.2	269.9	$mg.kg^{-1}$	3	25.6	3.1	3.8	2.5
P-Alkalinity	$mg.kg^{-1}$	0	0	0	$mg.kg^{-1}$	0	0	0	0	0
Chloride (Cl^-)	$mg.kg^{-1}$	12.55	12.33	180.2	ppb	132.9	535.5	5.14	75.88	0.61
Sulphate ($SO4^-$)	$mg.kg^{-1}$	37.76	34.12	328.4	$\mu g.kg^{-1}$	146.21	403.5	1.62	5.69	0.85
Silica (SiO_2)	$mg.kg^{-1}$	9	8	41	$\mu g.kg^{-1}$	141	931	18	231	4
Iron (Fe)	ppb				ppb					
Oil	ppb	0	0	0	ppb	0	0	0	0	0
Turbidity	NTU	6.52	0.201	0.391	NTU	0.217	0.214	0.307	0.313	0.221
Copper	$mg.L^{-1}$	0			$mg.L^{-1}$					
TOC	ppm				ppm					
Flow	m^3/h	162	162	15.4	m^3/h	96	13.6	84.9	3.6	81.3
T	^0C			25.1	^0C	25.1		24.2		24.5
P	kPa			1010	kPa	760	740	400	140	152
Conductivity Analyser	$\mu S.cm^{-1}$				$\mu S.cm^{-1}$	2.85		0.718		0.054

Table 48: Results from the sample analysis on 12 February 2014

Parameter	Unit	UF feed	UF perm	RO1 Brine	Unit	RO1 Perm	RO2 Brine	RO2 Perm	CEDI Brine	Demin
pH_{25}			7.48	8.08		5.98	7.91	6.07	6.45	6.11
Conductivity (K_{25})	$\mu S.cm^{-1}$		190.4	990	$\mu S.cm^{-1}$	3.4	66.1	1.6	17.2	1.3
Sodium (Na^+)	$mg.kg^{-1}$		9.04	55.9	$mg.kg^{-1}$			31.7	12.3	1.4
Potassium (K^+)	$mg.kg^{-1}$				$mg.kg^{-1}$					
Calcium Hardness	$mg.kg^{-1}$ as $CaCO_3$		32	199	$mg.kg^{-1}$ as $CaCO_3$	0	0	0	0	0
Magnesium Hardness	$mg.kg^{-1}$		33	191	$mg.kg^{-1}$	0	0	0	0	0
Total Hardness	$mg.kg^{-1}$		65	390	$mg.kg^{-1}$	0	0	0	0	0
M-Alkalinity	$mg.kg^{-1}$		42.6	262.9	$mg.kg^{-1}$	2.6	30.5	1.9	9	1.9
P-Alkalinity	$mg.kg^{-1}$		0	0	$mg.kg^{-1}$	0	0	0	0	0
Chloride (Cl^-)	$mg.kg^{-1}$		12.3	93.3	ppb	93.9	773.2	0.83	259.7	0.59
Sulphate ($SO4^-$)	$mg.kg^{-1}$		30.1	224.3	$\mu g.kg^{-1}$	73.3	618	0.2	82.3	0.2
Silica (SiO_2)	$mg.kg^{-1}$		9	48	$\mu g.kg^{-1}$	77	441	28	160	8
Iron (Fe)	ppb		0	0	ppb	0	0	0	0	0
Oil	ppb		0	0	ppb	0	0	0	0	0
Turbidity	NTU		0.261	0.452	NTU	0.229	0.339	0.261	0.313	0.396
Copper	$mg.L^{-1}$		0	0	$mg.L^{-1}$	0	0	0	0	0
TOC	ppm		7.68	33	ppm	65.6	163	58	97.4	60.5
Flow	m^3/h	138	138	15.4	m^3/h	96.4	11.8	87.3	4.62	83.7
T	^oC			23.1	^oC	23.1	24.4	24.4	24.3	24.3
P	kPa			998	kPa	740	720	402	84	105
Conductivity Analyser	$\mu S.cm^{-1}$				$\mu S.cm^{-1}$	2.86		0.844		0.053

Appendix K: Photos of the desalination plant

Figure 71: Desalination plant with UF skids, first and second RO stages and chemical dosing stations

Figure 71 above shows the desalination plant with the UF skids (large skids on the left), RO first stage skids and RO second stage skids (at the far end of the building on the left). The dosing stations are shown on the right hand side.

Figure 72: Ultrafiltration skid

The figure above shows a single UF skid with the membrane vessels (white vessels).

Figure 73: Pressure indicator at UF inlet

Inlet pressure indicators for the ultrafiltration section are shown in Figure 73.

Figure 74: Turbidity analyser after UF membranes

The turbidity analyser after the UF section that analyse the turbidity and determines the effectiveness of the filtration stage.

Figure 75: RO1 high pressure feed pump

The figure above shows the motor and pump configuration with the variable speed drive that provides the high pressure feed for the first RO stage.

Figure 76: RO1 inter-stage booster pump

The figure above shows the motor and pump configuration with the variable speed drive that makes up the inter-stage booster pump.

Figure 77: Pressure indicator before RO1 booster

Figure 78: Pressure indicator after the RO1 booster pump

Figures 77 and 78 show the pressure indicators before and after the inter-stage booster pump on the first RO sections.

Figure 79: RO1 permeate conductivity

The photo above shows the permeate conductivity analyser on the permeate stream of the RO 1 section of the desalination plant.

Figure 80: Flow meter of RO1 brine

The photo above shows the flow meter analyser on the brine stream of the RO 1 section of the desalination plant.

Figure 81: RO2 high pressure feed pump

The figure above shows the motor and pump configuration with the variable speed drive that provides the high pressure feed for the second RO stage.

Figure 82: RO2 permeate conductivity

The photo above shows the permeate conductivity analyser on the permeate stream of the RO 2 section of the desalination plant.

Figure 83: RO2 brine pressure indicator

Figure 84: RO2 brine flow meter

The photos above show the brine pressure and flow meter analyser on the RO 2 section of the desalination plant.

Figure 85: CEDI booster pumps

Figure 85 shows the booster pumps on for the CEDI polishing plant with the motors, VSD and pump configuration.

Figure 86: CEDI modules

The photo above shows the CEDI modules that polish the permeate from the RO sections to produce demin water.

Figure 87: Flow meter on CEDI permeate

The flow meter above shows the flow of the demineralised boiler feed water from the desalination plant.

Appendix L: Uncertainty Analysis

An uncertainty analysis was performed in order to determine the accuracy of the pressure transmitters and salinity calculations.

The uncertainty is the quantified measure of doubt that exists about the measurement. The uncertainty of certain experimental results and the deviation of the measurement from reality are determined by completing an uncertainty analysis (NIST, 2014).

Two types of uncertainty analyses can be performed (NIST, 2014).

Type A is typically used for typically used for instrumentation where statistical measures can be used. This can be done for any measurement that can be repeated a minimum of four times. The uncertainty is calculated as:

$$u_A = \frac{\sigma}{\sqrt{n}} \qquad \textbf{Equation 61}$$

where u_A is the uncertainty for type A, σ is the standard deviation and n is the number of measurements (NIST, 2014).

Type B uncertainty analyses are usually done when information is not as available or when a specific measurement cannot be accurately reproduced a number of times (NIST, 2014).

A rectangular or normal distribution is assumed for the data set. Normally a rectangular distribution is assumed, unless calibration data from the manufacturer provides sufficient reason to assume a normal distribution (NIST, 2014).

$$u_B = \frac{a}{d} \qquad \textbf{Equation 62}$$

where u_B is the uncertainty for type B, a grade of uncertainty and d is dependent on the assumed distribution (normal = 2, rectangular =$\sqrt{3}$) (NIST, 2014).

The individual uncertainties of the equipment are then combined as follows (NIST, 2014):

$$u_c = \sqrt{u_1^2 + u_2^2 + u_3^2 + \cdots + u_i^2} \quad \textbf{Equation 63}$$

Where u_c is the combined uncertainties of the equipment and u_i is the uncertainty of the individual constituents of the equipment (NIST, 2014).

The expanded uncertainty can be calculated by finding the product of the confidence level with the combined uncertainty. This is done as follows:

$$U = ku_c \quad \textbf{Equation 64}$$

where U is the uncertainty and k is the confidence level. (k = 1, 68% confidence; k = 2, 95% confidence; k = 2.58, 99% confidence level) (NIST, 2014)

For this study, a confidence level of 95% (k = 2) was chosen.

For the salinity measurements, type A was used. The chlorine content of an identical water sample was repeated five times in order to calculate the required statistical data. The results are as follows:

Table 49: Results from the chlorine sample analysis

Analysis number	Chlorine (ppm)
1	13.31
2	13.48
3	13.16
4	13.09
5	13.24
Average	13.256
Standard Deviation	0.149833241

From Table 49, the uncertainty was calculated as $\pm$0.0749 ppm with an expanded uncertainty of $\pm$0.1498 ppm. This is a percentage offset of $\pm$1.13% for the chlorine content.

The pressure indicators and transmitters for this uncertainty investigation were investigated under type B. This is due to the fact that the variable speed drive on the pump constantly changes the feed pressure to the skids. If the feed pressure is constantly changing, (due to the changing water quality and temperature) the brine and permeate pressure will change. This prevents the measurements from being done under identical conditions which is required for type A. The results from this investigation are given in Table 50.

Table 50: Results from the uncertainty analysis for the pressure indicators

Type B: Pressure Indicators and flow meters													
Instrument	Description	Range Min	Range Max	Unit	Variables	± Value	Distribution	Standard uncertainty	u^2	k	Combined Uncertainty	Expanded uncertainty (kPa)	**Percentage offset**
Pressure Indicator	Yokogawa EJX630B	10	2000	kPa	Accuracy	0.0475	1.73205081	0.027424138	0.000752	2	1.156770868	2.313541735	**0.115677087**
					Power Supply Stability	0.00052	1.73205081	0.000300222	9.01E-08				
					Stability	2	1.73205081	1.154700538	1.333333				
					Ambient Temp effects	0.11	1.73205081	0.06350853	0.004033				
Pressure Indicator	Yokogawa EJX630D	0.35	70	MPa	Accuracy	45.5	1.73205081	26.26943725	690.0833	2	52.1112272	104.2224544	**0.148889221**
					Power Supply Stability	0.00052	1.73205081	0.000300222	9.01E-08				
					Stability	70	1.73205081	40.41451884	1633.333				
					Ambient Temp effects	34.3	1.73205081	19.80311423	392.1633				
Flow meter													

The values for the grade of uncertainty are from the respective manual of the instruments (Yokogama, 2014).

The results from this shows a percentage offset of 0.12% for the low pressure indicators and 0.15% for the high pressure indicators.